



universität
wien

DIPLOMARBEIT

Titel der Diplomarbeit

Analysis of long-period seismic signals
near Bad Ischl

Verfasser

Franziska Mayrhofer

angestrebter akademischer Grad

Magistra der Naturwissenschaften (Mag. rer.nat.)

Wien, 2012

Studienkennzahl lt. Studienblatt: A 416

Studienrichtung lt. Studienblatt: Geophysik

Betreuer: Univ.-Doz. Dr. Wolfgang Lenhardt, ZAMG

Abstract

In the vicinity of Bad Ischl, located in the Northern Calcareous Alps in Upper Austria, 43 long-period seismic events were detected by ZAMG between 1999 and 2011. They are supposed to be an effect of local mass movements. On the basis of a second data set, containing twelve tectonic earthquakes from the same region, a differentiation of source mechanisms by means of analyzing seismograms is done.

With the help of signal processing these long-period seismic events can be detected and separated from tectonic earthquakes. Therefore, the spectral content (including maximum amplitude, mean value and sum in the range of 0.5 to 3 Hz), auto correlation (including sum and time after 95 % of signal has passed), Arias intensity (including exponential fit), local and body-wave magnitude, coda, root mean square of amplitudes and signal energy is calculated. It turned out that the results of the last three methods are less indicative and thus not useful.

The spatial division of the events into three clusters leads to a good correlation with the regional geology and geotechnical setting (mainly the system "Hart auf Weich"). The information taken from literature verifies the assumption that the long-period seismic data set can be related to regions of higher mass movement activity. However, an analysis of local precipitation data does not indicate a strict causal connection between mass movements and preceding rainfall.

Zusammenfassung

In der Umgebung von Bad Ischl, welches sich in den nördlichen Kalkalpen in Oberösterreich befindet, wurden in einem Zeitraum von 1999 bis 2011 43 langperiodische seismische Ereignisse von der ZAMG registriert. Es wird vermutet, dass deren Ursprung in Hangbewegungen liegt. Basierend auf einem zweiten Datensatz, der aus 12 tektonischen Erdbeben aus derselben Region besteht, wird eine mögliche Unterscheidung der verschiedenen seismischen Quelltypen mittels detaillierter Analyse der Seismogramme gesucht.

Mit Hilfe von Signalprozessing können die langperiodischen Ereignisse erkannt und von denen der Erdbeben unterschieden werden. Dazu wird Folgendes berechnet: Frequenzgehalt (mit maximaler Amplitude, Mittelwert und Summe der Frequenzen von 0,5 bis 3 Hz), Autokorrelation (mit Summe und Dauer von 95 % des Signals), Arias Intensität (mit exponentiellem Fit), lokale und Raumwellenmagnitude, Coda, Effektivwertquadrat und Energiesignal. Die Ergebnisse der drei letztgenannten Berechnungen sind im Vergleich zu den anderen nicht aussagekräftig und daher nicht notwendig.

Die räumliche Trennung der Events in drei separate Cluster führt zu einer guten Korrelation mit der lokalen Geologie und der jeweiligen geotechnischen Situation (zumeist das System „Hart auf Weich“). Anhand einer vielfältigen Auswahl an Literatur wird die Annahme bestätigt, dass die Cluster von langperiodischen Ereignissen mit Gebieten erhöhter Massenbewegungen zusammenhängen. Eine Analyse lokaler Niederschlagsdaten deutet auf keinen direkten Zusammenhang hin, wenn auch vereinzelt eine Auslösung der Hangbewegung nicht ausgeschlossen werden kann.

Contents

1	<u>INTRODUCTION.....</u>	<u>1</u>
2	<u>DATA ACQUISITION.....</u>	<u>5</u>
2.1	EVENT LIST	5
2.2	SEISMIC STATIONS	8
2.2.1	STATION MOLLN (MOA).....	9
2.2.2	STATION KÖLNBREINSPERRE (KBA)	9
3	<u>LONG-PERIOD SEISMIC SIGNALS</u>	<u>11</u>
3.1	LANDSLIDES	11
3.1.1	TERMS AND DEFINITIONS FOR LANDSLIDES.....	11
3.1.2	LANDSLIDE CAUSES AND TRIGGERING MECHANISMS.....	14
3.1.2.1	Natural Occurrences	14
3.1.2.2	Human Activities	15
3.1.3	SEISMIC SIGNALS ASSOCIATED WITH LANDSLIDES.....	15
3.2	OTHER MASS MOVEMENTS	17
3.2.1	LONG-PERIOD VOLCANO SEISMICITY.....	17
3.2.2	ROCKFALL INDUCED SEISMIC SIGNALS	19
3.2.3	SEISMIC SIGNALS FROM ROCK/SNOW/ICE AVALANCHES	20
4	<u>MASS MOVEMENTS NEAR BAD ISCHL</u>	<u>23</u>
4.1	GEOLOGICAL OVERVIEW	23
4.2	GEOTECHNICAL CONDITIONS	24
4.3	CORRELATION OF SEISMOLOGICAL DATA AND GEOLOGY	25
4.3.1	LPES NEAR HALLSTATT	27
4.3.2	LPES IN THE REGION BETWEEN BAD GOISERN AND BAD ISCHL.....	30
4.3.3	LPES NORTHWEST OF BAD AUSSEE	32
5	<u>DATA PROCESSING AND QUANTIFICATION</u>	<u>35</u>
5.1	SEISMIC ANALYSIS CODE (SAC)	35
5.2	NOISE.....	37
5.3	USEFUL SIGNAL.....	38
5.4	SPECTRAL CONTENT	41
5.4.1	COMPARISON OF AMPLITUDE SPECTRA	44
5.5	MAGNITUDES	48

5.6	ARIAS INTENSITY.....	50
5.7	ENERGY SIGNAL.....	53
5.8	ROOT MEAN SQUARE	55
5.9	AUTO - CORRELATION	57
5.10	CODA.....	63
6	<u>CORRELATION</u>	<u>67</u>
6.1	CORRELATION WITH PRECIPITATION DATA	67
6.1.1	METEOROLOGICAL STATIONS	68
6.1.2	PRECIPITATION DATA	69
6.1.3	QUANTIFICATION	70
6.2	CORRELATION WITH THE GEOLOGICAL AND GEOTECHNICAL SETTING	79
7	<u>DISCUSSION</u>	<u>85</u>
8	<u>CONCLUSION.....</u>	<u>95</u>
	<u>ACKNOWLEDGEMENTS.....</u>	<u>97</u>
	<u>REFERENCES.....</u>	<u>99</u>
	<u>CURRICULUM VITAE.....</u>	<u>105</u>

1 Introduction

Every year about 7000 tremors are analyzed by the Seismological Service of Austria (Österreichischer Erdbebendienst) at Central Institute for Meteorology and Geodynamics (Zentralanstalt für Meteorologie und Geodynamik, ZAMG) whereby 5900 of these events take place in foreign countries. Little more than 500 of the remaining 1100 events refer to mining activity in Austria. The leftover is classified as tectonic earthquakes with 30 to 60 of them being noticed by the population. Some of the strongest earthquakes with magnitudes greater than 5.0 happened the last 100 years in Schwadorf, Lower Austria (1927), Namlos, Tyrol (1930) and Seebenstein, Lower Austria (1972) (ZAMG, 2012).

In the vicinity of the town of Bad Ischl, Upper Austria, seismic events with unusual frequency content have been detected within the tectonic earthquake data set. Over the last 13 years 43 of these events have been collected that are either definitely long-period seismic events (LPE) or it is at least doubtful, whether their seismograms belong to tectonic earthquakes or not. This data set is the basis of this diploma thesis. Figure 1-1 shows the region of interest with the LPEs (red circles varying with magnitude) while Figure 1-2 gives an example of a typical seismogram of such an event.

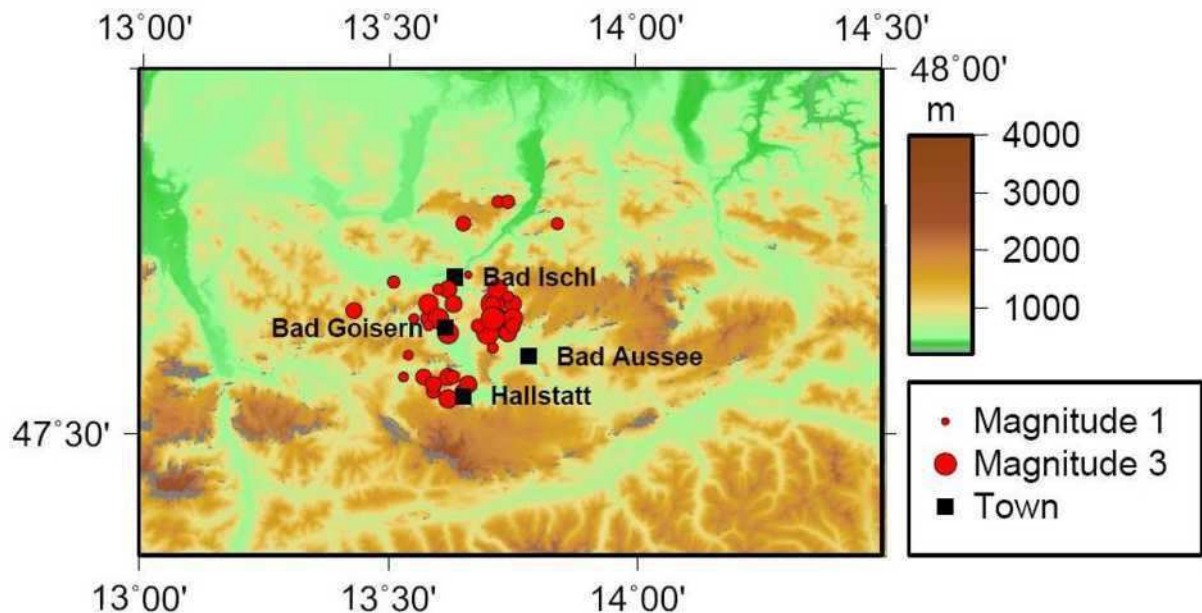


Figure 1-1 Epicentres (red circles) of the long-period data set in the surrounding of Bad Ischl. The size of the red circles indicate the magnitude.

1. Introduction

The question arises whether these LPEs can be detected and easily separated from tectonic earthquakes with the help of signal processing. Thus, a second data set of twelve true earthquakes, which are from the same region and cover approximately the same magnitude range are used for comparison. An example is shown in Figure 1-2.

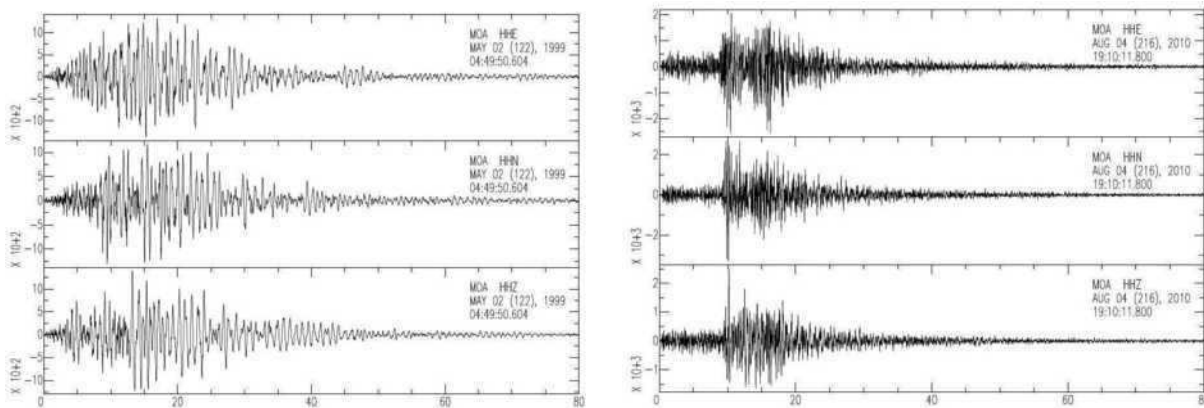


Figure 1-2 Three components of a seismic record of a long-period event (LPE) (left) and of a tectonic earthquake (right) of similar magnitude recorded approximately at the same distance.

Consequently the main purpose of this diploma thesis is a detailed analysis of the seismograms to find out more specific and expressive characteristics (e.g. spectral content, Arias intensity) to make LPEs easily distinguishable from tectonic earthquakes.

To detect the differences in these two types of seismograms the two nearest seismic stations from the Seismological Network of Austria are used: Molln (MOA) and Kölnbreinsperre (KBA). Figure 1-3 shows the region of interest with the data set of both LPEs (red) and tectonic earthquakes (green) and the two seismic stations.

The other part of the thesis places special emphasis on the origin of the ground motion. Figure 1-1 reveals three clusters of LPEs: an accumulation of epicentres is located between Bad Goisern and Bad Ischl; another one can be defined northwest of Bad Aussee while the third cluster can be found west of Hallstatt. After a short summary of possible long-period sources mass movements on the earth's surface are considered as the most probable. Thus, a short outline of the regional geology and geotechnical situation raises the question of a correlation with mass movements from the three spatial separated regions. General information and data of mass movements was provided by the Geological Survey of Austria (GBA).

Another idea to figure out a relation with an external factor is the correlation with precipitation data. Thus, time series of precipitation of the nearest meteorological stations of the last four weeks

1. Introduction

(28 days) before each LPE source was possibly triggered by rainfall, were correlated with the recorded seismic activity.

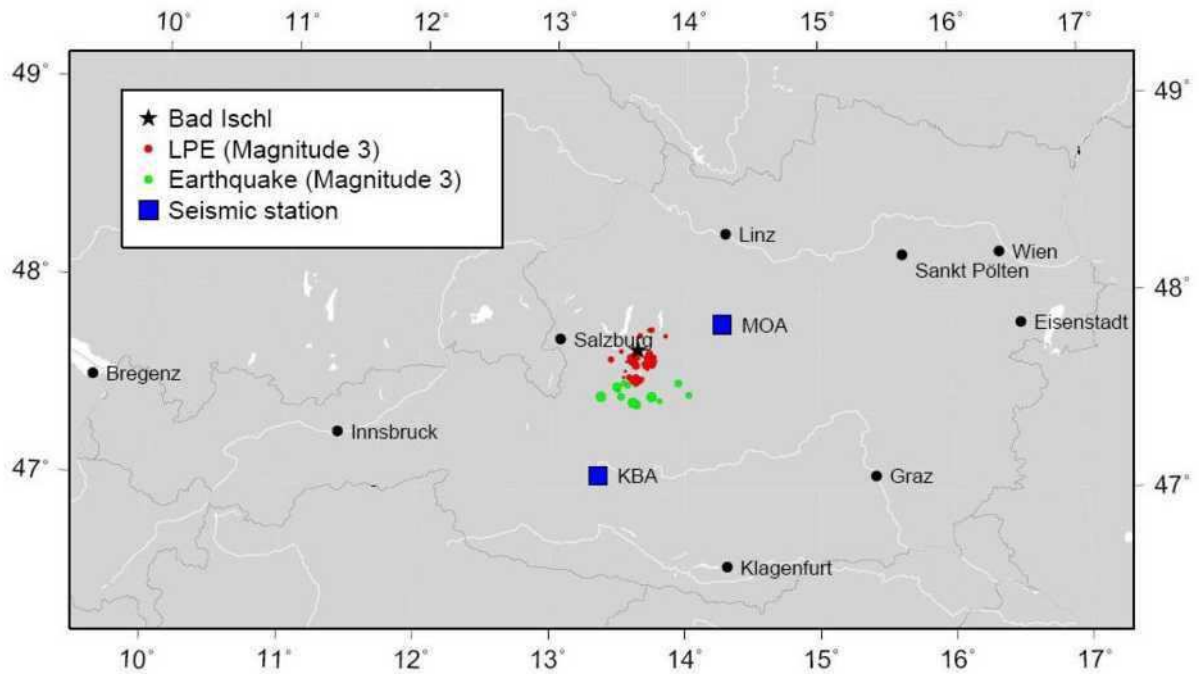


Figure 1-3 Map of Austria showing the location of Bad Ischl (asterisk), the long-period data set (red circles) and the earthquake data set (green circles) as well as the two seismic stations Molln (MOA) and Kölnbreinsperre (KBA).

1. Introduction

2 Data Acquisition

2.1 Event List

The data contain events from the time period of 1999 until 2011. All in all there are 43 events that were suspected of having non-earthquake sources in the respective time window in the area of interest. During data processing some of the events were eliminated due to a lack of long-period characteristics. Table 2-1 lists the events for processing, thus naming the date, focal time, latitude and longitude, magnitude and intensity, if available, as well as the village next to the epicenter. The events were all located within 20 km from Bad Ischl. The data were retrieved from the earthquake database of ZAMG.

To get an overall view of the data, two histograms are presented below. Figure 2-1 shows the distribution of the data concerning the month of occurrence (left side) and the number of events per magnitude class (right side).

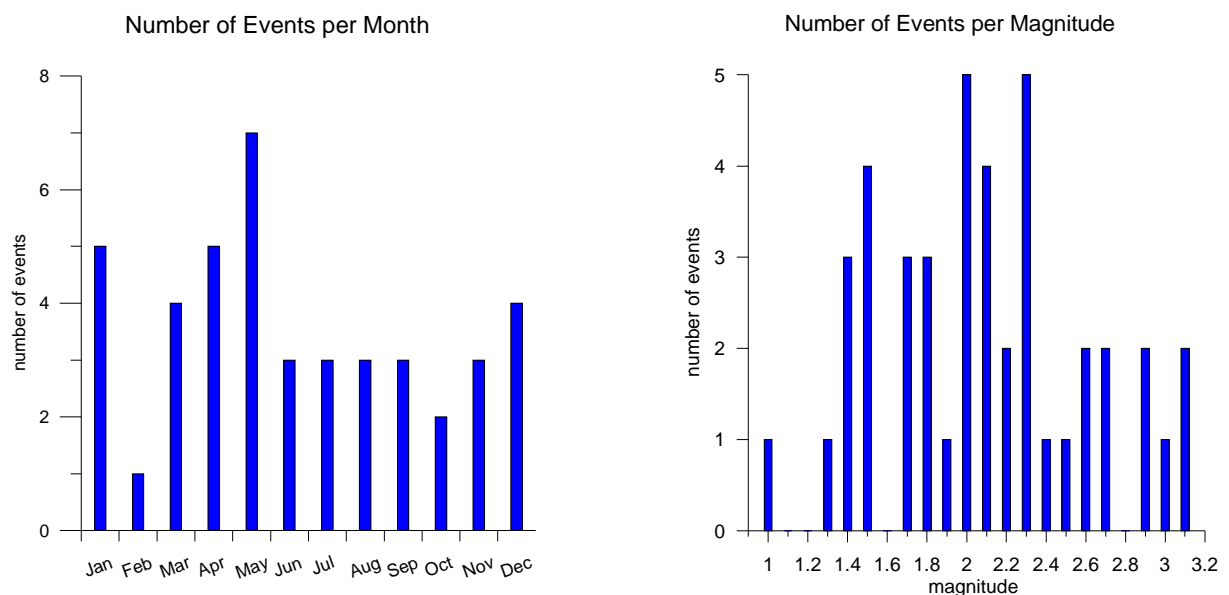


Figure 2-1 Histograms of the number of events per month (left) and the number of events per magnitude class (right).

As can be seen from Figure 2-1 there is no annual trend of occurrence of LPEs concerning the month. It only shows a small tendency for a higher probability of those events in spring, which could be related to the snow melting. The magnitude for the events ranges from 1.0 to 3.1. Again no correlation between magnitude and number of events is apparent except for a small peak between magnitude 2.0 and 2.3.

2. Data Acquisition

During the course of this study, comparisons with earthquakes from the respective region were carried out to extract characteristics of the LPEs. ZAMG provided the data that are listed in Table 2-2.

To get access to the raw data (time series) the AutoDRM (Automatic Data Request Manager) is used. An email had to be sent to autodrm2@zamg.ac.at in the following format:

```
BEGIN GSE2.1
MSG_TYPE REQUEST
MSG_ID 001_seismo geotool
EMAIL a0500656@unet.univie.ac.at
TIME 2010/08/04 19:21:00 to 2010/08/04 19:27:00
STA_LIST MOA,KBA
CHAN_LIST HHZ,HHN,HHE
WAVEFORM GSE2.1
STOP
```

An essential input is the time period with the starting time and the end time. In general, a time window of six minutes was selected whereas later on in the processing steps, the data length is reduced to its appropriate length of 80 seconds. Also the station codes (STA_LIST) and the respective channels (CHAN_LIST) and the waveform format must be defined. AutoDRM sends a response-email for processing with the requested time series to the given email address (EMAIL). ZAMG provides the data in the GSE 2.1 format.

Besides time series, a request for P and S wave first arrival picks and magnitudes can also be made via AutoDRM. The content of the email to autodrm2@zamg.ac.at reads as follows:

```
BEGIN
MSG_TYPE REQUEST
MSG_ID 2008 earth
TIME 2008/07/18 22:54:00 TO 2008/07/18 22:55:00
BULLETIN
STOP
```

Again, the time window needs to be defined. The given magnitudes as well as the picks for the first arrivals are then extracted from the email for further processing. Unfortunately the online bulletin only contains data since 2008. Therefore, the missing data has to be requested from the ISC homepage (<http://www.isc.ac.uk/>).

2. Data Acquisition

Table 2-1 List of LPEs for processing provided by ZAMG.

date yyyy mm dd	focal time hh mm ss.s	latitude [°]	longitude [°]	magnitude	intensity	epicenter
1999 05 02	04 49 43.5	47.68	13.71	3.1		Altaussee
2000 04 18	15 15 18.0	47.70	13.62	2.3		Bad Ischl
2000 06 25	17 02 45.0	47.70	13.72	2.6		Bad Ischl
2000 08 29	14 21 34.1	47.66	13.58	2.1		Bad Goisern
2000 11 09	15 33 04.2	47.82	13.72	1.7		Ebensee
2001 04 25	16 03 05.7	47.56	13.59	1.8		Gosau-Hintertal
2002 06 30	00 14 56.7	47.65	13.72	2.0		Altaussee
2002 07 20	02 35 58.6	47.66	13.73	2.1		Altaussee
2002 11 18	22 16 53.2	47.79	13.65	2.0		Höllengebirge
2003 07 14	03 24 34.9	47.64	13.62	2.9	4	Bad Goisern
2003 09 18	22 47 12.3	47.56	13.65	2.1		Hallstatt
2004 05 08	10 23 44.7	47.62	13.71	1.5	3 - 4	Altaussee
2004 10 12	06 56 45.8	47.64	13.73	1.5		Altaussee
2006 02 22	03 38 59.9	47.64	13.70	3.0	4	Altaussee
2006 03 28	03 26 44.3	47.65	13.68	1.8		Bad Goisern
2006 04 27	20 12 39.6	47.70	13.60	1.5		Bad Ischl
2006 05 18	00 39 33.1	47.68	13.58	2.6	4	Bad Ischl
2006 05 27	19 10 29.4	47.68	13.75	2.3		Altaussee
2006 08 22	00 44 57.2	47.58	13.62	2.3	3	Hallstatt
2006 09 26	10 08 37.2	47.82	13.74	1.9		Ebensee
2006 11 24	00 33 21.1	47.71	13.51	1.7		Strobl
2006 12 15	13 44 42.1	47.66	13.60	2.9	3 - 4	Bad Goisern
2006 12 16	09 45 59.1	47.66	13.72	2.7		Altaussee
2007 03 18	13 27 05.0	47.58	13.53	1.4		Gosau
2007 03 27	18 26 14.0	47.58	13.57	2.2		Gosau
2007 06 04	10 33 04.4	47.72	13.66	1.0		Bad Ischl
2007 12 10	06 26 18.9	47.65	13.75	2.0		Altaussee
2008 01 22	20 00 42.2	47.61	13.54	1.4		Gosau
2008 03 02	13 00 09.5	47.58	13.63	1.8		Hallstatt
2008 05 03	11 37 40.0	47.55	13.62	2.5	3	Hallstatt
2008 07 23	16 36 07.6	47.68	13.71	2.0		Altaussee
2009 01 06	10 09 27.4	47.65	13.58	1.3		Bad Goisern
2009 05 06	14 33 55.4	47.57	13.59	2.1		Gosau-Hintertal
2010 01 19	18 43 59.6	47.66	13.75	2.7	2 - 3	Altaussee
2010 01 23	21 27 24.7	47.64	13.74	2.3		Altaussee
2010 01 24	00 46 32.3	47.57	13.66	2.3		Hallstatt
2010 04 23	12 53 04.9	47.66	13.55	1.4		Bad Goisern
2010 05 03	09 14 21.7	47.67	13.43	2.2		Postalm
2010 09 18	22 13 20.2	47.79	13.84	1.7		Offensee
2010 10 23	19 36 09.1	47.68	13.63	2.4	3 - 4	Bad Ischl
2011 04 05	07 14 25.8	47.66	13.71	3.1	4	Altaussee
2011 08 10	16 16 37.5	47.65	13.75	2.0		Altaussee
2011 12 26	01 34 29.2	47.69	13.74	1.5		Altaussee

2. Data Acquisition

Table 2-2 List of earthquake provided by ZAMG for comparison

date yyyy mm dd	focal time hh mm ss.s	latitude [°]	longitude [°]	magnitude	intensity	epicenter
2001 04 15	18 05 10.1	47.55	13.94	2.6	4	Bad Mitterndorf
2001 11 10	05 08 06.8	47.49	14.02	2.4	4	St. Martin am Grimming
2004 02 22	20 09 09.0	47.54	13.56	2.4	4	Gosau-Hintertal
2004 06 18	08 10 45.2	47.48	13.36	3.6	5	St. Martin am Tennengebirge
2005 06 23	12 12 00.0	47.46	13.8	1.9	4	Haus im Ennstal
2008 05 21	07 21 00.7	47.44	13.63	3.0	3 - 4	Ramsau
2008 05 21	13 39 57.0	47.45	13.60	3.6	4	Hoher Dachstein
2008 07 18	22 54 03.3	47.48	13.74	3.8	5	Haus im Ennstal
2010 08 04	19 09 59.0	47.53	13.48	3.3	4 - 5	Gosaukamm
2010 08 04	19 14 46.1	47.55	13.53	2.1		Gosau-Hintertal
2010 08 04	19 21 44.9	47.51	13.49	1.4		Gosaukamm
2010 08 05	15 07 46.2	47.48	13.51	2.7	3 - 4	Gosaukamm

2.2 Seismic Stations

Figure 2-2 gives an overall view of the Seismic Network of Austria. As the majority of events did not exceed a local magnitude of 2.5, only data of the two nearest stations could be used for this study. In this case, these are the seismic stations named MOA and KBA. General information is given in Table 2-3 (ISC-Code, abbreviated name of station by the International Seismological Centre). Both, MOA and KBA are equipped with Streckeisen STS-2 broadband sensors and Quanterra digitizers. Detailed information of the seismic instrument is given on the following homepage www.passcal.nmt.edu.

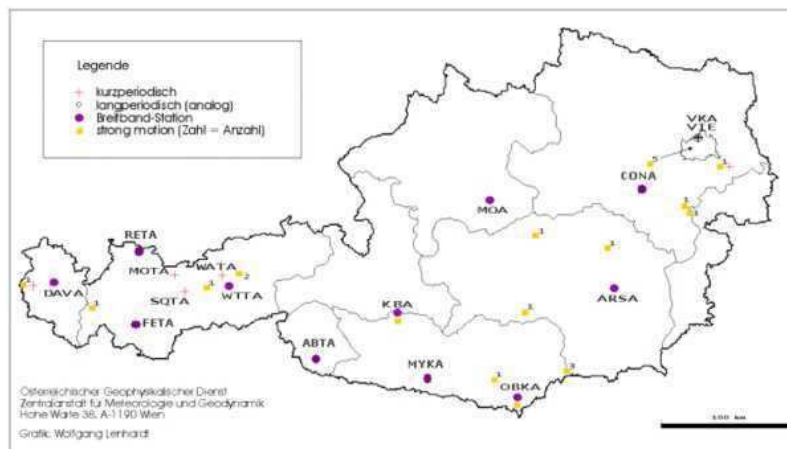


Figure 2-2 Seismological broad-band station network of Austria. KBA and MOA are denoted with purple dots. (© ZAMG, 2011)

2. Data Acquisition

Table 2-3 General information about the seismic stations by ZAMG.

ISC-Code	Location	Latitude	Longitude	Elevation	since	distance from Bad Ischl
KBA	Kölnbreinsperre	47.0784	13.3447	1721 m	1997	49.5 km
MOA	Molln	47.8495	14.2659	572 m	1996	74.1 km

2.2.1 Station Molln (MOA)

The station Molln (MOA) is located in the Upper Austrian Alpine foreland in the so called Pyhrn-Eisenwurzen at 572 metres above sea level. From a geological point of view it is situated in an Austroalpine cover, being rich in limestone and belonging to the Permian Mesozoic. Figure 2-3 shows on the left side a detailed map of Molln and its surrounding. The red circle represents the location of the seismic station MOA. To the right, a photo gives an impression of the entrance of the access tunnel, where the seismic instrument is installed.



Figure 2-3 Left side: Map of Molln and its surrounding area. The center of the circle indicates the position of the station. Right side: Entrance of the seismic station.

2.2.2 Station Kölnbreinsperre (KBA)

The station KBA is established at the dam toe of the Kölnbrein reservoir. It is located in the so called Ankogel Gruppe at a height of 1721 m. Geologically it belongs to the Tauern window (Penninic nappes). Figure 2-4 shows a map of the Kölnbrein reservoir (left) and its surrounding area (right).

Station information and the relating maps as well as pictures are provided by the Department of Geophysics/ZAMG.

2. Data Acquisition



Figure 2-4 Map of the Kölnbrein reservoir and its surrounding. The red circle indicates the location of the seismic station.

As already mentioned above, all data in this thesis has its origin in the vicinity of Bad Ischl. To get an impression of the location of the town of Bad Ischl and the seismic stations MOA and KBA, Figure 2-5 features a map of Austria, which only contains those three locations. The map also highlights the fact that the two seismic stations are located in two different directions seen from the location of origin of the observed LPEs.

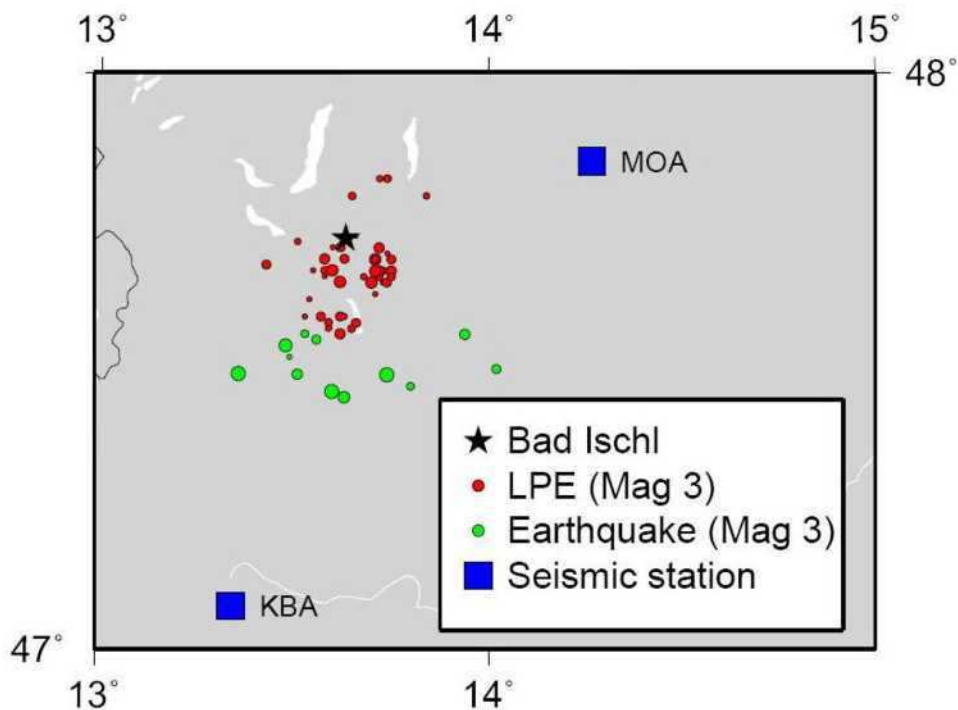


Figure 2-5 Map of LPEs (red circles), earthquakes (green circles), Bad Ischl (asterisk) and seismic stations (blue squares).

3 Long-period Seismic Signals

Certainly there are a great number of causes that produce seismic signals. In this study the data to be considered has led to a classification of the seismic events based on the frequency content. More precisely, the main emphasis is on long-period seismic signals.

Different events in nature can produce these long-period seismic signals. For example, the seismograms of mass movements such as landslides, debris flows, rockfalls or avalanches or even volcanoes consist of these low frequencies aside other characteristics. An overview of the above mentioned sources will be given on the following pages to consider all possible causes that result in longer periods in recorded seismic spectra. A special focus is put on landslides as they are the most likely reason for the LPEs in the Alps.

The importance of seismically identifying and locating such LPEs is obvious. As the global population is constantly expanding more hazardous regions are habituated and a greater number of people are exposed to the risk of mass movement hazards.

“The success in identifying and in some cases locating these events in near real time demonstrates that local and regional seismic networks can play a valuable role in reducing hazards from large, rapid mass movements.”

(NORRIS, R., 1994)

3.1 Landslides

3.1.1 Terms and Definitions for Landslides

The International Union of Geological Sciences proposed a system to classify landslides according to their post failure velocity (G. HUNTER and R. FELL, 2001). Generally they can be divided into “slow landslides” with an upper limit of 1.8 m/s and “rapid landslides” with a lower limit of 1.8 m/s. Table 3-1 gives a more detailed insight into the velocity classification for landslides, whereas the first four classifications relate to slow landslides.

As the velocity does not give detailed information about the source mechanism or the amount of mass to be transported, another approach for classification is used. One part is the initial slide classification, which describes the initiation of landslides in the source area; the other part is the travel classification, which describes the movement along the travel path.

3. Long-period Seismic Signals

Velocity Classification	Description of Velocity	Velocity limits	Velocity in mm/sec
7	Extremely rapid	> 5 m/sec	> 5×10^3
6	Very rapid	3 m/min to 5 m/sec	50 to 5×10^3
5	Rapid	1.8 m/hour to 3 m/min	0.5 to 50
4	Moderate	13 m/month to 1.8 m/hour	5×10^{-3} to 0.5
3	Slow	1.6 m/year to 13 m/month	50×10^{-6} to 5×10^{-3}
2	Very slow	16 mm/year to 1.6 m/year	0.5×10^{-6} to 50×10^{-6}
1	Extremely slow	≤ 16 mm/year	$\leq 0.5 \times 10^{-6}$

On the left side of Figure 3-1 the soil behaviour is described. At the top the failure is due to contraction while at the bottom it is due to dilatation on shearing. In the middle there is the initiating slide classification, which is composed of flow slide, slide through soil mass and defect controlled slide.

The term “flow slide” is related to contraction on shearing and most often takes place in saturated soils. Static liquefaction on shearing concludes in a large loss in undrained strength, which leads to a failure of the slide mass. “Slide through the soil mass” as well as “defect controlled slide” originate in soils that are dilative on shearing. In the first case the surface of rupture is situated in the soil/rock mass whereas in the second case the origin of sliding lies in a defect in the soil or weathered rock mass (G. HUNTER and R. FELL, 2001).

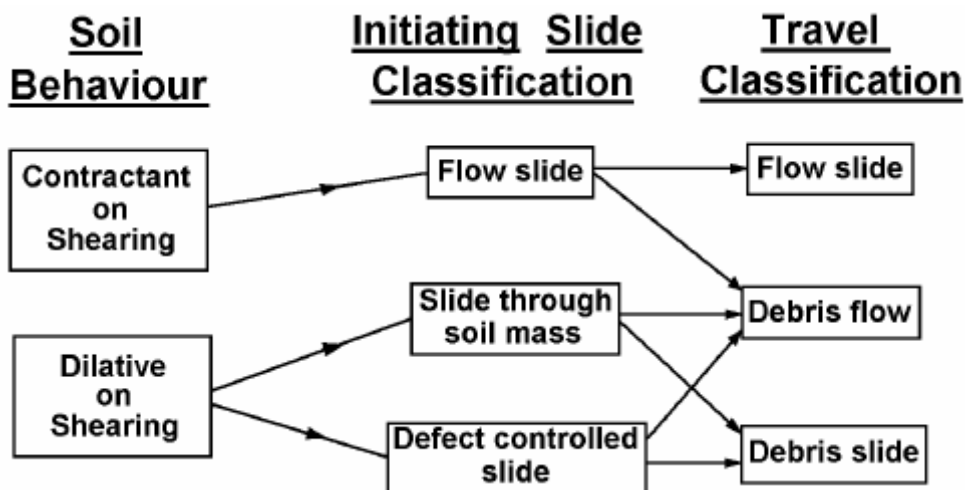


Figure 3-1: The classification system and main slides types (G. HUNTER and R. FELL, 2001).

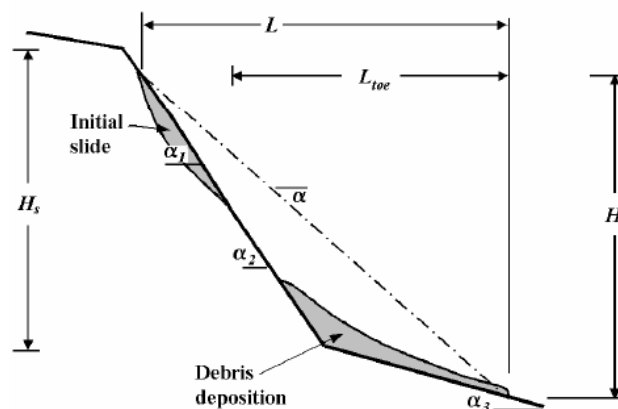
3. Long-period Seismic Signals

On the right side of Figure 3-1 there are three end terms of the travel classification, whereby a mixture of the three terms is likely to occur in nature. Two distinct types can be pointed out in general, where on the one hand the moving mass stays in its initial structure (flow slide), while on the other hand the mass moves more as a turbulent flow (debris flow). For a debris slide the mass moves along a defined basal surface while it is not mixed up a lot. They are typically transported far beyond the source area.

To describe the geometry of a slope and its travel geometry (Figure 3-2), several parameters are needed (Table 3-2). This is also another possibility to distinguish different types of gravitational mass movements. There are five different types that are basically different from each other by the position of the initial slides and its deposits which are strongly linked to the topography (more precisely dependent on the travel distance angle and the slope angle) and the transportation velocity.

Table 3-2 Definitions of terms used to describe the geometry of landslides.

Abbreviation	Explanation
H_s	slope height
H	slide height
L	travel distance
α	travel distance angle
L_{toe}	horizontal distance beyond the toe of the initial failure
D	failure depth
α_1	source area slope angle
α_2	down-slope angle immediately down-slope of the failure zone
α_3	down-slope angle over the distal portion of the travel path



2 Slope failure geometry (G. HUNTER and R. 01).

3. Long-period Seismic Signals

3.1.2 Landslide Causes and Triggering Mechanisms

The following information is based on and extracted from “The Landslide Handbook - A Guide to Understanding Landslides” (HIGHLAND and BOBROWSKY, 2008) as it highlights the fundamentals of landslide causes.

There are two main categories of sources causing landslides – they are either natural- or human caused whereby the actual reason of failure is always a physical one. Therefore Table 3-3 lists the most frequent occurring physical causes triggering landslides.

3.1.2.1 Natural Occurrences

Natural occurrences are divided into three endterms: water, seismic activity and volcanic activity. These three major triggering mechanisms are likely to occur in combination as they depend on several factors (e.g. shape of terrain, steepness of slope, soil type and underlying geology).

The main link between landslides and water is the saturation. After intense rainfall or snowmelt the slope material might be oversaturated and this is likely to result in failure. The deposit of the mass after the slide is in many cases linked with secondary effects such as blocking waterways. This leads to backwater flooding behind a dam, and in case of a breaking dam in downstream flooding.

Table 3-3 Physical Causes – Triggers of landslides. (HIGHLAND and BOBROWSKY, 2008)

Physical Causes—Triggers
• Intense rainfall
• Rapid snowmelt
• Prolonged intense precipitation
• Rapid drawdown (of floods and tides) or filling
• Earthquake
• Volcanic eruption
• Thawing
• Freeze-and-thaw weathering
• Shrink-and-swell weathering
• Flooding

Table 3-4 Natural causes for landslides (HIGHLAND and BOBROWSKY, 2008).

Natural Causes	
Geological causes	Morphological causes
<ul style="list-style-type: none"> • Weak materials, such as some volcanic slopes or unconsolidated marine sediments, for example • Susceptible materials • Weathered materials • Sheared materials • Jointed or fissured materials • Adversely oriented mass discontinuity (bedding, schistosity, and so forth) • Adversely oriented structural discontinuity (fault, unconformity, contact, and so forth) • Contrast in permeability • Contrast in stiffness (stiff, dense material over plastic materials) 	<ul style="list-style-type: none"> • Tectonic or volcanic uplift • Glacial rebound • Glacial meltwater outburst • Fluvial erosion of slope toe • Wave erosion of slope toe • Glacial erosion of slope toe • Erosion of lateral margins • Subterranean erosion (solution, piping) • Deposition loading slope or its crest • Vegetation removal (by forest fire, drought)

The risk of earthquakes triggering landslides is deeply connected with mountainous regions, where either the ground shaking itself or liquefaction of susceptible sediments is responsible for triggering them. Another reason is due to shaking-caused dilation of soil-material. Water can rapidly infiltrate in the opening cracks and cause a landslide. This also shows the connection of the endterms of classifying the natural occurrences of landslides.

The most devastating types of failures occur in relation with volcanic activity. First, the rising of the heat can lead to an enormous amount of ice melting on

3. Long-period Seismic Signals

top of the volcano in quite a short period of time, which, when mixed with rock, soil and ash, results in a debris flow named lahar. They typically reach great distances and therefore are of great danger. The other reason for landslides at volcanoes is due to the very young and unconsolidated geological structures, which can easily collapse and cause rockslides, landslides and debris avalanches.

Table 3-4 gives a more detailed insight into the natural causes for landslides divided into geological and morphological causes to get a better impression of natural landslides sources.

3.1.2.2 Human Activities

Table 3-5 Human causes for landslides (HIGHLAND and BOBROWSKY, 2008).

Human Causes
<ul style="list-style-type: none">• Excavation of slope or its toe• Use of unstable earth fills, for construction• Loading of slope or its crest, such as placing earth fill at the top of a slope• Drawdown and filling (of reservoirs)• Deforestation—cutting down trees/logging and (or) clearing land for crops; unstable logging roads• Irrigation and (or) lawn watering• Mining/mine waste containment• Artificial vibration such as pile driving, explosions, or other strong ground vibrations• Water leakage from utilities, such as water or sewer lines• Diversion (planned or unplanned) of a river current or longshore current by construction of piers, dikes, weirs, and so forth

The permanent growth of world population forces people to explore new land. This goes hand in hand with changing drainage patterns, destabilizing slopes, and removing vegetation. These human-induced factors are also likely to initiate landslides (HIGHLAND and BOBROWSKY, 2008).

More examples and detailed information for human causes are listed in Table 3-5.

3.1.3 Seismic Signals associated with Landslides

“A landslide generates seismic waves by both shearing and loading the surface as the mass moves from a steep to a shallow slope. “

(BRODSKY E. E. et al., 2003)

“The landslides produced seismic signals characterized by high amplitude and very emergent onset, irregular envelope, frequency content in the band 0.1-5 Hz, and a duration of many minutes”

(LA ROCCA M. et al., 2004)

Based on the two citations from the articles “Landslide basal friction as measured by seismic waves” (BRODSKY E. E. et al., 2003) and “Seismic Signals Associated with Landslides and with a Tsunami at

3. Long-period Seismic Signals

Stromboli Volcano, Italy" (LA ROCCA et al., 2004) landslides as sources of seismic waves and their characteristics are discussed.

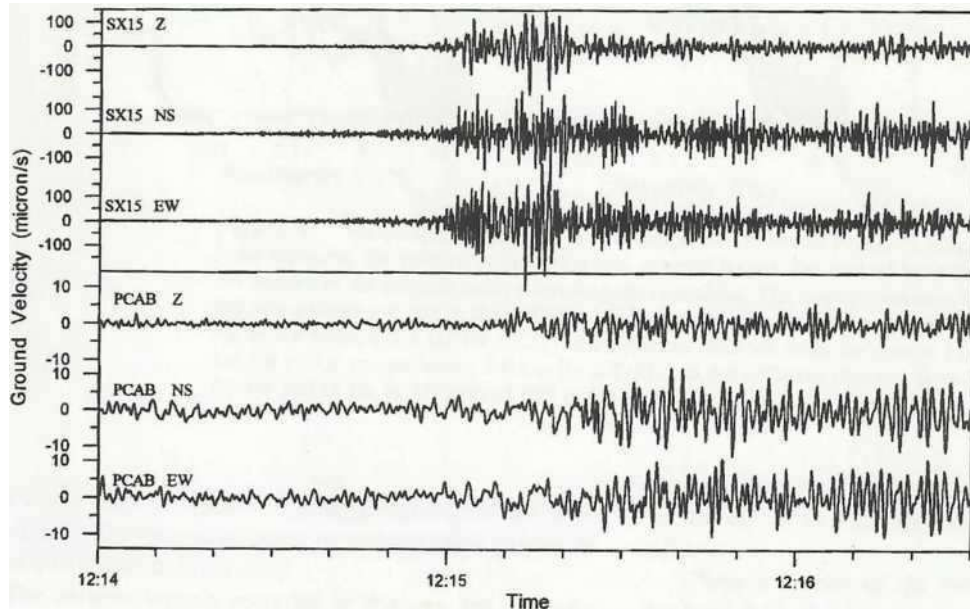


Figure 3-3 Example of a high-frequency signal recorded by stations SX15 (Stromboli, 2.8 km from source) and PCAB (Panarea Island, 21 km from source).

Considering the emergent onset, the following can be said: As there is no sharp pulse that precisely defines the beginning of the seismogram it is generally difficult to make a clear statement about the time of origin of the landslide. At stations close to the event the precursor can be interpreted by the opening of cracks and the rolling and sliding of small blocks down the slope before the actual failure of the major mass. The duration of several minutes of a seismogram that results from a landslide might have the same origin but starts significantly after the actual failure of the major mass (LA ROCCA et al., 2004).

Typically for landslides are relatively low frequencies of recorded ground motions. The high-amplitude peaks can be detected in the 0.01 to 5 Hz frequency band whereas in specific cases a more detailed analysis has to be made regarding the site and kind of seismometer (LA ROCCA et al., 2004).

Another interesting and often applied method to deal with seismic signals of landslides is the analysis of particle motion as it enables the comparison with a source model. To find a model that approximates the source of a landslide best, a single-force model has been introduced by several authors such as KANAMORI and GIVEN (1982), OKAL (1990) and DAHLEN (1993). When a large mass starts sliding down the recoil of the ground produces a force and exactly this force is represented by a shallow single-force model (LA ROCCA et al., 2004).

3. Long-period Seismic Signals

Considering the force drop during a landslide it is proportional to the amplitude of the seismic waves whereas the gravitation is the driving force, thus enabling one to calculate an absolute value of the frictional force (BRODSKY E. E. et al., 2003).

Furthermore, standard spectrogram/sonogram analysis is a useful tool for detecting mass movements such as avalanches (SURINACH et al., 2005).

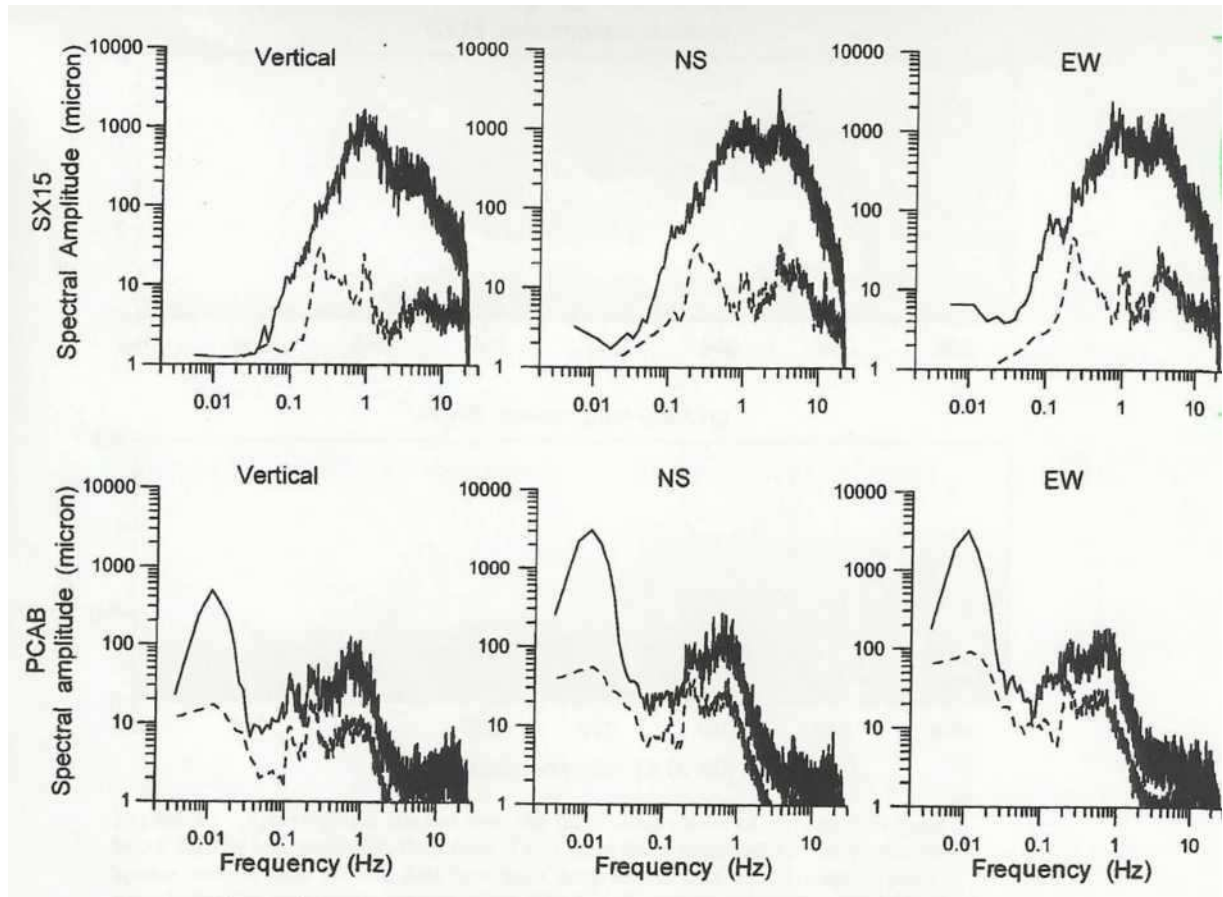


Figure 3-4 Examples of amplitude spectra of seismograms produced by landslides. The spectra relate to the seismograms shown in Figure 3-3. Only continuous lines are of interest as they represent the landslide.

3.2 Other Mass Movements

3.2.1 Long-Period Volcano Seismicity

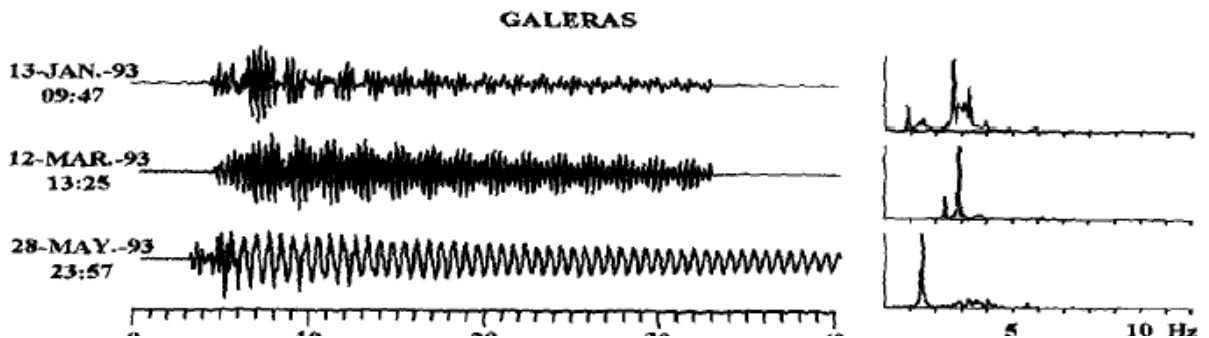
Referring to the article "Prediction of Volcanic Activity" from wikipedia.org (http://en.wikipedia.org/wiki/Prediction_of_volcanic_activity, last access 21/03/2012) volcanic

3. Long-period Seismic Signals

seismicity can be separated in three major forms, which are short-period earthquakes, long-period earthquakes and harmonic tremor. In literature, there are many different notations for these three characteristic endterms of seismic signatures of volcanic activity as for example CHOUEY (1996) denotes them as tremor, long-period events and volcano-tectonic earthquakes. He also states that the origin of the volcanic seismicity is divided into two distinct types of the process. Tremors and long-period events originate in the fluid while the volcanic earthquakes have their source in the solid rock. Spectral analyses are needed to determine the differences of the source properties.

DIEGO et al. (1996) describes these long-period events as unusual low-frequency seismic signals and states that these signals have been observed at several volcanoes under different conditions: short-term precursor, after eruption, during seismic swarms and during quiescence. Referring to CHOUEY (1996) typical sources for long-period events are volumetric modes of deformation. Due to unsteady mass transport within the magma, a pressure fluctuation occurs. This is most likely to happen at the place of interaction of the groundwater system and the magma conduit.

While the duration of small tectonic earthquakes can be similar to long-period events, there is a significant difference in the frequency range and the harmonic signature. Typical for these events is a high-frequency onset that can be best recognized when a station is placed near the source. Following this onset is a harmonic waveform that is characterized by one or up to several dominant periods (typically 0.2-2 seconds). CHOUEY (1996) also suggests that it is easier to recognize long-period seismicity when comparing it with other events, in this case volcano driven tectonic earthquakes.



d their respective

DIEGO et al. (1996) gives some examples for these unusual low-frequency seismic signals with their respective spectra. They call these events "tornillos", which is Spanish for screw, because the shape of the seismic signal resembles that. Figure 3-5 shows one of these examples for the Galeras volcano in Colombia and the according spectra with sharp peaks in the lower frequency range.

3. Long-period Seismic Signals

3.2.2 Rockfall Induced Seismic Signals

To describe and quantify rockfall induced seismic signals VILAJOSANA et al. (2008) performed time series, time-frequency evolution and particle motion analysis as well as seismic energy estimation. They had their focus on rockfall events with volumes ranging between 1 and 10^3 m^3 and, therefore, obtained their data from an experiment with two seismic stations located below the rock wall at the level of the rock impact about 110 m (station A) and 50 m (station B) sideways aided by a video-documentation (Figure 3-6). Their investigations had three aims: detection of rockfall events, localization and determination of the size. Similar to seismic signals of landslides, they detected an irregular envelope with several energetic pulses in the time series analysis. Figure 3-6 shows the seismogram of the vertical component of the two stations deployed for the experiment whereby the numbers indicate the beginning of a new wave packet.

Concerning the detection of rockfall events it can be said that the impact of a rock is reflected in the seismogram with strong energy attenuation whereas on contrary the mass flow seismic signal shows a gradual increase in spectral amplitudes.

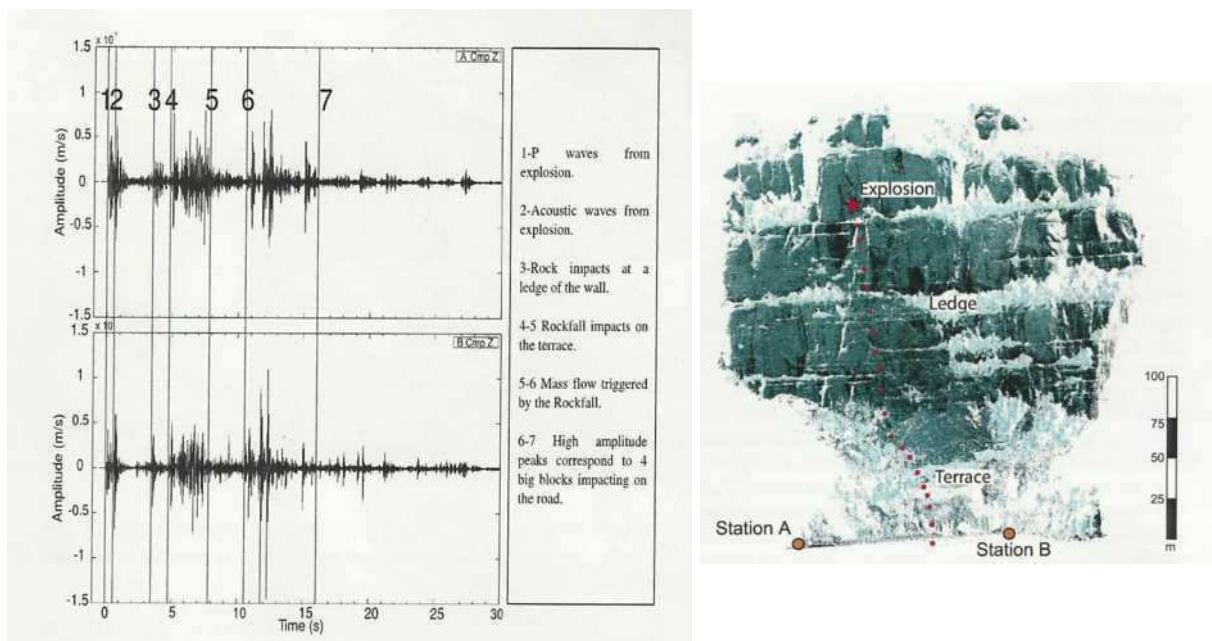
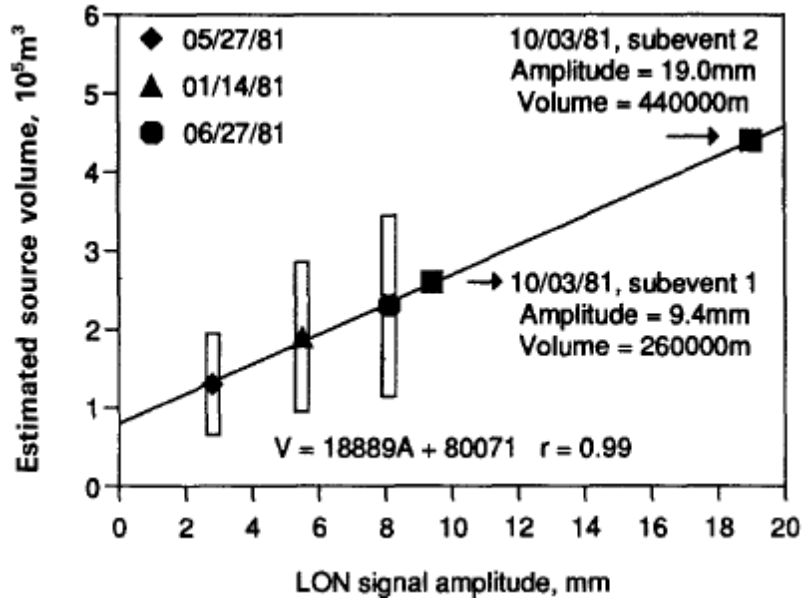


Figure 3-6 Seismograms of the vertical component with identification of different wave packets on the left side. Right: Location of seismic station A and B.

Contrary to VILAJOSANA et al. (2008) there are some studies on seismic signals generated by large rockfall events from 10^4 to 10^7 m^3 (NORRIS, 1994) which allows a useful record of the data far off from the source location. In addition, NORRIS (1994) compares the maximum signal amplitude with the estimated source volumes of the respective rockfall. He concludes that the signal amplitude

3. Long-period Seismic Signals

varies linearly with the source volume with the following limitation: The rockfalls compared have to originate as large-block failures that descend similar shaped slopes (Figure 3-7).



ock rockfalls in
e, Washington

3.2.3 Seismic Signals from Rock/Snow/Ice Avalanches

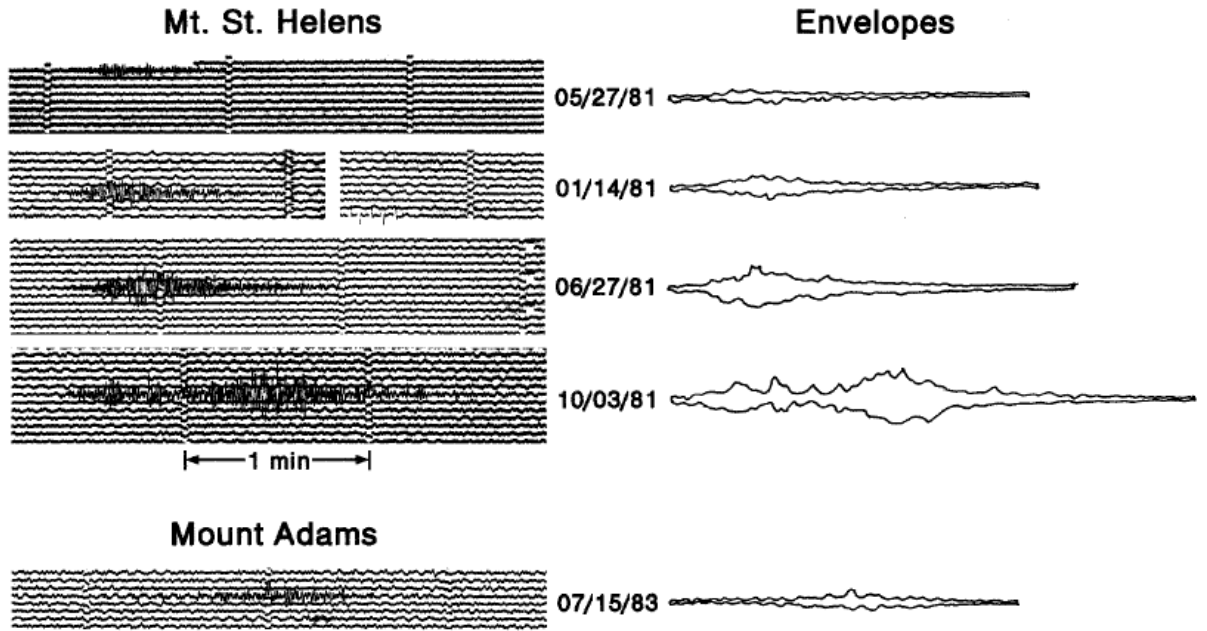
Based on an article from CAPLAN-AUERBACH and HUGGEL (2007) seismic signals associated with avalanches are discussed in the following.

The first characteristic of such a seismogram is its increasing amplitude with time. This can be explained by entraining friable rock along the travel path which leads to a higher density of avalanche material. Due to the greater load, a larger force is imposed on the ground. Extreme high signal amplitudes are assumed to be an effect of the change in the path or slope, which transmits more energy to the ground. Additionally, the maximum amplitude is low relatively to duration (NORRIS, 1994).

Also typically for avalanches – the same as for other mass movements – is the spectral content (1-8 Hz) as well as the so called spindle shape of the seismogram with an emergent onset. NORRIS (1994) analyzes the envelopes of vertical components and describes them as a teardrop or spindle-shaped envelope for both avalanches and rockfalls (Figure 3-8). The first three envelopes, referring to rockfalls, also show that the maximum amplitude occurs 25 to 30 seconds after the onset and the durations only vary within 6 seconds.

3. Long-period Seismic Signals

Rockfall and Avalanche Seismograms
(LON-SPNS Component)



at St. Helens on top, one

3. Long-period Seismic Signals

4 Mass movements near Bad Ischl

4.1 Geological Overview

Geologically the area of interest is situated in the central part of the Northern Calcareous Alps (NCA), which belongs to the Upper East Alpine unit (FAUPL, 2003) (Figure 4-1). It is the uppermost tectonic element of the Eastern Alps spanning 500 km from the Rhine Valley to the Vienna Basin (FRISCH and GAWLICK, 2002) and about 50 km from North to South.

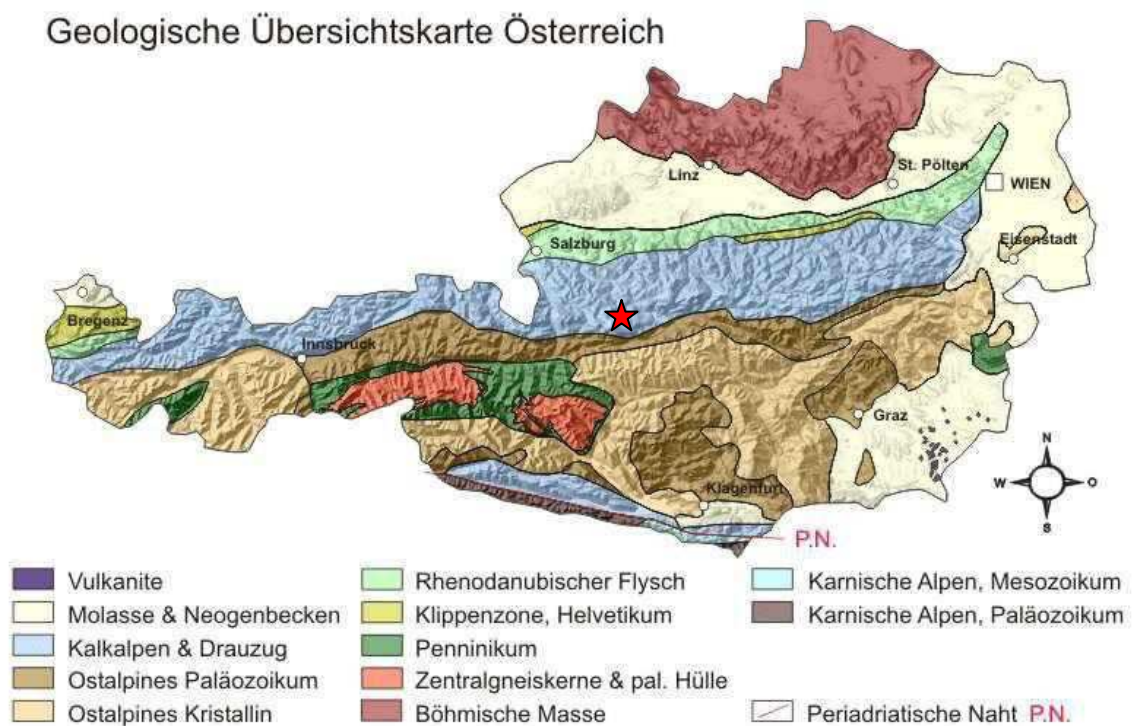


Figure 4-1 Geological map of Austria. The Northern Calcareous Alps (NCA) are illustrated in blue. The red asterisk marks the town of Bad Ischl.

The permomesozoic stratigraphic sequence consists predominantly of carbonate-dominated Triassic sediments (starting in Anis with the Wetterstein formation and ending with the Dachstein limestone in Rhätium) which can achieve kilometres of thickness. They were originally deposited several 100 km further south at a passive continental margin that was subjected to subsidence rates due to rifting of the Tethys Ocean (e.g. HAAS et al., 1995; MANDL, 2000).

4. Mass movements near Bad Ischl

The general outline of the regional geology in the area of interest is very well given in the diploma thesis of EHRET (2002) serving as a basis for the following paragraphs.

The sedimentation of the NCA began at the end of the Palaeozoic. Onshore clastic material of the Permian Rotliegendes was deposited, and from the late Permian onwards it was overlain by fine-grained and evaporate sediments due to a shallow subtidal marginal marine depositional environment (SPÖTL, 1987). During the dehydration stage, a salt pan developed and thus evaporitic sequences arose. These are the evaporates from the Alpine Haselgebirge, also known as East Alpine Salinar. It generally consists of components of shales, sandstones, anhydrites, carbonates and occasional magmatic rocks within a clay-rich evaporitic matrix.

In Early Triassic, terrigenous, fine-grained sediments deposited, which are known as the Werfener Schichten. Due to a continually transgression, this terrigenous impact decreased while at the same time the content of carbonate in the sediment increased. Thus the previously mentioned Triassic carbonate sediments were deposited, whereas a differentiation in terms of the facies took place. Three main facies domains developed (Figure 4-2): the Hauptdolomit Facies (lagoonal sediments), the Dachstein Limestone Facies (a carbonate platform with reefs and lagoons) and the Hallstatt Facies (connection of the shelf with the open sea) (e.g. HAAS et al., 1995)

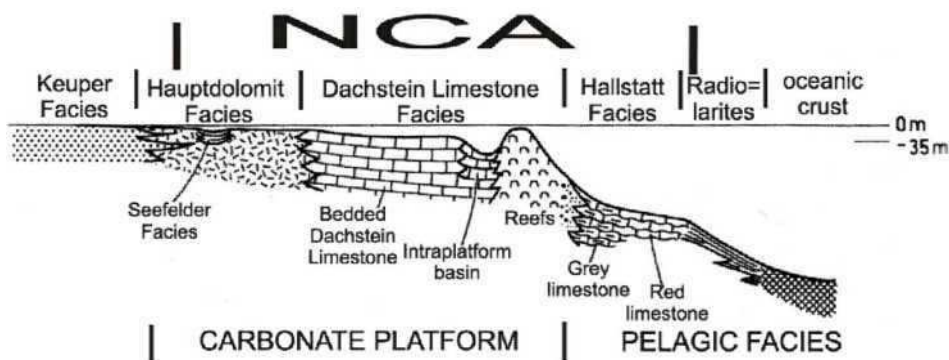


Figure 4-2 Major facies zones on the passive continental margin during Triassic (HAAS et al., 1995).

Of course, the geology of the region of interest is a lot more complex and due to the alpine orogeny not fully reconstructed, but the above mentioned stratigraphic information will suffice for discussing in general the situation of mass movements in the surrounding of Bad Ischl.

4.2 Geotechnical conditions

The main focus has to be laid on the interaction between the ductile evaporitic footwall, which is the Alpine Haselgebirge, and the overlying brittle reacting carbonates. This geotechnical constellation known as "Hart auf Weich" is a widespread phenomenon of slope instability in this region (MOSER et

4. Mass movements near Bad Ischl

al., 2003). Very briefly the system can be explained as follows: POISEL and EPPENSTEINER (1989) propose that the creeping and sliding of the basement cause the brittle cap-rock to become unstable. The brittle cap-rocks resting upon a weak ductile reacting basement cause block toppling and block sliding of the pinnacles at the edge of the hanging wall. Also the ductile sequence is more susceptible to water through the cracks and gaps in the overlying rock and therefore for weathering and erosion, which leads to a self-strengthening effect.

MOSER et al. (2003) state that there are two main hazards, namely the potential rockfall hazard at the edge of the brittle cap-rocks as well as earth flows and debris flows in the weak sequences in consequence of mobilisation of the ductile rock masses.

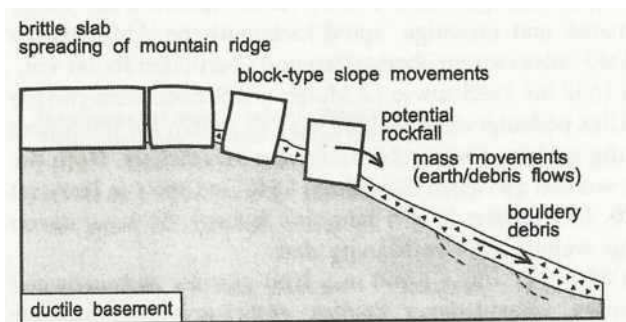


Figure 4-3 Brittle cap-rock overlying a thick ductile basement.

4.3 Correlation of Seismological Data and Geology

After this brief introduction to the regional geology and the geotechnical situation of the investigated area, we proceed to concentrate on a direct link between the above mentioned information and the seismological long-period data set. For that purpose the epicentres of the LPEs are plotted on a geological map (Figure 4-4). It is necessary to combine two geological map sheets provided by the Geological Survey of Austria (GBA): map 95 SANKT WOLFGANG im Salzkammergut (1:50 000) and map 96 BAD ISCHL (1:50 000). For a closer consideration one can find the maps including the legends online at www.geologie.ac.at.

As already mentioned, three main clusters of events can be defined with the help of event list provided by ZAMG. In Figure 4-4 these three clusters are highlighted in different colours for a better visualization. In the region of Bad Ischl and Bad Goisern, the events are represented by green circles, for the cluster northwest of Bad Aussee red circles are chosen, whereas the LPEs of the region of Hallstatt are in yellow. Considering the locating error, these clusters can be associated with three regions of active mass movements (pers. comm. Lotter). Examples are discussed on the following pages in detail.

Some events are not represented on the map as - from a personal point of view - they do not belong to any cluster or do not define an additional region of higher mass movement activity (Table 4-1). But

4. Mass movements near Bad Ischl

this definitely does not identify them as earthquakes; it only means that these events do not correlate with the three clusters mentioned above. Thus they will not be discussed anymore in this chapter, because no general correlation can be made with a region high in landslide hazards as defined by the GBA.

Table 4-1 List of remaining events.

date yyyy mm dd	focal time hh mm ss.s	latitude [°]	longitude [°]	magnitude	epicenter
2000 11 09	15 33 04.2	47.82	13.72	1.7	Ebensee
2002 11 18	22 16 53.2	47.79	13.65	2.0	Höllengebirge
2006 09 26	10 08 37.2	47.82	13.74	1.9	Ebensee
2006 11 24	00 33 21.1	47.71	13.51	1.7	Strobl
2007 03 18	13 27 05.0	47.58	13.53	1.4	Gosau
2008 01 22	20 00 42.2	47.61	13.54	1.4	Gosau
2010 05 03	09 14 21.7	47.67	13.43	2.2	Postalm
2010 09 18	22 13 20.2	47.79	13.84	1.7	Offensee

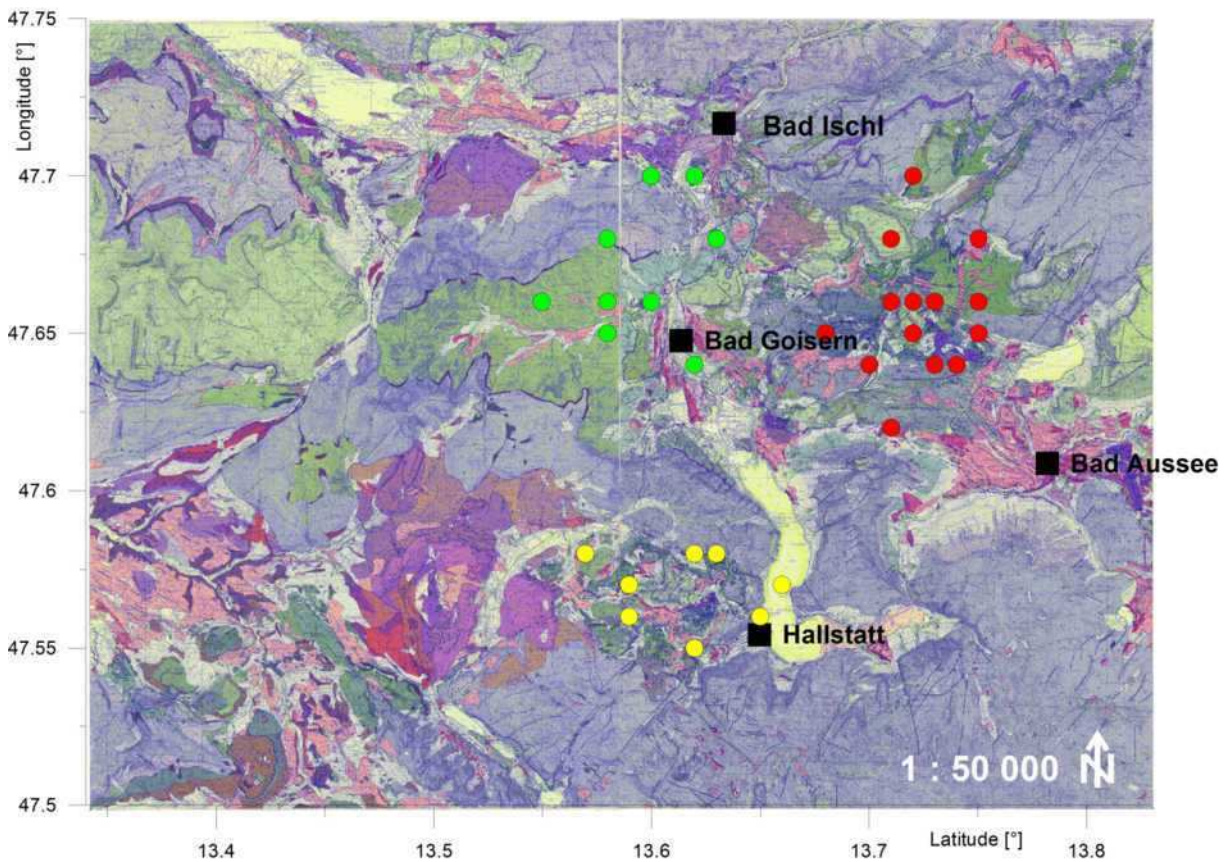


Figure 4-4 Geological map of the area of interest. Map sheets 95 and 96 of the GBA are combined and towns (black squares), events (coloured circles), north arrow and scale are added.

4.3.1 LPEs near Hallstatt

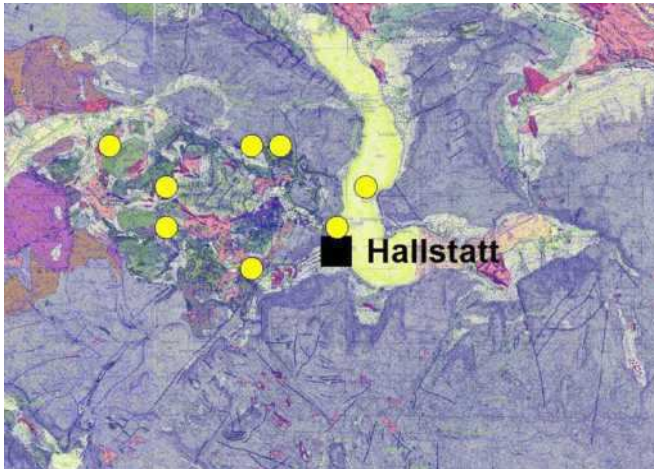


Figure 4-5 Detail from Figure 4-4.

First of all, the region around Hallstatt will be discussed, as the correlation with geological and geotechnical information is the best considering the three defined clusters. As can be clearly seen in the map, the LPEs plot in or around a region of different geological units (featured by a greater variety of colours) surrounded by the compact carbonates of the Dachstein massif (grey-violet colour). Thus one tends to conclude that west of Hallstatt a geological active region is located and therefore mass movements are more likely to occur.

For the purpose of discussing this region in greater detail the diploma thesis of EHRET (2002) serves as a good example. EHRET (2002) carried out a geotechnical investigation of the mass movements between Hallstatt and Plassen; Plassen is the remarkable massif west of Hallstatt reaching an altitude of 1954 metres above sea level.

In his diploma thesis he distinguishes three major geotechnical units (Figure 4-6):

- Greatly influenced part of mass movements from the geotechnical system “Hart auf Weich” with a brittle cap-rock and a ductile basement (e.g. Plassen)
- Regions of mass movements in changeable hard rock, which is either a halite-clay-stone, alternate layers of limestone and marl or sandstone and mudstone.
- Stable region with minimal mass movement activity.

As in a previous chapter the geotechnical situation of the system “Hart auf Weich” was mentioned, the region of Plassen is discussed now in greater detail. The more than 700 metres massive brittle cap-rock is located on an elastic basement. For the most part the weak basement is build up by the Alpine Haselgebirge. Due to drilling it is known that the formation beneath the “Plassen” reaches at least down to the level of Lake Hallstatt at 508 metres above sea level.

The biggest and most obvious mass movements can be found on the southeastern part of the mountain in the direction of Hallstatt, where the Alpine Haselgebirge reaches its maximum distance from the summit of “Plassen”. Thus distinct extension structures and the formation of slabs take place. EHRET (2002) also describes the formation of rock towers in the region of the Lahngangkogel, which is strongly linked to the occurrence of recent rockfalls. As an example, in Figure 4-8 a convergence of the rock tower and the rock wall was measured. In the years 1994 to 1998 the two

4. Mass movements near Bad Ischl

masses separated from each other by 10 mm (LOTTER, 2001). He made some great illustrations that show the mechanism of the mass movements and verified it with photos.

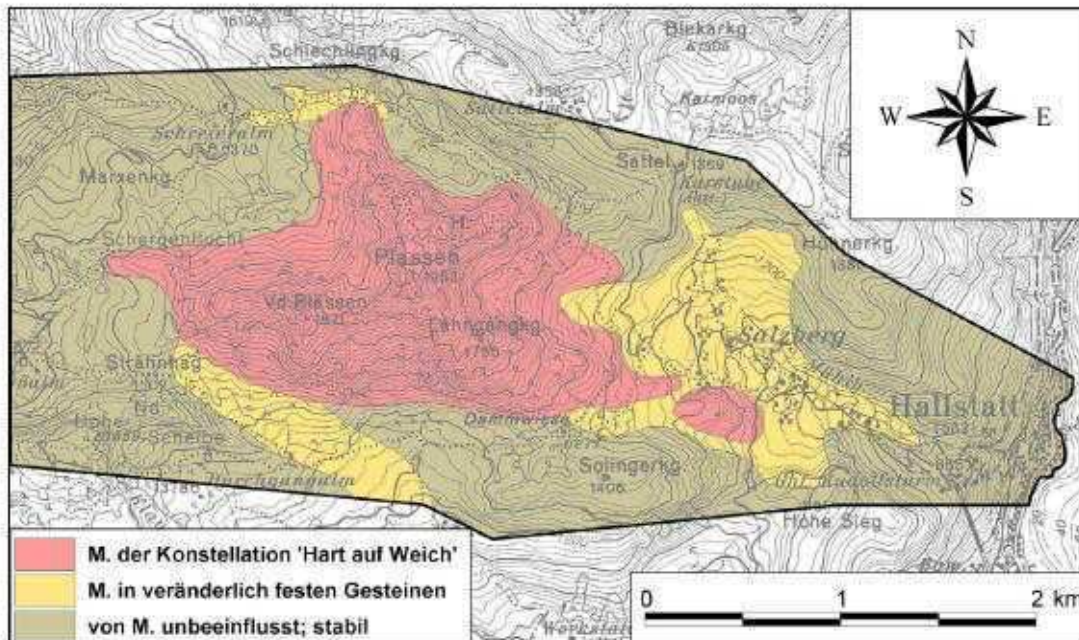


Figure 4-6 Segmentation of the area of work into regions with similar geotechnical properties (red: mass movements “Hart auf Weich“, yellow: mass movements in varying hard rock, green: stable region) from EHRET (2002).

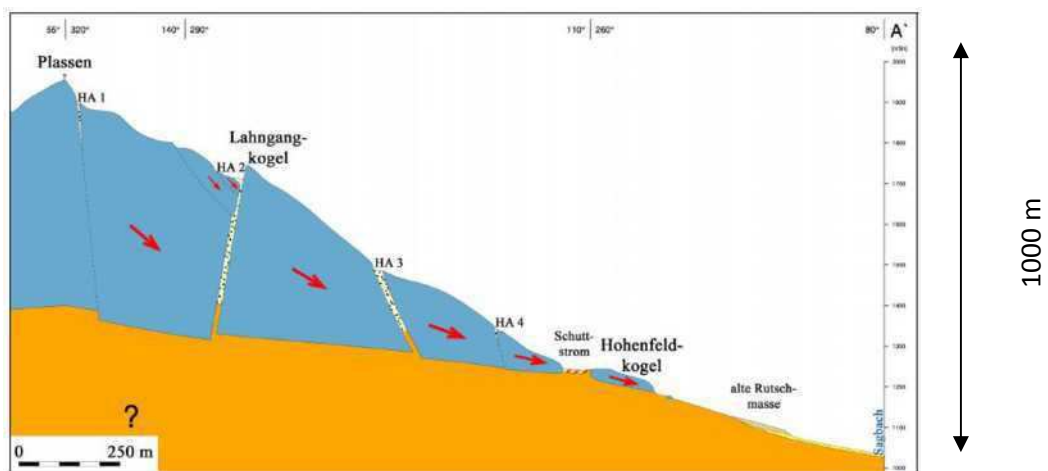


Figure 4-7 Geotechnical profile through the “Plassen” – Lahngangkogel – Hohenfeldkogel – Sagbach. The red arrows indicate the direction of movement (EHRET, 2002).

4. Mass movements near Bad Ischl



Figure 4-8 South eastern side of the “Plassen” with the Lahngangkogel-slab and important edges on the left side. Right: Rock tower with a volume of 5 000 m³ from EHRET (2002).

EHRET (2002) discussed many more phenomena (e.g. slides etc.) in the context of mass movements to the west of Hallstatt. He also mentions previous divergence measurements and carried out some by himself at different locations. He remeasured the distances about two month later and displacements -0.35 and +2.97 mm were observed. From the greatest relative displacements an annual movement of 16.6 mm was concluded.

In addition to the diploma thesis of EHRET (2002) there is a great number of literature that deals with the mass movements in the region of “Plassen”, as this has been an area of interest for the last 200 years. Various publications focus on the local geology (MANDL (1984, 2000), TOLLMANN (1964, 1976, 1982, 1985) and many more) while others concentrate on geotechnical data (HAUSWIRTH and SCHEIDEGGER (1988), LOTTER (2001), MOSER and CZURDA (1999) etc.).

All the above mentioned information indicates clearly mass movements in this area of the defined cluster west of Hallstatt. Thus, it is most likely that the LPEs generated next to Hallstatt can be attributed to those rock movements.

4. Mass movements near Bad Ischl

4.3.2 LPEs in the region between Bad Goisern and Bad Ischl

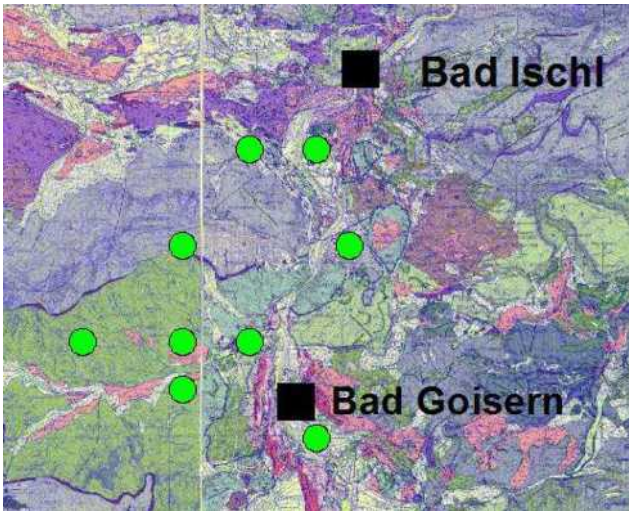


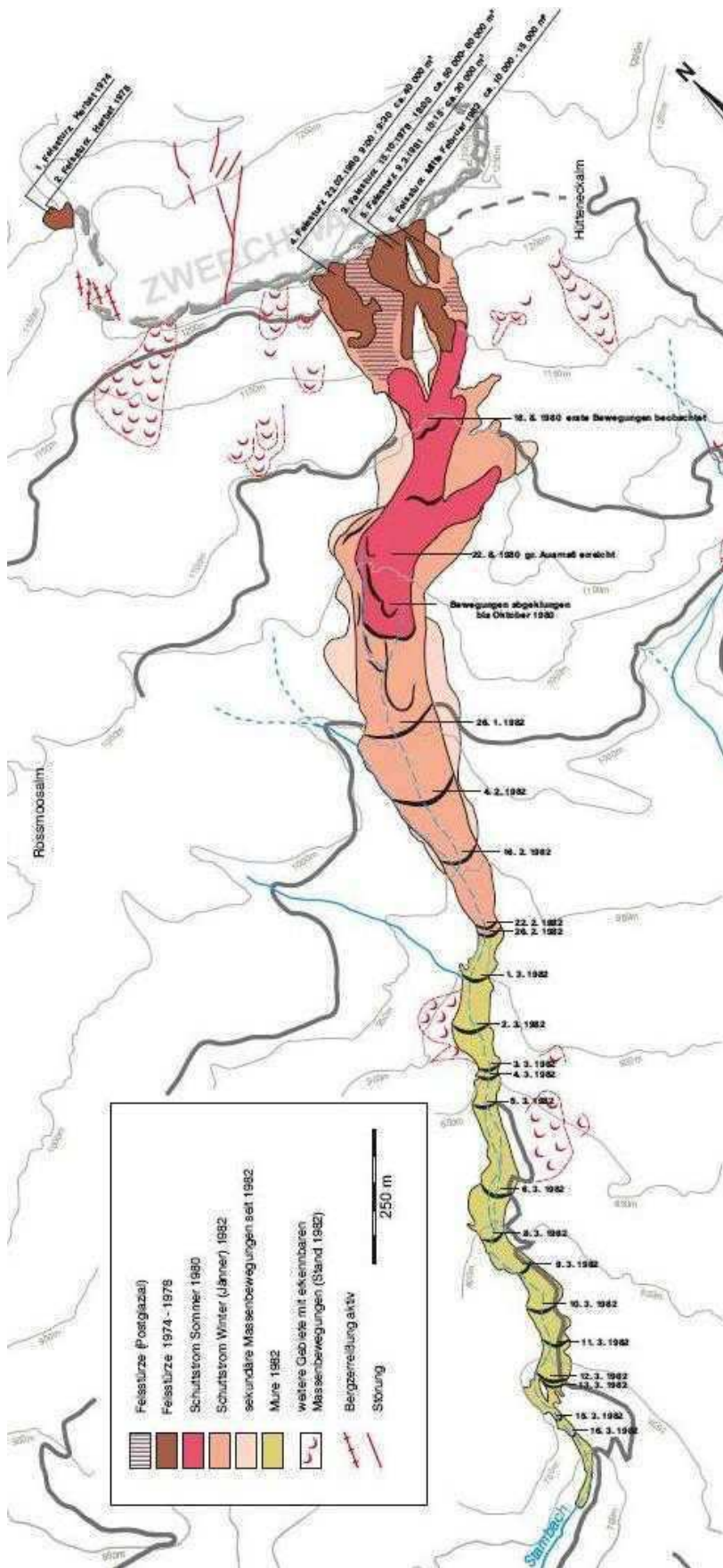
Figure 4-9 Detail from Figure 4-4.

Considering the correlation of geology and geotechnical information, the epicentres of the LPEs located by ZAMG in the region between Bad Goisern and Bad Ischl obviously do not form such a distinct cluster as the LPEs of Hallstatt, but still a great number of mass movements were documented in literature.

One region worth mentioning is the Stambach catchment, which starts at the Zwerchwand (1326 m.a.s.l) and ends at the river Traun (525 m.a.s.l). VAN DEN HAM (2006) describes the Stambach slope as a dormant earth flow. It was

active in 1982 for the last time and radiocarbon dating on organic material proves that it was at least three times activated since the Pleistocene (ROHN et al., 2004). Again the characteristic geology is marls and salt clays overlain by large and thick rigid slabs of limestone. VAN DEN HAM (2006) describes the mechanism at the Stambach slope as follows: Due to the uphill propagation source area of the creeping slope, namely the underlying Alpine Haselgebirge, the base of the 80 m high vertical rock face, namely Zwerchwand, is destabilised. Thus rock pillars break down onto the upper part of the slope and trigger the earth flow as a consequence of greater pore water pressures. VAN DEN HAM (2006) says that the last rock pillar had a volume of about 30 000 m³ while the next one is already toppling outwards the rock face. Its volume is estimated to be approximately 20 000 m³ currently moving downhill with around 12 mm per year. (ROHN, 1991)

4. Mass movements near Bad Ischl



Of course, there are more detailed analyses of the mechanism of activation (e.g. HUTCHINSON and BHANDARI, 1971) and other source areas (e.g. VAN DER HAM, 2006), but this general overview appears to be sufficient to prove the presence of mass movements in the region of interest. Thus it is likely that the LPEs are generated by some kind of mass movement, e.g. earth flows.

Figure 4-10 Temporal sequence of the mass movements (rockfalls from the Zwerchwand and earth flow in the Stambach) south of the Zwerchwand. The different colours indicate different time periods and the solid black curves show the position and date of reactivation (provided by GBA).

4.3.3 LPEs northwest of Bad Aussee

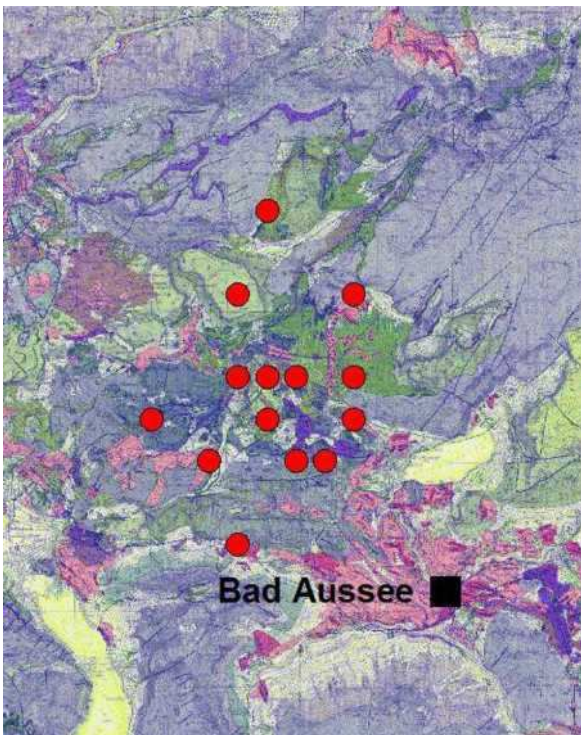


Figure 4-11 Detail from Figure 4-4.

Also the LPEs in the region northwest of Bad Aussee form a cluster. As an example the area of the “Sandling” is chosen.

To explain the situation at “Sandling” in detail the term lateral spreading has to be introduced as it is the main mechanism triggering mass movements there, possibly similar to the system “Hart auf Weich”. Additionally, the individual slabs do not move as a unit but the movements follow different directions. As they move further on, they can break up into smaller units, which disperse. A vertical subsidence of the separate slabs can then be observed together with bulging of the elastic base (DÖLLMANN, 2000). Figure 4-12 visualizes the term of lateral spreading.

RÖNNAU (2001) states, that “Sandling” is built up of the Allgäu formation, which consists of marly and siliceous series, and the previously described Alpine Haselgebirge covered by Plassenkalk (like in the region west of Hallstatt). After the Würm glaciations excessively steep slopes of Allgäu formation and Alpine Haselgebirge could not bear the material of the massive limestone slabs anymore and became unstable. The overlain limy slab broke up into individual units (Figure 4-13). DÖLLMANN (2000) confirmed the slab movement with the help of a GPS measurement network.

RÖNNAU (2001) states, that “Sandling” is built up of the Allgäu formation, which consists of marly and siliceous series, and the

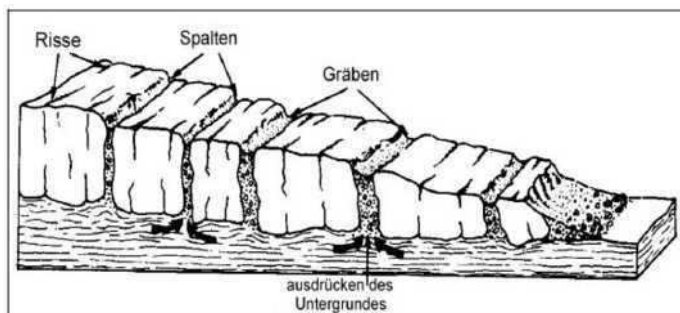
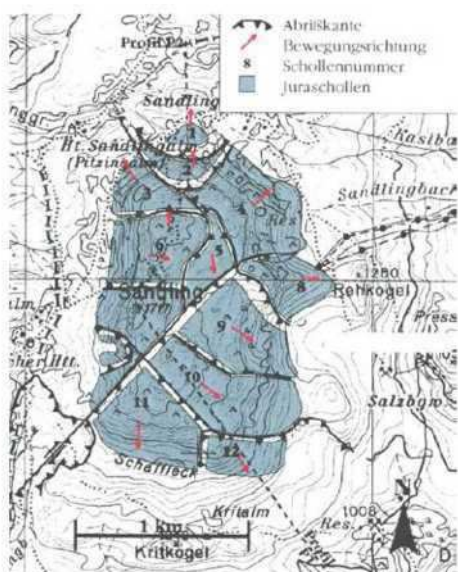


Figure 4-12 Lateral spreading in theory. (RÖNNAU, 2001).

Figure 4-13 Limy slabs broken into several separate units (RÖNNAU, 2001).

4. Mass movements near Bad Ischl

Both DÖLLMANN (2000) and SCHNEIDER (1998) describe a mass movement at the south side of "Sandling". HÖCHERL (1991) concentrates in his master thesis among other issues on the approximately 3.7 km long and 250 m wide "Sandling" earth flow activated by the collapse of a nearly 200 m high rock tower next to the western wall of the "Sandling" in September 1920. The result was an earth flow with a mean velocity of 45 m/h ending 33 days later. HOECHERL (1991) also correlated the event with available precipitation data. He mentions also other active earth flows in the proximity of the "Sandling".

Again this information proves the existence of a great number of mass movements in the region of interest. It verifies that the most probable reason for the LPEs lies in some kind of mass moving within few 100 metres from surface.

4. Mass movements near Bad Ischl

5 Data Processing and Quantification

All time series, as mentioned previously, are provided by ZAMG in the GSE2.1 format. For the essential processing steps the Seismic Analysis Code Software (SAC) is used. As SAC cannot read GSE2.1 data a conversion tool is necessary. `codeco3`, available on www.seismo.ethz.ch, meets the necessary demands for waveform conversion as it both supports GSE formats as well as SAC-ASCII.

5.1 Seismic Analysis Code (SAC)

SAC was downloaded from www.iris.edu (last access 01/04/2012). All necessary information about using SAC e.g. commands, formats or error messages are also listed on this website.

For basic processing steps, such as Fourier transforms or filtering, the SAC-ASCII data is read from disk and converted with a simple command into the SAC binary format. Afterwards the data can be reconverted in a SAC-ASCII format and exported, if necessary, for usage in other programs for e.g. visualisation.

All data in the following chapters was processed with a high pass filter with a corner frequency of 0.1 Hz to get rid of the baseline offset. Unless otherwise stated, a band pass filter from 0.5 to 35 Hz is applied additionally.

It is also necessary to apply a distance correction to make the traces better comparable. On the average the distance between an event and the seismological station MOA is approximately 50 km whereas about 69 km separate KBA and the epicentre of an LPE. Thus, each trace “ s_i ” is multiplied by a distance (x) dependent correction term as formula (3.1) features:

$$s_i = 1.66 * \log(x) \quad (3.1)$$

The factor “1.66” was found to compensate sufficiently the distance-dependent amplitude decay in the Alps (pers. comm. Lenhardt). For any signal processing steps including the Fourier transform a more complex correction term has to be applied. This is related to the effects of attenuation, which has to be considered additionally. Formula (3.2) shows the exact term (LAY and WALLACE, 1995)

$$S_i = a_i * \exp\left(-\pi f \frac{x}{Q_p v_p}\right) \quad (3.2)$$

5. Data Processing and Quantification

" Q_p " is the quality factor that is approximated by a constant value of 400, the propagation velocity " v_p " is chosen 5700 m/s (pers. comm. Lenhardt). The distance " x " is also given in metres. " f " refers to the frequency, " a_i " is the respective amplitude at each frequency and " S_i " is then the distance corrected amplitude value. As a working hypothesis, the source can be mainly treated as impact event and thus the values for the quality factor " Q_p " and the velocity " v_p " concern P waves.

Any further processing steps will be given in the respective chapters.

5.2 Noise

First of all, a detailed consideration of the noise at the two stations MOA and KBA shall improve the comparison of data measured at the two spatially divided locations. As already mentioned in chapter 2, station KBA is located at a dam toe and is therefore suspected to experience a higher noise level due to anthropogenic noise due to operations at the reservoir.

To rule out the possibility that a comparison is not useful due to clearly diverse noise levels, the noise of each trace is analyzed 10 seconds prior to the P wave arrive. Afterwards the discrete Fourier transform (e.g. SCHERBAUM, 2001), is applied and the sum of each spectra is calculated. The comparison of noise follows

$$N_r = \frac{\sum a_i}{\sum b_i} \quad (3.3)$$

with “ a_i ” referring to the amplitude values of noise at station MOA and “ b_i ” at station KBA respectively.

Figure 5-1 shows the results of “ N_r ” as a function of time. A 2nd order polynomial fit is applied to all three components to get a good impression of the daily trend. At night, there is a noise minimum at station MOA, while at midday the noise level is higher. As station MOA is located less than 10 kilometres away from a highway, anthropogenic causes are clearly the source of noise. In addition, mining activity takes place in its close vicinity. Contrary, at station KBA the main noise source is the hydro power plant itself. The least variation takes place at the Z-component, while the east and north components both show a similar trend with an overall higher noise level.

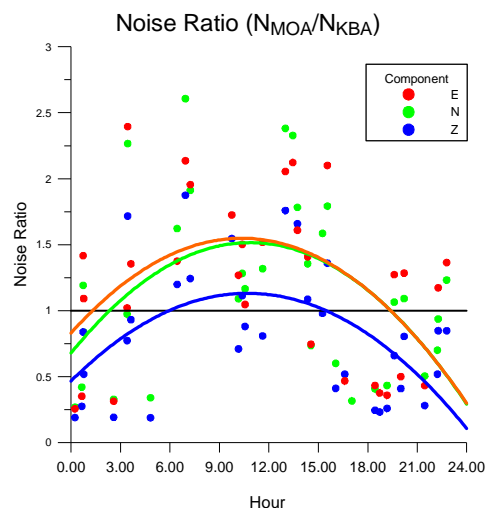


Figure 5-1 Noise ratio of data recorded at station MOA and KBA for each event in terms of magnitude. Red dots represent component E, green ones N and blue ones Z. The black line refers to values of the same noise level.

5.3 Useful Signal

Another aspect has to be considered before starting the actual evaluation: the length of the time window for analyzing an event. For that reason two time windows of ten seconds are chosen, whereby one of them only consists of noise. After applying the discrete Fourier transform the sum of the amplitudes is calculated. The quotient “ S_U ” of these two sums serves as an indicator of the signal quality (pers. comm. Lenhardt).

$$S_U = \frac{\sum a_i}{\sum n_i} \tag{3.4}$$

“ a_i ” refers to the amplitude in the defined time window that is suspected of still containing a useful signal whereas “ n_i ” represents the same for the noise.

For first considerations a time window starting 60 seconds after the P wave arrival is chosen. A limit of 2.0 for “ S_U ” is taken to verify the content of useful signal. Figure 5-2 shows the results for both stations.

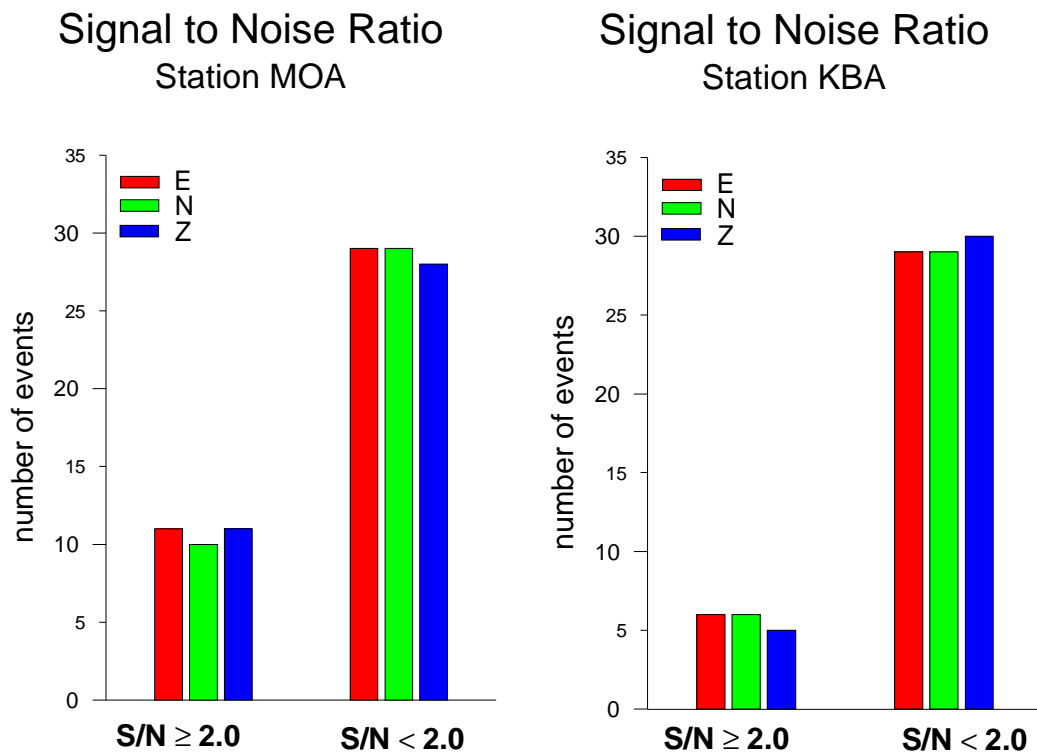


Figure 5-2 Signal to Noise ratio implying the existence of useful signal in a time window starting 60 seconds after the P arrival lasting 10 seconds. Results for station MOA are shown on the left side and for station KBA on the right side. All three components are represented.

5. Data Processing and Quantification

Obviously the traces at station MOA contain more information than the ones at station KBA 60 seconds after the P arrival. While at the most 20 percent of the traces at KBA still include information about an event, the ones at station MOA add up to nearly 40 percent at maximum. With exception of one very distinctive value (10th of August 2011) all corresponding magnitudes are 2.3 or greater.

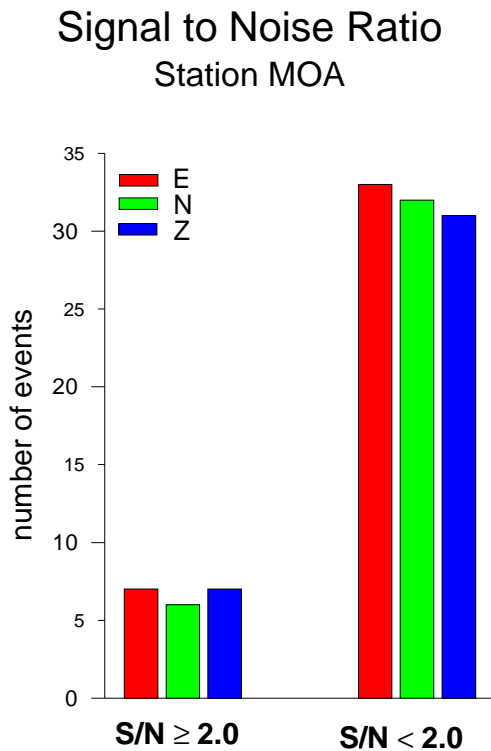


Figure 5-3 Signal to Noise Ratio implying the existence of useful signal in a time window starting 70 seconds after the P arrival lasting 10 seconds. The data represents values at station MOA for all three components

Because there is still a great amount of useful signal in the data at station MOA, the processing step is repeated for a time window of ten seconds starting 70 seconds after the P arrival to define the ultimate length of the traces for the further analysis dealt with in this chapter.

The amount of the useful signal at station MOA is considerably decreased to about 20 percent (Figure 5-3). Therefore, the ultimate length of the traces for further processing amounts to 80 seconds in total. Generally speaking, the magnitude of the events still containing useful signal is greater than 2.7 not taking into account the event of the 3rd of May 2008, which had a magnitude of 2.5 and is still represented in component Z with a ratio of 2.11.

An approach for the interpretation might be the different travel paths of the waves through the Alps. As station MOA is located along and accordingly approximately east of Bad Ischl, the waves travel through different geological layers when compared with KBA, which is located south of Bad Ischl. Therefore, the attenuation and the scattering of the seismic waves are certainly different.

It is also worth mentioning that no significant differences in the loss of signal concerning the three components of the seismometer arise.

To study the horizontal excitation the sum of the amplitudes in the frequency spectra of the E-component is divided by the N-component to see whether one component contains more information than the other.

A time window of 80 seconds starting at the P arrival was used for analysis. The spectral content is calculated with the help of the discrete Fourier transform. Then the sum of the amplitudes is calculated whereby values for frequencies smaller than 0.1 Hz and greater than 40 Hz are neglected. The ratio "SR" is then defined as the ratio of the two sums.

5. Data Processing and Quantification

Figure 5-4 shows the results for SR for both stations, which scatter around 1.0. In some cases the amplitudes on the E-component are larger while in other cases the ones at component N are more pronounced. For example the amplitudes on the E-component are greater at station MOA whereas they are smaller at station KBA for the event on the 4th of May 1999. The same applies to the first event in 2009 (6th of January).

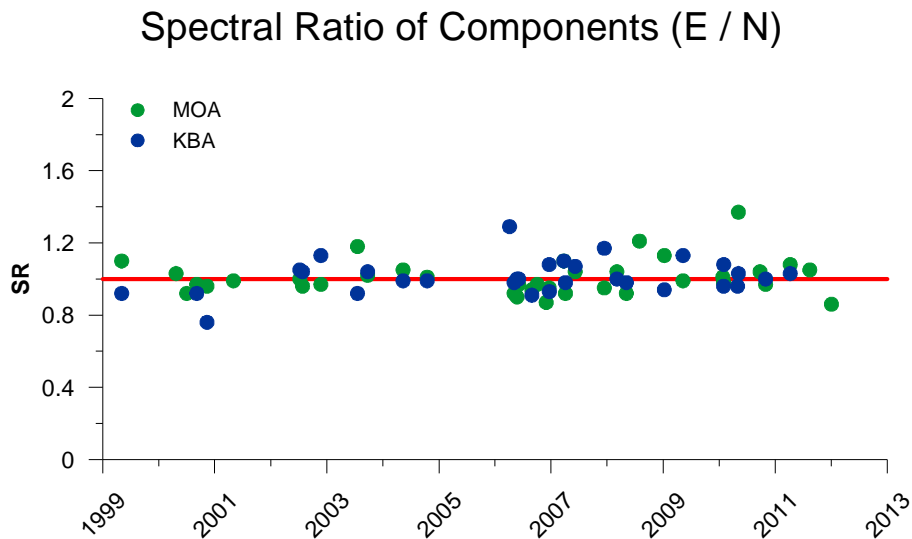


Figure 5-4 Ratio of the sum of the amplitudes of the frequency spectra of component E and N for station MOA represented by green dots and KBA by blue ones. The results are shown in terms of the date. The red line visualizes the ratio of equal sums.

Also worth mentioning is the noticeable increase in data from 2006 onwards. This is due to the enlargement of the seismological network in Austria, which made it possible to locate more events.

5.4 Spectral content

An approach to determine whether a tremor is a natural earthquake or not, is to analyze its spectral content. It is an established method to distinguish event types (e.g. ALLMANN et al., 2008).

For calculations the discrete Fourier transform is applied to the data with SAC. For this method the band pass filter from 0.5 to 35 Hz is not applied.

On the next pages the amplitude spectra of the LPEs (Figure 5-5) and the earthquakes (Figure 5-6) are plotted. Each figure shows the results from the two stations; MOA on the left side and KBA on the right side, for each component with E on top, N in the middle and Z below. Each colour represents one event, outliers are discussed separately.

At first, it can be seen that there is a peak at approximately 0.1 Hz. This signal is not unique to LPEs as it is also existent in the spectra of earthquakes. It is known as microseism (LAY and WALLACE, 1995).

To be able to compare characteristics of the spectral content of earthquakes and LPEs, two events are selected. Figure 5-7 emphasizes the diverse characteristics of the spectral content. On the one side LPEs have a maximum between 0.5 and 3 Hz while they lack at frequencies greater than 5 Hz, which are typical for the earthquakes. Thus, there are two main differences that can be used to separate those two types of events.

5. Data Processing and Quantification

AMPLITUDE SPECTRA FOR LPEs

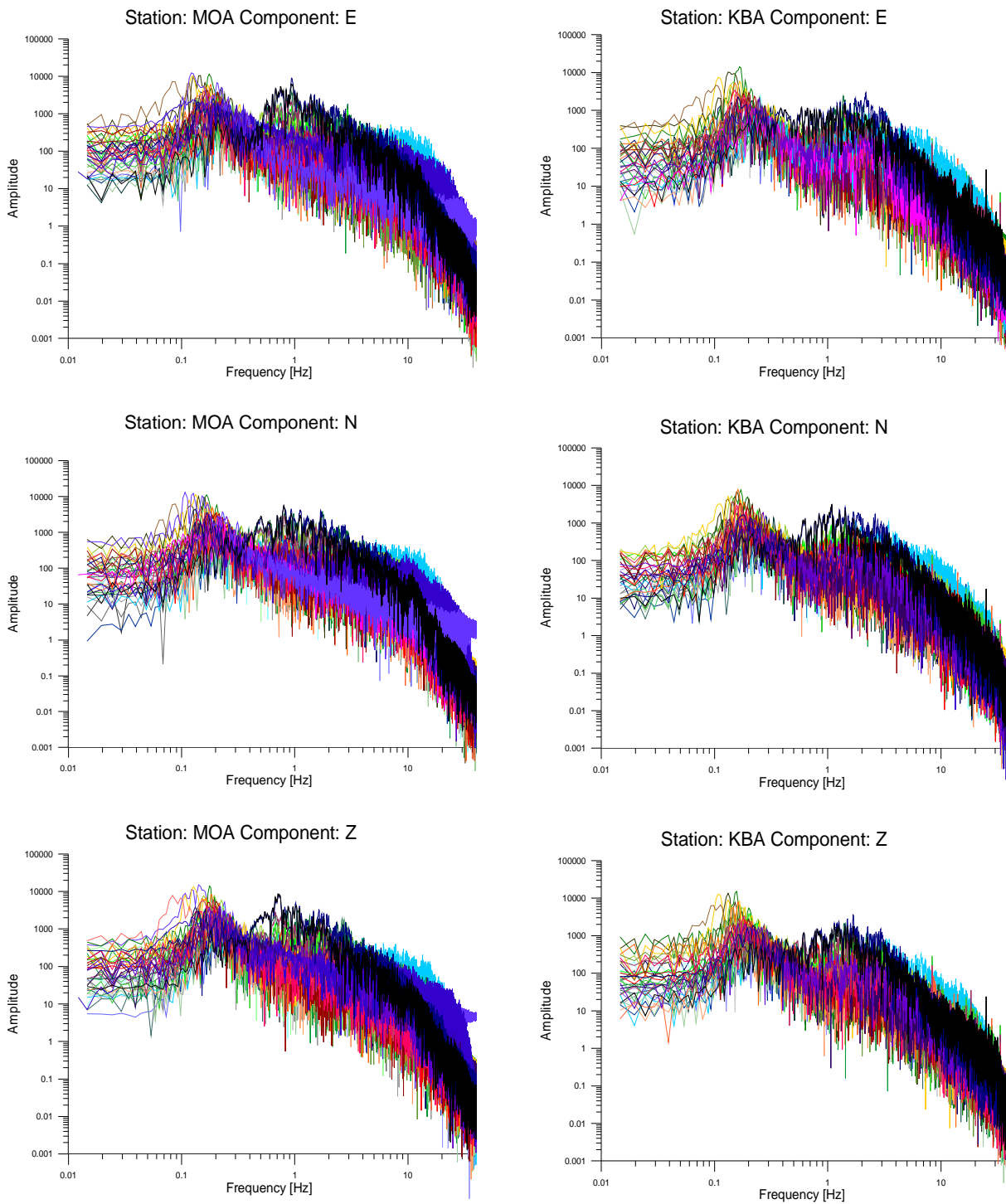


Figure 5-5 Amplitude spectra for the LPEs recorded at stations MOA on the left side and KBA on the right side. From top to bottom are the components E, N and Z.

5. Data Processing and Quantification

AMPLITUDE SPECTRA FOR EARTHQUAKES

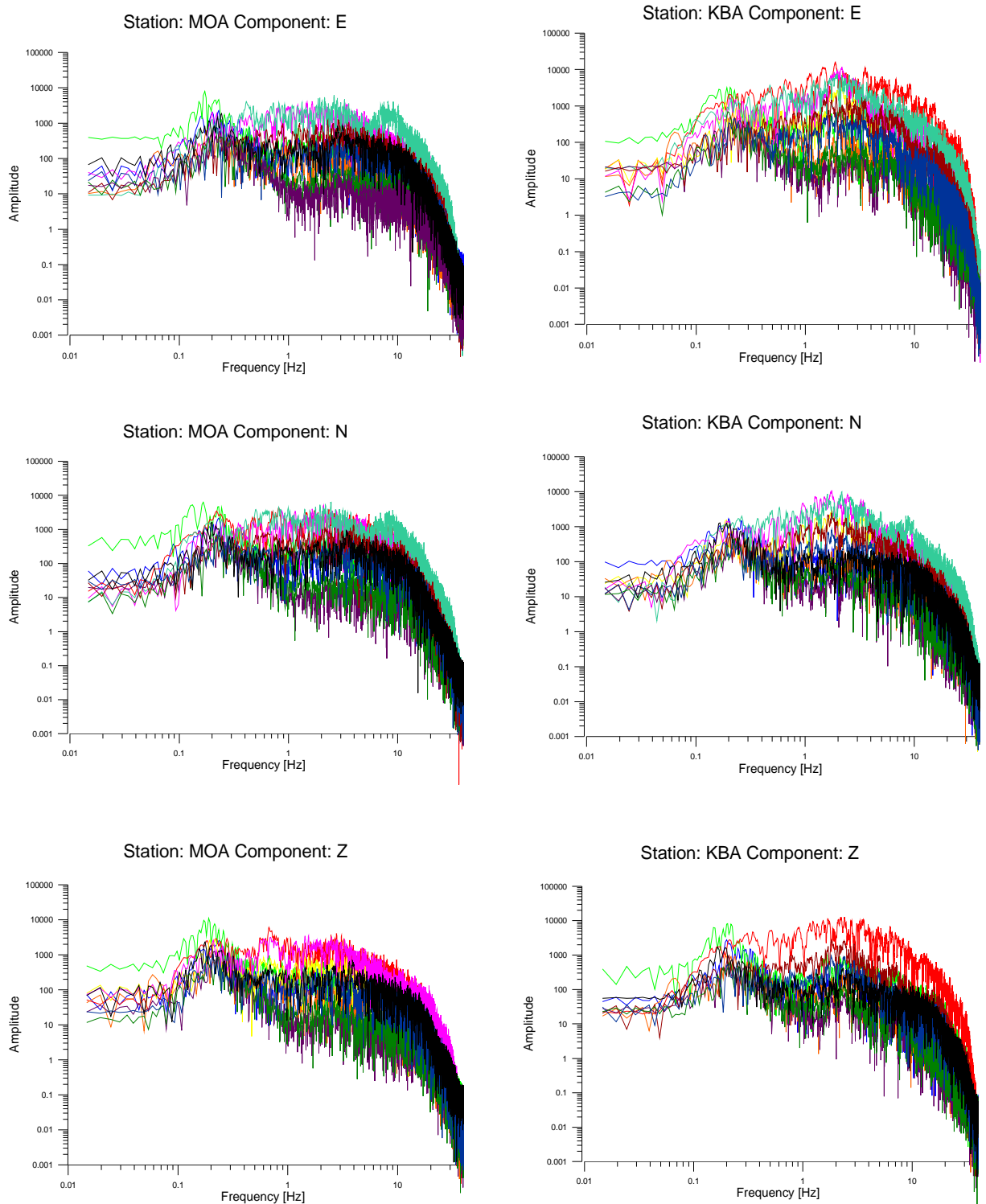


Figure 5-6 Amplitude spectra for earthquakes recorded at stations MOA on the left side and KBA on the right side. From top to bottom are the components E, N and Z.

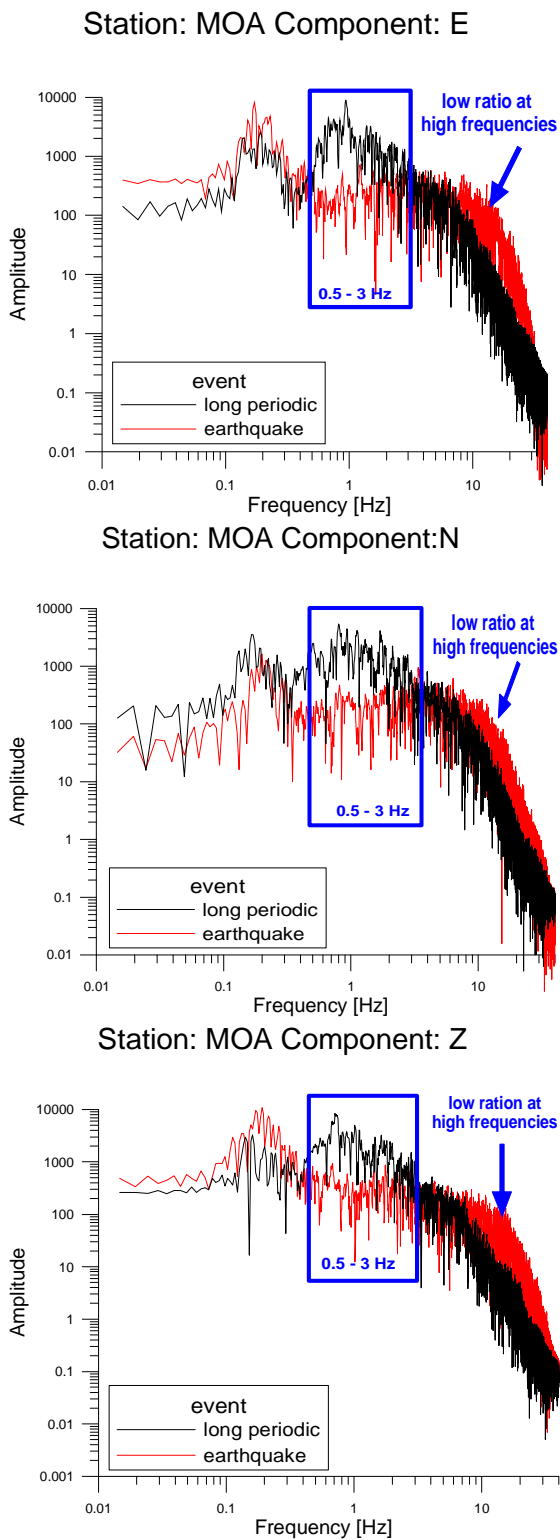


Figure 5-7 Comparison of the amplitude spectra of a characteristic earthquake in red and a LPE in black from the area of interest. The data refers to station MOA with component E on top, N in the middle and Z at the bottom.

5.4.1 Comparison of Amplitude Spectra

Spectra

Figure 5-7 clearly signals two main differences in the spectral content concerning two diverse source mechanisms. On each component the distinction in the frequency domain from 0.5 to 3 Hz is explicitly recognizable. Roughly speaking there is a difference of about a factor ten. The other mismatch is the lack of high frequencies for long periodic events. Quite to the contrary those frequencies seem to be representative for the earthquakes in this study. Also noticeable is the way of the drop of the frequencies. The black graph can be approximated by a more or less straight line. The comparison of the amplitude spectra is shown only for the station MOA as there are no significant differences worth mentioning for station KBA.

Figure 5-5 also illustrates that not all events reveal those characteristics. Therefore, the events are considered individually. A correlation with the existence of the above named frequency window in terms of the magnitude of the single events is considered as well as the lack of frequencies higher than 5 Hz, which is represented by a more or less continuously decrease in amplitude. For frequencies greater than 0.5 Hz and smaller than 3 Hz the maximum amplitude value is picked for each component. Also the same values are selected from the earthquake data and added. Similar plots are created regarding the mean value of the above defined frequency window as well as the sum for each long periodic event and each earthquake. This is visualized in Figure 5-8.

5. Data Processing and Quantification

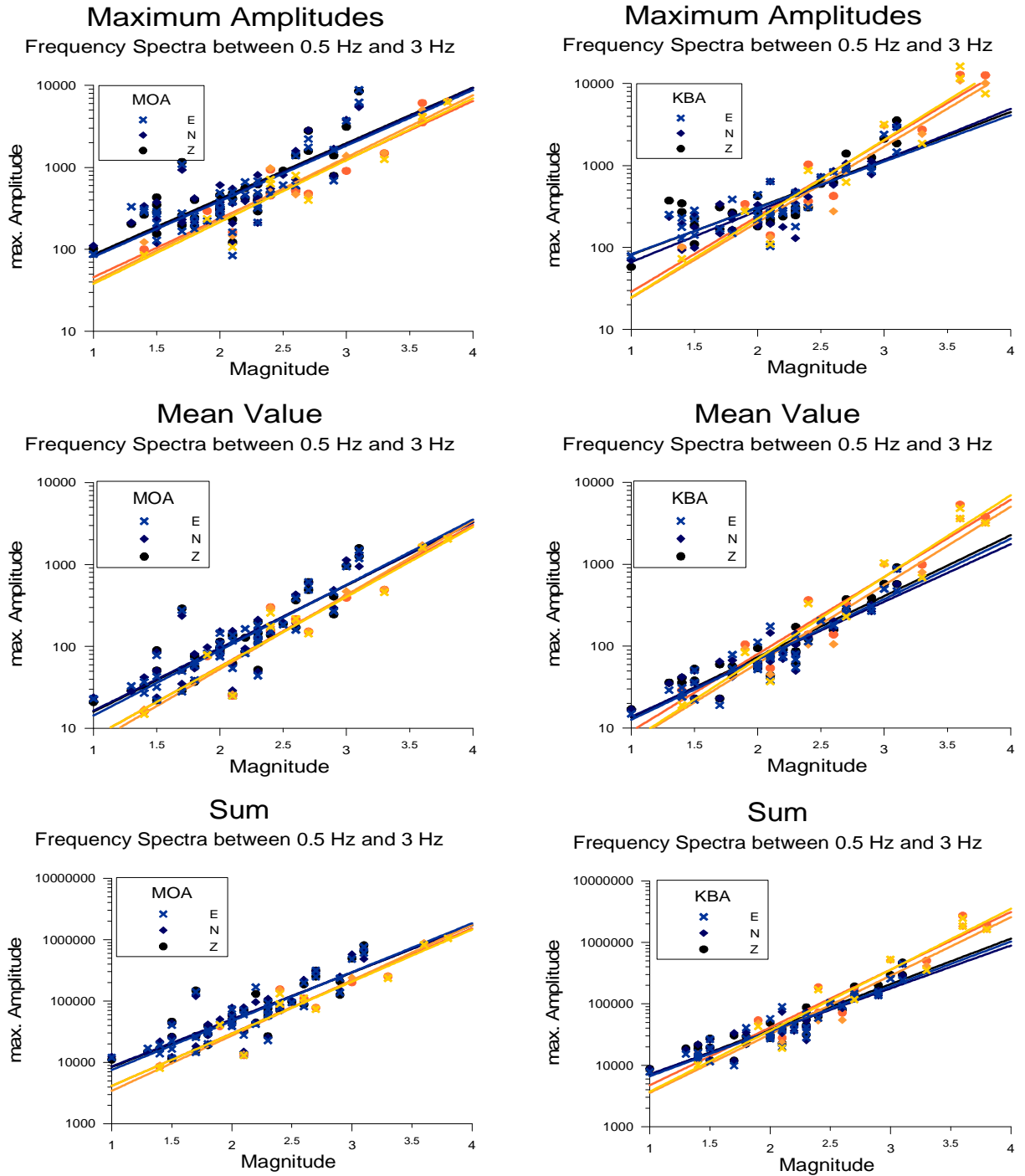


Figure 5-8 Maximum amplitudes (top), mean values (middle) and sum of the amplitude values of the frequency window 0.5 to 3 Hz for the station MOA on the right side and KBA on the left are plotted against magnitudes. Each component is represented by a distinct symbol. The blue colour represents LPEs while the yellow colour represents earthquakes. An exponential fit is applied.

5. Data Processing and Quantification

Detailed explanation of Figure 5-8:

For station MOA, the value of the maximum amplitude represents a good method evaluating whether the event in question belongs to a certain event type. The values of the LPEs are always greater than the ones of earthquakes. Closer examination reveals an outlier in the left graph at magnitude 1.7, with values varying from 1000 to 1200 nm/s, whereas the average amounts to less than 400 nm/s. These values refer to the event of 18th of September 2010. There are also three questionable values, each from one component, for the magnitude of 2.9 that all refer to the event of 14th of July 2003. Although this event was classified as a LPE, the values are far too small. Thus, they are interpreted as outliers that better match the characteristics of an earthquake. Also in the other two graphs on the left side outliers at magnitude 1.7 and 2.9 are apparent.

Also shown in Figure 5-8 are the mean values and the sum of the amplitudes in the frequency window from 0.5 to 3 Hz. A disassociation of the two event types is again visible. At station MOA the values for the LPEs exceed again the ones from earthquakes, but for greater magnitudes the exponential fits show a convergence of the two lines.

Considering the results at station KBA the convergence of the exponential fits becomes more distinct. Within the magnitude range of 2.0 to 2.5, these lines intersect and the values calculated for earthquakes exceed the ones of LPEs. Thus, no discrimination of different event types can be made in this range at station KBA. Besides that, the maximum amplitude values seem to be a useful tool to distinguish an LPE from an earthquake at station MOA.

The above mentioned outlier for the 14th of July 2003 is also evident in Figure 5-8 (blue colour). It can be seen best at station MOA on the components N and Z. From that figure, it is also apparent that this event is a tectonic earthquake while for the event of the 18th of September 2010 no high ratio in high frequencies is visible. Thus no decision about the origin is possible, based on the frequency spectra only. One more outlier can be seen in that figure. The deep blue colour represents the event of the 10th of August 2011 which indicates a tectonic earthquake.

Table 5-1 gives an overview over the outliers identified with the help of the frequency spectra and further methods.

5. Data Processing and Quantification

Table 5-1 Events, that do not match the characteristics of LPEs based on frequency content.

date yyyy mm dd	magnitude	method	value	
			observed	calculated (approx.)
2003 07 14	2.9	frequency spectra	long periodic	earthquake
		maximum amplitude	> 1500 nm/s	< 1000 nm/s
		mean value	> 500 nm/s	< 300 nm/s
		sum	> 250 000 nm/s	< 150 000 nm/s
2010 09 18	1.7	maximum amplitude	< 500 nm/s	> 1000 nm/s
		mean value	< 100 nm/s	> 250 nm/s
		sum	< 60 000 nm/s	> 120 000 nm/s
2011 08 10	2.0	frequency spectra	long periodic	earthquake

5.5 Magnitudes

A common way to quantify seismic energy is the magnitude. Depending on the distance and the variable wave phases there is a number of different scales. In general, a magnitude can be written down as

$$M = \log\left(\frac{A}{T}\right) + f(\Delta, h) + C_s + C_r \quad (3.5)$$

e.g. LAY and WALLACE (1995). “M” is magnitude, “A” denotes the ground displacement of the phase, “T” is the period of the signal, “f” is a function of the epicentral distance “Δ” and the focal depth “h”, whereas “C” implies a correction term for the location of a station (“C_s”) and the source region (“C_r”) respectively.

In literature an approach to differentiate between earthquakes and long periodic events, such as rockslides, suggests to plot several magnitude types against each other (e.g. WEICHERT et al. 1994). In this thesis the local magnitude “M_L” and the body-wave magnitude “m_b” are compared.

The local magnitude “M_L” was created by C. F. Richter in the early 1930s and contains only terms of the displacement “A”, measured from shear wave amplitudes and the distance “Δ”. Because Richter only developed a formula for the Wood-Anderson torsion seismometer that time, it is a modification of (3.5)

$$M_L = \log A - 2.48 + 2.76 \log \Delta \quad (3.6)$$

e.g. LAY and WALLACE (1995). In practice other constants are added for e.g. different crustal models or other instruments.

On the contrary the body-wave magnitude “m_b” is derived from the direct P wave:

$$m_b = \log\left(\frac{A}{T}\right) + Q(h, \Delta) \quad (3.7)$$

e.g. LAY and WALLACE (1995). “A” denotes the actual ground-motion amplitude in micrometers with “T” being the corresponding period in seconds. “Q” represents in this case the empirically determined correction term for distance “Δ” in degree and the focal depth “h” in km, which is equivalent to $f(\Delta, h)$ in (3.5).

5. Data Processing and Quantification

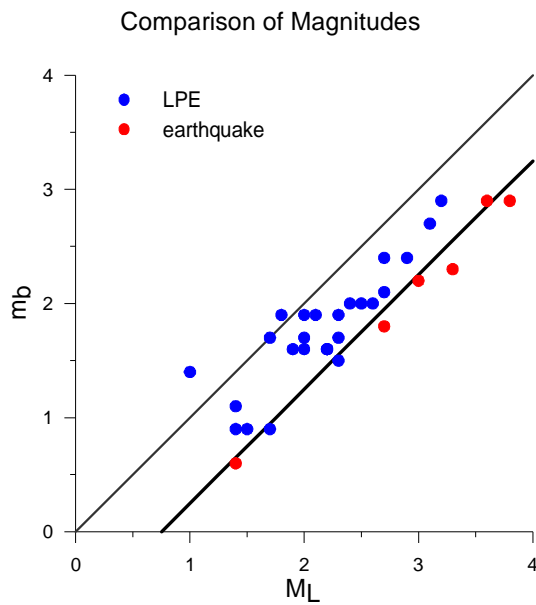


Figure 5-9 Comparison of the body-wave magnitude “ m_b ” and the local magnitude “ M_L ”. Red dots refer to LPEs, blue dots to earthquakes.

Figure 5-9 indicates that LPEs can be graphically separated from earthquakes. This is based on the calculation of different magnitude scales. While the body-wave magnitude is calculated from P waves, the local magnitude refers to the S wave. In case of an earthquake the P wave amplitude is always significantly smaller than the one of the S wave and, therefore, the body-wave magnitudes are less than the calculated local magnitude for the same event. In comparison, LPEs tend to have similar body-wave and local magnitudes. This clearly indicates that the shear wave and the P wave amplitudes are of similar size, which is a characteristic of such events.

In the following chapters local magnitudes are cited.

5.6 Arias Intensity

Dealing with the effect of transient seismic waves on the surface Arturo Arias defined an intensity of ground shaking, that describes the potential of earthquakes triggering e.g. landslides or rock avalanches.

$$I_A = \frac{\pi}{2g} \int_0^{T_d} a(t)^2 dt \quad (3.8)$$

(ARIAS, 1970) with “a(t)” as the ground acceleration, “g” as the acceleration due to gravity and “T_d” the duration of signal above a certain threshold, usually 90 % of the signal’s energy. Known as the Arias Intensity (AI) the time-integral of the square of the ground acceleration describes the square root of the energy per mass with units of m/s.

As the Arias Intensity values are typical for certain effects in nature, HARP and WILSON (1995) grouped them in three categories (Table 5-2).

Table 5-2 Some Arias Intensities and their meaning.

AI-Minimum value	category	description
0.11 m/s	I	Falls, disrupted slides, avalanches
0.32 m/s	II	Slumps, block slides, earth flows
0.54 m/s	III	Lateral spreads and flows

To find out whether using different Arias Intensity categories as a criterion for seismograms reflecting landslides is reasonable or not, the data is differentiated in SAC. In addition, a distance correction was applied to compensate attenuation. This correction shall assist in estimating Arias intensities of the source for composing the values with those from Table 5-2.

$$s_i = 4,3 * \log (x) \quad (3.9)$$

Each trace “s_i” is multiplied by a distance (x) dependent correction term as stated in formula (3.9). Then, the sum of the squared acceleration values is calculated. The results are presented according to the components of the seismometer (E, N and Z) for each station in Figure 5-10. For comparison, the Arias Intensity values for earthquakes are shown below (note, that the axes of the logarithm of the Arias Intensity are not the same).

5. Data Processing and Quantification

As can be seen in Figure 5-10 it is useful to apply an exponential fit to the values of the Arias Intensity. At station KBA they seem to fit better on the exponential line, whereas at station MOA they vary a lot. Considering the different dimensions of the ordinates for earthquakes and LPEs, Figure 5-10 clearly shows the different slopes of the respective fits. To quantify the values and to compare them, the slope of the exponential fit and the intersection point with the ordinate are presented in Table 5-3.

Also noticeable are some outliers. Three of which can be seen at station MOA at magnitude 2.0 which represent the event on 10th of August 2011. Because no data was available for this event at station KBA, the outliers are missing on the right graph. There are also three more outliers for the event on the 14th of July 2003 with a magnitude of 2.9. The apparent Arias Intensity exceeds values of 0.5 and 1.0 depending on the component at station MOA, but they can be detected better at station KBA, where the values are greater than 1.0 for all three components.

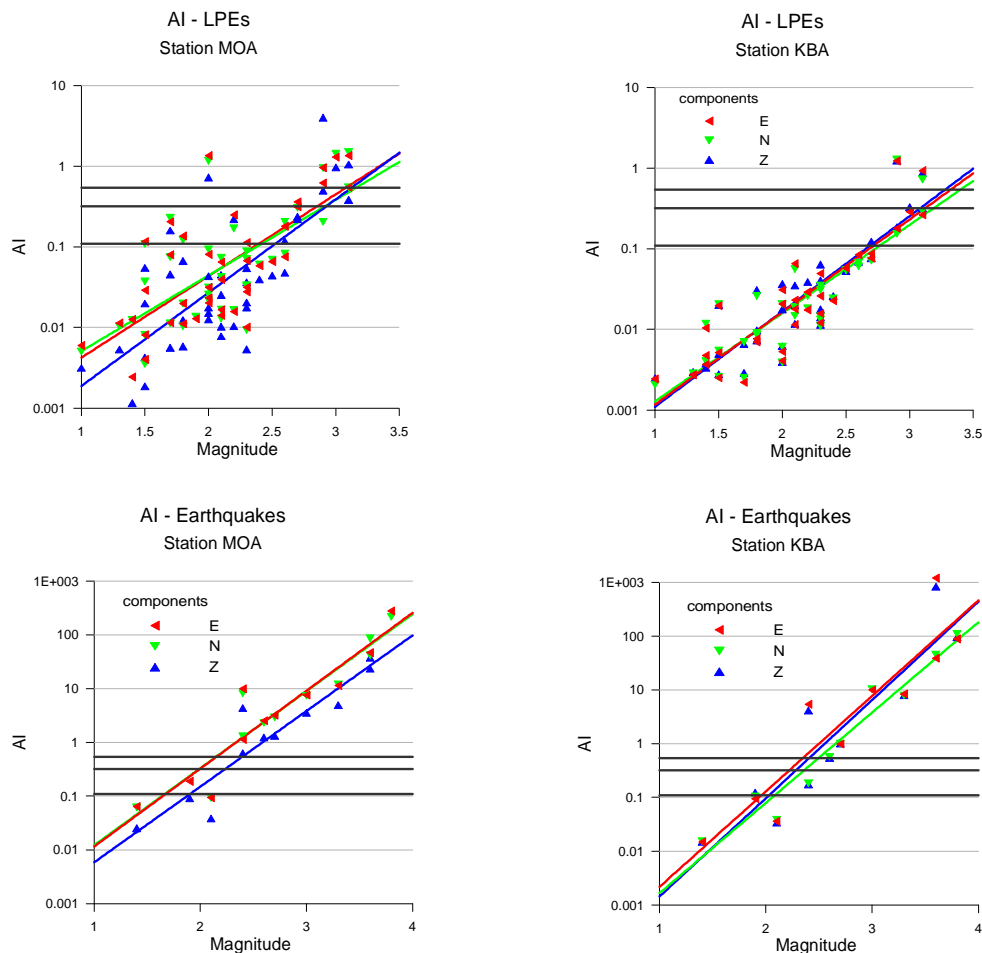


Figure 5-10 Estimated Arias Intensity values of LPEs (top) and earthquakes (bottom) for the stations KBA and MOA for each of the three components are plotted against the local magnitude of each event. Red left pointing triangles represent the E-component, green downward triangles the N-component and Z-component in blue (upward triangle). The black lines indicate the limits of the AI-categories defined by HARP and WILSON.

5. Data Processing and Quantification

Discussing the results for station KBA, the following can be said: For magnitudes 2.5 there is a distinct difference in the calculated values as for earthquakes they are greater than 0.1, which can be clearly seen on the exponential fit. On the contrary, for LPEs all the Arias Intensities are smaller than 0.1. This gap between the two exponential fits becomes more significant for larger magnitudes, which Table 5-3 also points out as the slope k for earthquakes has values between 3.86 and 4.21, whereby the ones for LPEs are only between 2.52 and 2.73.

Table 5-3 Values characterizing the exponential fit of the Arias Intensities.

EXPONENTIAL FIT		$y = d * \exp(k*x)$			
station	component	LPE		Earthquake	
		$d \times 10^{-3}$	k	$d \times 10^{-3}$	k
MOA	E	0,409	2,3335	0,414	3,3345
	N	0,585	2,1631	0,455	3,2962
	Z	0,131	2,6663	0,231	3,2387
KBA	E	0,083	2,6429	0,037	4,0883
	N	0,103	2,5206	0,035	3,8668
	Z	0,072	2,7216	0,022	4,2071

It is harder to make decisive statements for the values at station MOA as the distribution of the single values around the line of the exponential fit is greater than at station KBA. But another aspect has to be mentioned: The exponential fit for the components E and N are quite similar, whereas the one for component Z apparently differs.

It is not useful to interpret the figure concerning the Arias Intensity categories defined by HARP and WILSON in more detail as most of the values lie below the lowermost boundary. Worth mentioning is the fact that the intersection points of the fits with that lowest boundary vary for earthquakes (about magnitude 2.0) and LPEs (about 2.5). Hence, if data of an earthquake is available, a comparison of values for Arias Intensity of LPEs and earthquakes from approximately the same location can help determining whether an event was of tectonic origin or rather a gravitational driven rock mass movement.

Further, the discussion about the Arias Intensity entails that the two events in Table 5-4 might not be LPEs.

Table 5-4 Events, that do not match the expected Arias Intensities for LPEs.

date yyyy mm dd	Arias Intensity [m/s]	
	observed	expected
2003 07 14	$0.05 < AI < 0.2$	> 0.5
2011 08 10	< 0.05	> 0.1

5.7 Energy Signal

A further approach to distinguish the origins of signals in this thesis is the comparison of signal energies of LPEs and those of earthquakes.

The signal energy “E” of a real signal “s(t)” in the time window (t₁; t₂) is defined as

$$E = \int_{t_1}^{t_2} s^2(t) dt \quad (3.10)$$

e.g. LÜKE (1995). Having a focus on energy signals it concerns signals that are either real or complex with a finite energy signal along the whole time axis, which according to LÜKE (1995) correspond to

$$E = \int_{-\infty}^{+\infty} s^2(t) dt < \infty \quad (3.11)$$

Figure 5-11 shows the results of both, the long periodic events (blue) and the earthquakes (yellow), for both stations and each component. The values are plotted in respect to the magnitude. For a better interpretation an exponential fit is applied. Generally speaking, the calculation of the energy signal features greater values for earthquakes than for long periodic events.

Contrary to the so far applied methods for determining the source mechanism, calculating the energy signal for station MOA seems to be no satisfying means of classification, whereas the results from station KBA are much more promising. Considering the exponential fit, it clearly points out that, the greater the magnitude, the bigger the gap between the energy signal of earthquake and LPE. Such an observation cannot be made from the data recorded at station MOA. A close-up look shows that the main difference lies in the energy signal of the earthquake recorded at the two stations. The slope of the exponential fit at station KBA is steeper than the one at station MOA and thus is of use for separation of the event sources. Unfortunately, there are no obvious limits and, therefore, no outliers can be defined. Still, calculating the energy signal for larger magnitudes at station KBA might be useful in combination with other methods of classification.

5. Data Processing and Quantification

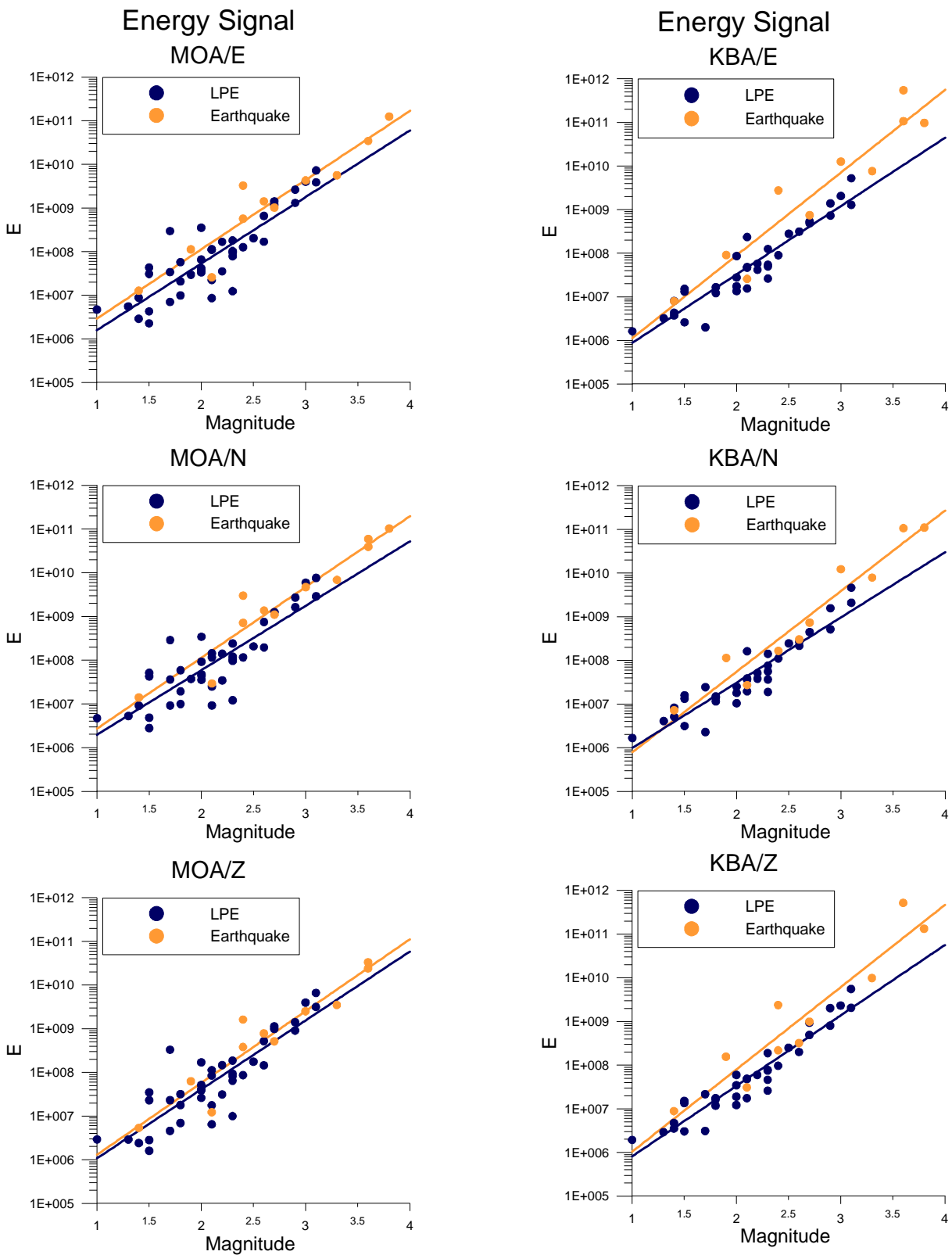


Figure 5-11 Energy signal of long periodic events represented in blue and of earthquakes in yellow plotted against the magnitude. The left side shows the results for the station MOA with component E on top, N in the middle and Z on the bottom, the right side gives the results for KBA respectively. An exponential fit is applied to both data sets.

5.8 Root Mean Square

Another idea for determining different source mechanisms is to calculate the Root Mean Square RMS of the signal. Defined as the square root of the arithmetic mean of the discrete data set, it represents a magnitude of the amplitude of a signal. For a set of n values the amplitudes “ $a(t)$ ” as a function of time “ t ” are given. RMS is then calculated with the following equation (3.12)

$$RMS = \sqrt{\frac{\sum_{i=1}^n a^2(t)}{n}} \quad (3.12)$$

The results are shown in Figure 5-12.

For station MOA this method did not appear to be suitable for classification. On all three components it can be seen, that the fit for values of the earthquakes is similar to these of LPEs, and the gap between the two fits is quite small and therefore not distinct.

For station KBA the results are more promising. The RMS values for small magnitudes, at least less than 2.0, have similar values for LPEs and earthquakes. However, applying an exponential fit clearly shows the divergence in the results with greater magnitudes. Still, it is not enough to distinguish between these two types for certain, but it has to be noted at this point that calculating the RMS for LPEs can be a useful tool when combined with other methods.

As both, “Energy Signal” and “Root Mean Square”, do not lead to as conclusive means for an event separation, no table with defined outliers is listed as they would not be more than mere surmise.

5. Data Processing and Quantification

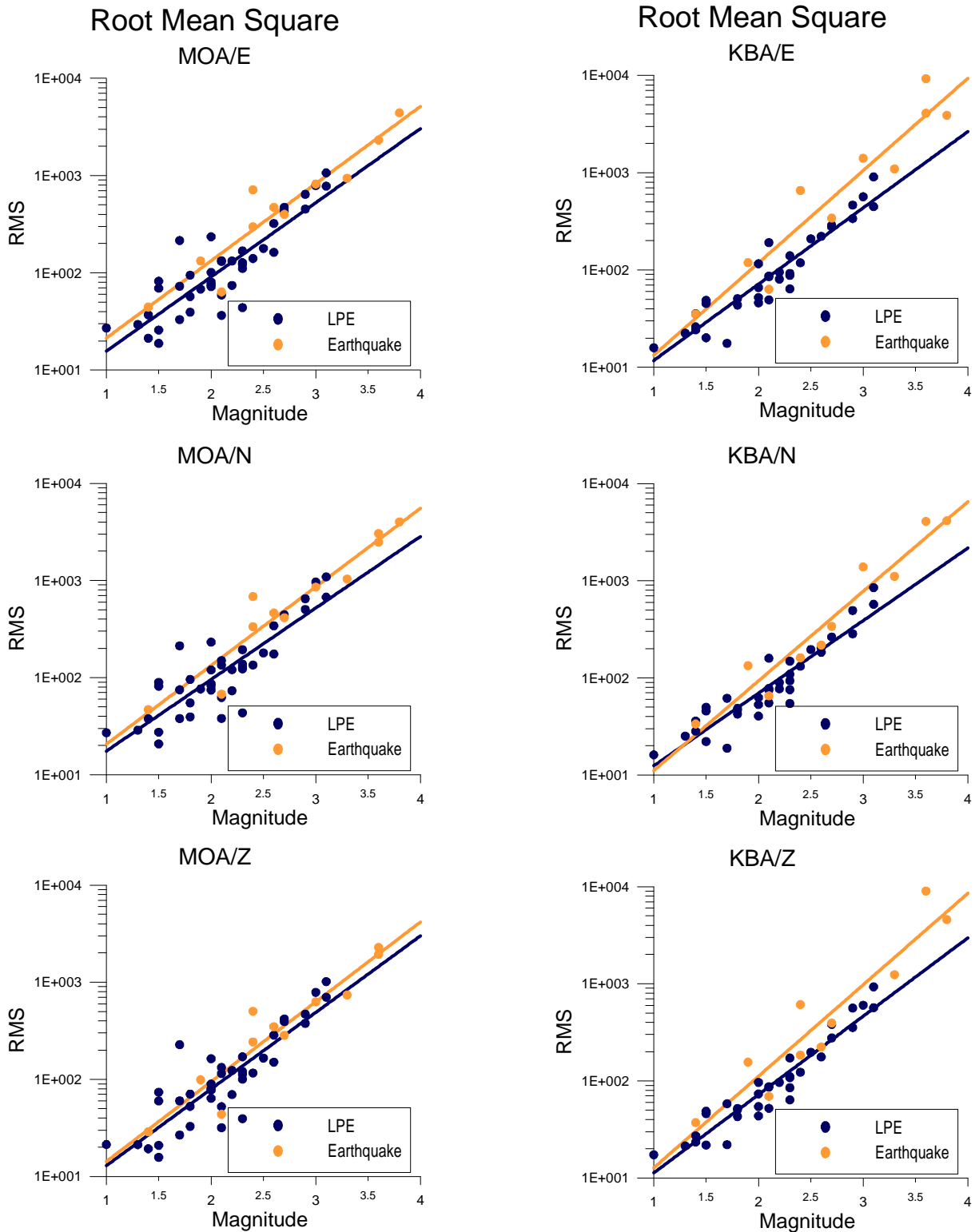


Figure 5-12 Root Mean Square for station MOA on the left side and KBA on the right. Blue dots represent the results for LPEs, yellow ones earthquakes. An exponential fit is applied to the data. Note: the RMS values are plotted on a logarithmic scale.

5.9 Auto - Correlation

The auto-correlation is a special case of the cross-correlation function “ k_{12} ”. To calculate “ k_{12} ” the two signals “ $x_1(t)$ ” and “ $x_2(t)$ ” are compared. It achieves maximum values for signals that coincide best in shape and occur at the same time. Moving one of the two signals respectively to the other one for a time interval τ modifies the value of “ k_{12} ”. Therefore, “ k_{12} ” is defined as a function of “ τ ”:

$$k_{12}(\tau) = \int_{-\infty}^{+\infty} x_1(t) x_2(t - \tau) dt \quad (3.13)$$

(GÖTZ, 1995). For the correlation of two time discrete signals “ $x_1(m)$ ” and “ $x_2(m)$ ” the integral in the cross-correlation function appears as a sum:

$$k_{12}(n) = \sum_{m=-\infty}^{+\infty} x_1(m) x_2(m - n) \quad (3.14)$$

While “ k_{12} ” represents the similarity of two signals, the auto-correlation is the cross-correlation of a time series with itself (STEIN and WYSESSON, 2003), where $x_2(t) = x_1(t)$.

To calculate the auto-correlation the 80 seconds long traces are band pass filtered from 1 to 35 Hz in SAC. They are exported in ASCII files and processed in MATLAB.

Figure 5-13 on the left side displays the auto-correlation of the LPE of the 5th of April 2011. By way of comparison on the right side the earthquake of the 21st of May 2008 also shows the result for calculating the correlation of the signal with itself. As both events are of a similar magnitude (3.0 for LPE and 3.1 for earthquake) the rough comparison can be made based on these two figures that the amplitude of the auto-correlation of LPEs decays much faster than the one for earthquakes.

For further comparison the absolute value of each amplitude of the auto-correlation is normalized with its total amount and converted into percent according to

$$S_i = \frac{|A_i|}{\sum_{j=0}^{6400} |A_j|} \cdot 100 \quad (3.15)$$

The number of samples (6400) derives from the length of the trace (80 seconds) multiplied the sampling frequency of 80 Hz. One purpose is to find out the point in time when 95 % of the signal has passed. That value is declared as “ S_{95} ” and the corresponding point in time as “ T_{95} ”. By way of illustration, Figure 5-14 shows the normalized summing up of the absolute values of the amplitude. The figure reveals that the LPEs’ duration is shorter than the one of earthquakes. For these two examples it can also be said that the curve for “ S ” values for the earthquake increases faster until

5. Data Processing and Quantification

about 70 % are obtained. Afterwards the values are smaller than for LPEs and therefore it lasts longer to achieve the 95 %.

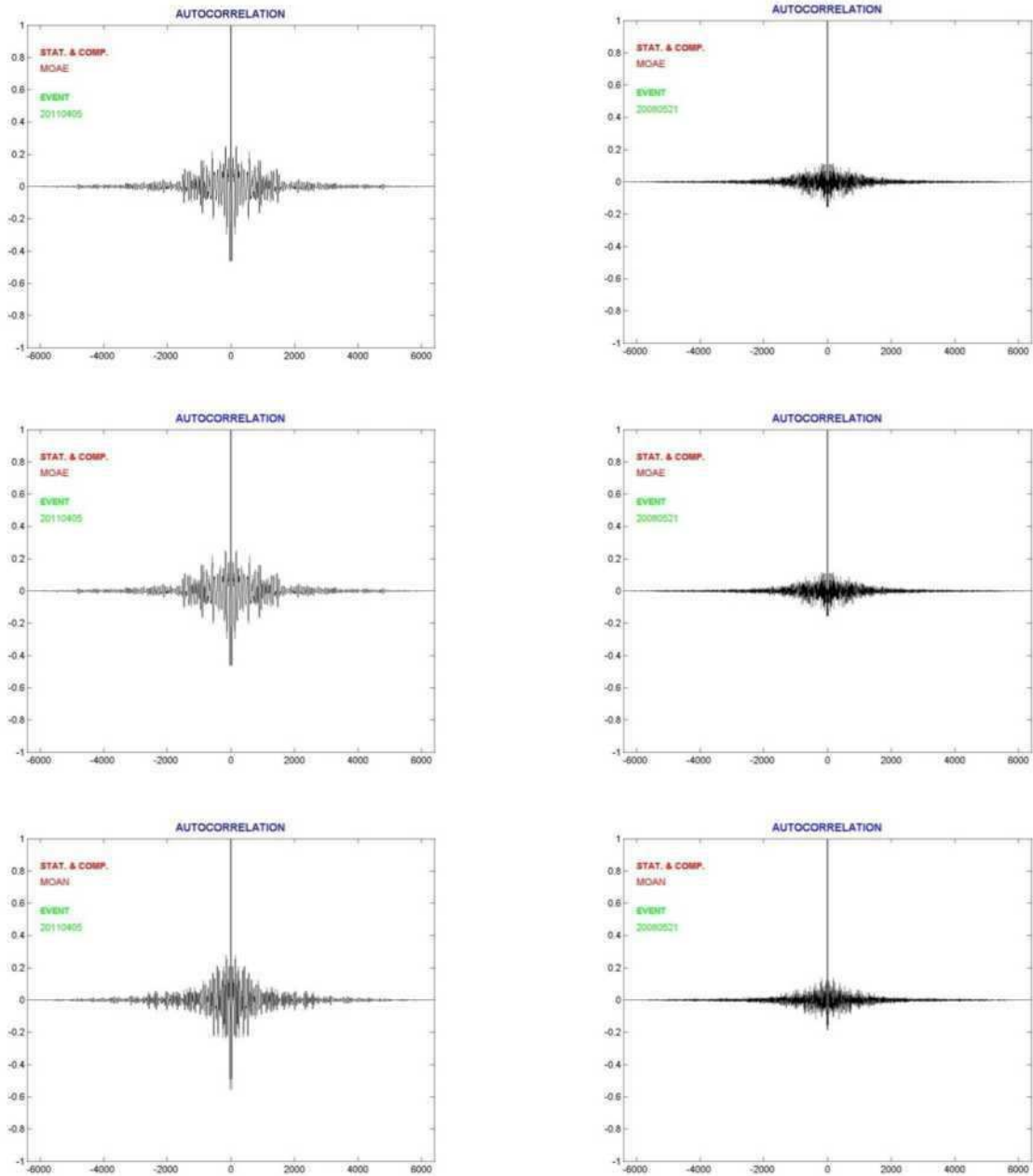


Figure 5-13 Auto-correlation of a LPE on the left side and of an earthquake on the right side. The data are from station MOA. All components are shown with E on top, N in the middle and Z below.

5. Data Processing and Quantification

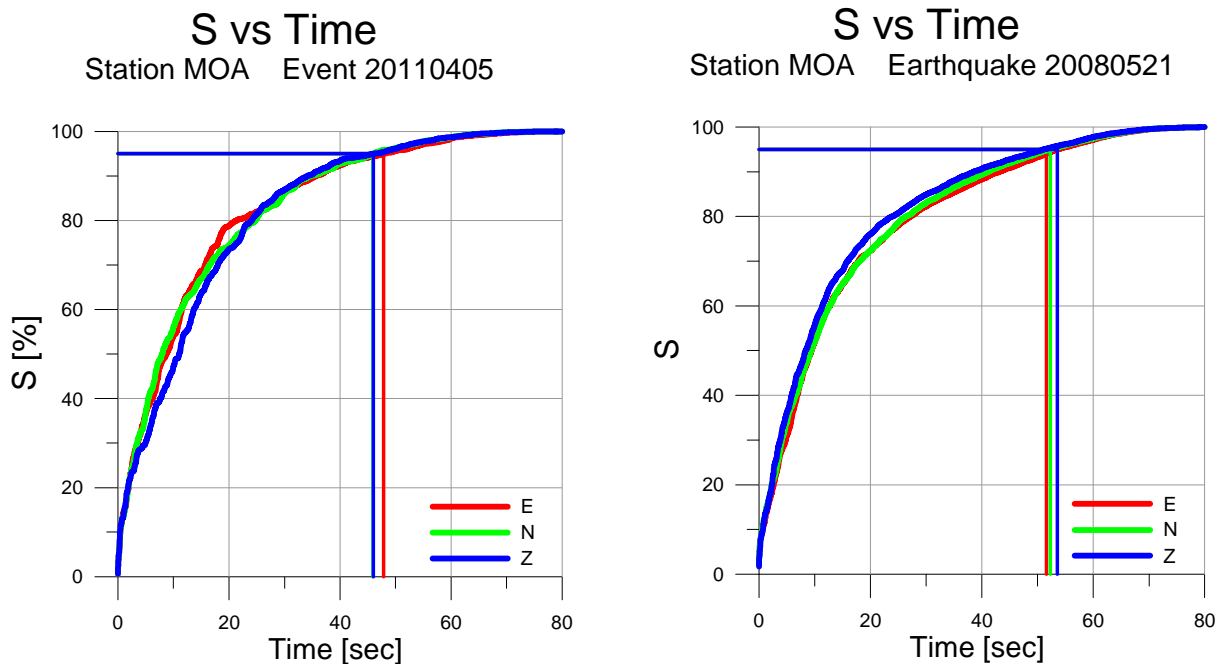


Figure 5-14 “S” for one LPE on the left side and for one earthquake on the right side. The horizontal line represents the 95 % limit with the vertical line indicating the point in time. All components are represented in the figure with red for E, green for N and blue for Z. The events were recorded at station MOA.

After explaining the theory, the actual data analysis is shown in the following figures. First, the “ S_{95} ” is shown as a function of the magnitude for both LPEs and earthquakes for each component. Secondly, its duration of time T_{95} is presented.

In Figure 5-15 the values for “ S_{95} ” show a substantial difference for LPEs and for earthquakes. The latter are plotting along a more or less straight line, whereas the values at station MOA vary less than the ones at station KBA. Basically, they are larger at KBA. These characteristics can be seen throughout all components. As opposed to this, “S” values of LPEs increase significantly with greater magnitudes while at station MOA they have smaller values for low magnitudes and similar ones for higher magnitudes. This results in a steeper slope of the linear fit with a better approximation of each value at station MOA than at station KBA.

Some outliers appear along the whole magnitude spectra. As they can be seen more precisely on the left side of the figure, the station MOA is discussed in more detail and afterwards an attempt to identify them at station KBA is made.

5. Data Processing and Quantification

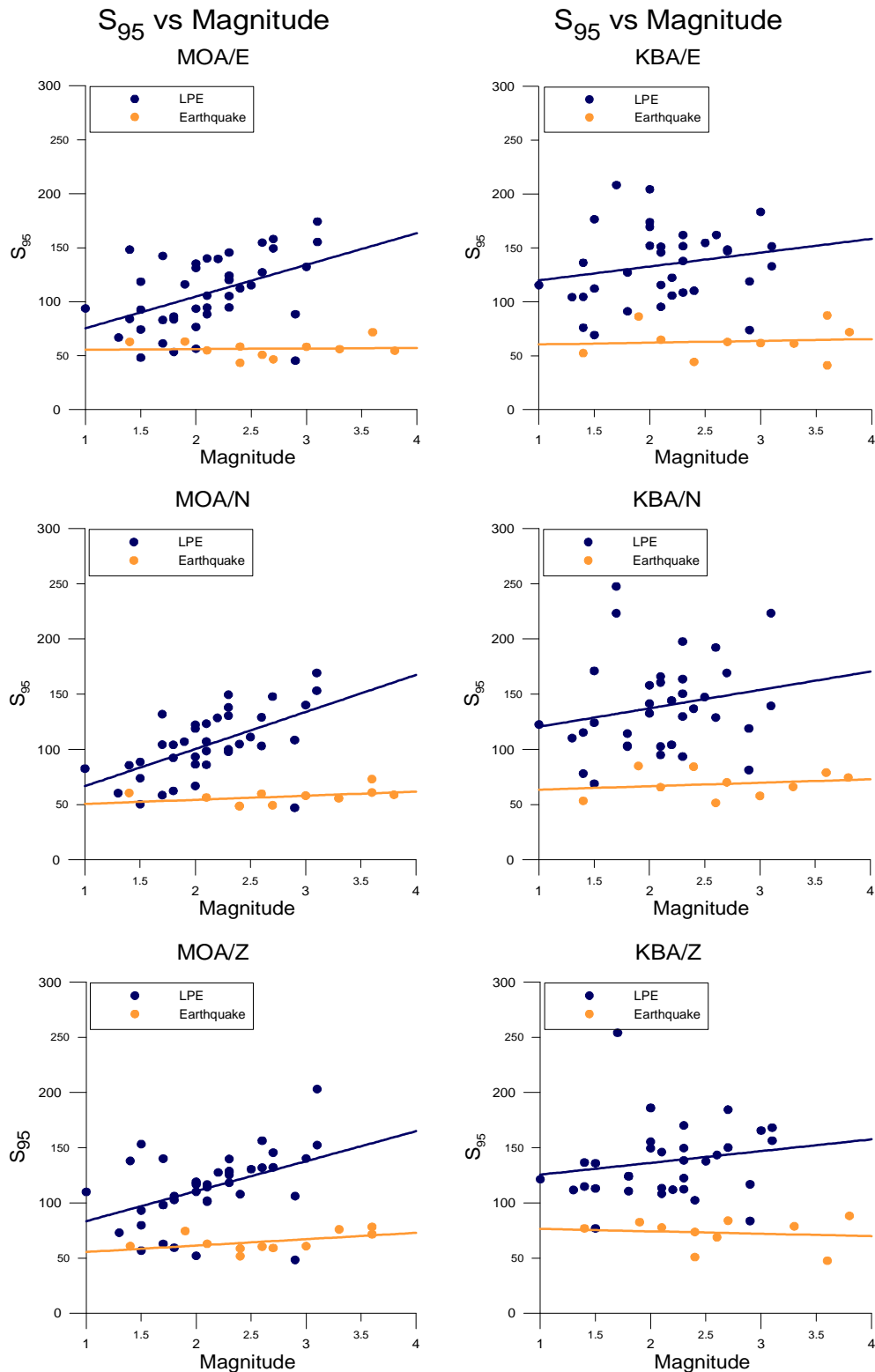


Figure 5-15 “ S_{95} ” as a function of magnitude. On the left side the results for the station MOA are shown with component E on top, N in the middle and Z at the bottom. Blue dots signify LPEs while yellow ones indicate earthquakes. The lines represent the linear fits. The right side shows data results of station KBA.

5. Data Processing and Quantification

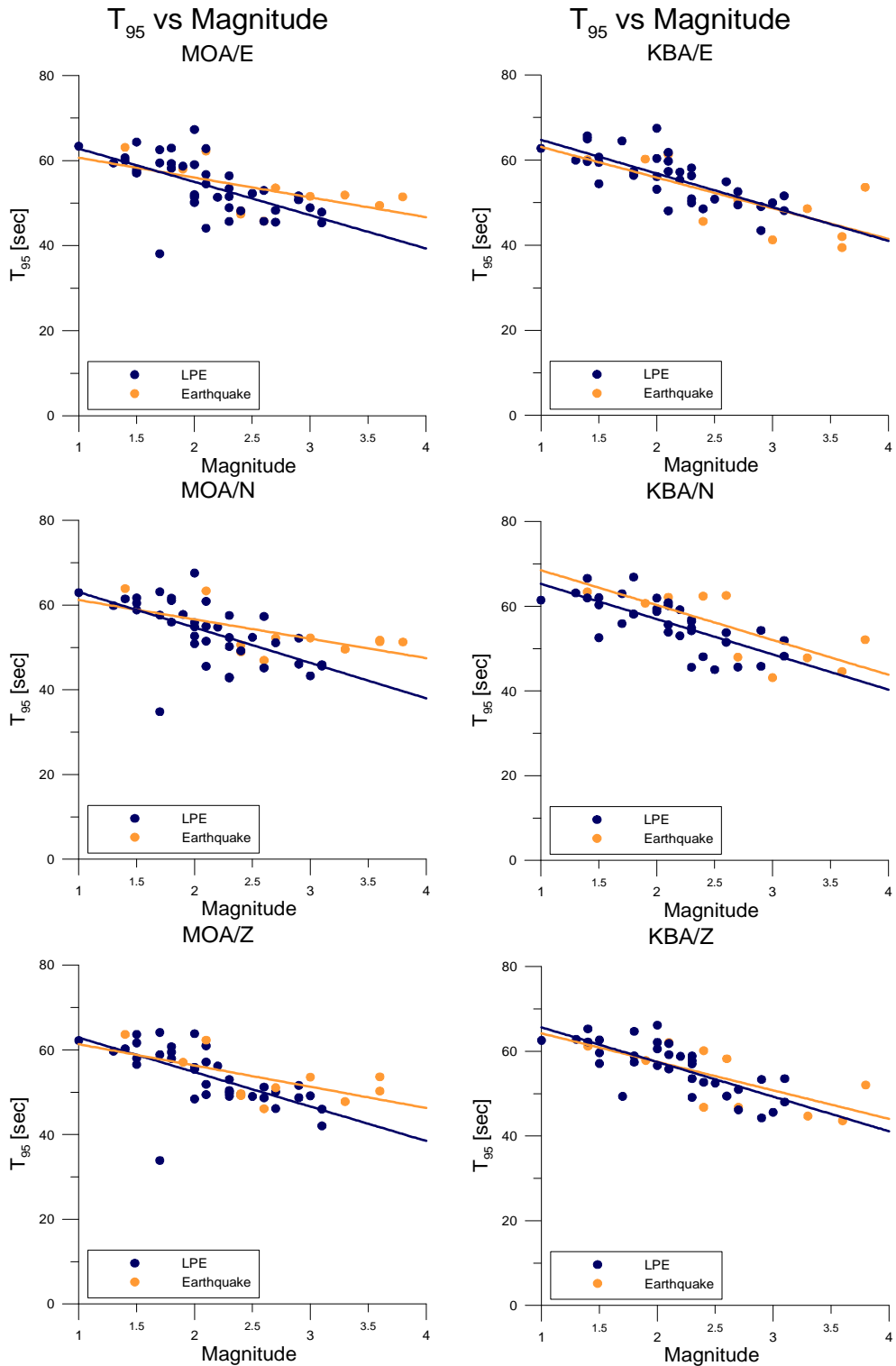


Figure 5-16 Signal length as a function of magnitude. On the left side the results for the station MOA are shown with component E on top, N in the middle and Z at the bottom. Blue dots signify LPEs while yellow ones indicate earthquakes. The lines represent the linear fits. The right side shows the results of station KBA.

5. Data Processing and Quantification

Station MOA reveals at least three outliers that even lie underneath the linear fit of the earthquake data for a magnitude of 1.5 (component E), of 2.0 (component Z) and of 2.9 (component E, N and Z). Two more can also be identified as outliers as they are located at or just above the defined line. These are an event of magnitude 1.7 and one of 1.8. One more can be located at magnitude 1.3 (component E and N), but due to the low magnitude no certain decision can be made, whether the event belongs to LPEs. More information for the specified events is listed in Table 5-5.

Table 5-5 Outliers of the long-period data set evaluated by calculating the sum of the absolute values of amplitudes.

date yyyy mm dd	magnitude	sum of absolute values of amplitudes [nm/s]		
		MOA E	MOA N	MOA Z
2003 07 14	2.9	45.34	47.14	48.47
2004 05 08	1.5	48.13	50.30	56.85
2011 08 10	2.0	56.43	66.95	52.16
2000 11 09	1.7	61.32	58.59	62.96
2006 03 28	1.8	53.46	62.45	59.47
2009 01 06	1.3	66.8	60.47	-
		KBA E	KBA N	KBA Z
2010 04 23	1.4	60.47	76.12	-

At station MOA only two of the defined outliers in Figure 5-15 can be distinguished. One appears at magnitude 1.5, which refers to the event of the 8th of May 2004, and the other one at 2.9, which belongs to the event of the 14th of July 2003. Another possible outlier can be assumed at the components E and N at a magnitude of 1.4 referring to the event of the 23rd of April 2010. Unfortunately, no data is available for component Z and from station MOA.

In Figure 5-16 the evaluated signal length is given as a function of the magnitude. The figure shows that for smaller magnitudes it takes longer to achieve an “S” of 95 %. Concerning station MOA an indication of a trend can be seen above magnitudes 2.8. It implies that the signal length of earthquakes is longer than the one of LPEs, which can be seen best at the components E and N, at the given distance of observation.

In conclusion, the calculation of “S₉₅” of the auto-correlation is a useful tool to distinguish the two types of events, whereas its corresponding duration “T₉₅” can, if at all, only be used in combination with other methods.

5.10 Coda

General information in this abstract refers to BORMANN (2009). Coda waves occur after the main generating wave phases have passed, mainly as a process of scattering and wave conversions in the heterogeneous crust. The coda length is mainly a function of the magnitude. For local earthquakes the wave amplitude envelope has a characteristic shape. After the amplitudes maximum follows usually an exponential decay of amplitudes, the coda.

For this processing, a band pass filtered from 1 to 35 Hz is additionally applied in SAC. Afterwards the envelope is generated, for which the program uses the Hilbert transform. Thereafter, the data are exported in ASCII files and further calculations are made with MATLAB.

First the maximum amplitude is assigned and each trace is divided into an increasing part, starting at the P arrival and lasting until the maximum amplitude, and a decreasing one. Then the logarithm of the data is taken and a linear fit is applied. To compare the fits of the data of LPEs with the ones of earthquakes, the intersection of the linear fit with the ordinate is defined as “a” whereas “b” denotes the slope. To get the exponential fit for the data, the logarithm of “a” is calculated and termed as “ a_{exp} ”.

Finally the formulas (3.16) describing the exponential fit shall give information for a classification as “b” is a function of the event type (pers. comm. Lenhardt) while “a” is a function of magnitude.

$$\ln A = a - b \cdot t$$

$$A = a_{exp} \cdot e^{-bt} \quad (3.16)$$

Figure 5-17 shows the result of the processing steps described above for component Z at station MOA for the event of the 2nd of May 1999.

To make sure that the shape of the traces for these characteristic events follows a systematic pattern on all three components, two LPEs are chosen. In previous methods these two events always turned out to have distinctive mismatches with the results for normal earthquakes. These are the event of the 2nd of May 1999 and the one of the 5th of April 2011. Their envelope and exponential fit are shown in Figure 5-18.

The figure displays the results for station MOA for the component E at the upper two pictures, for N at the at the mid-position and for Z at the lower end whereby in each case the upper one refers to the event of the 5th of April 2011 and the lower one to the 2nd of May 1999.

5. Data Processing and Quantification

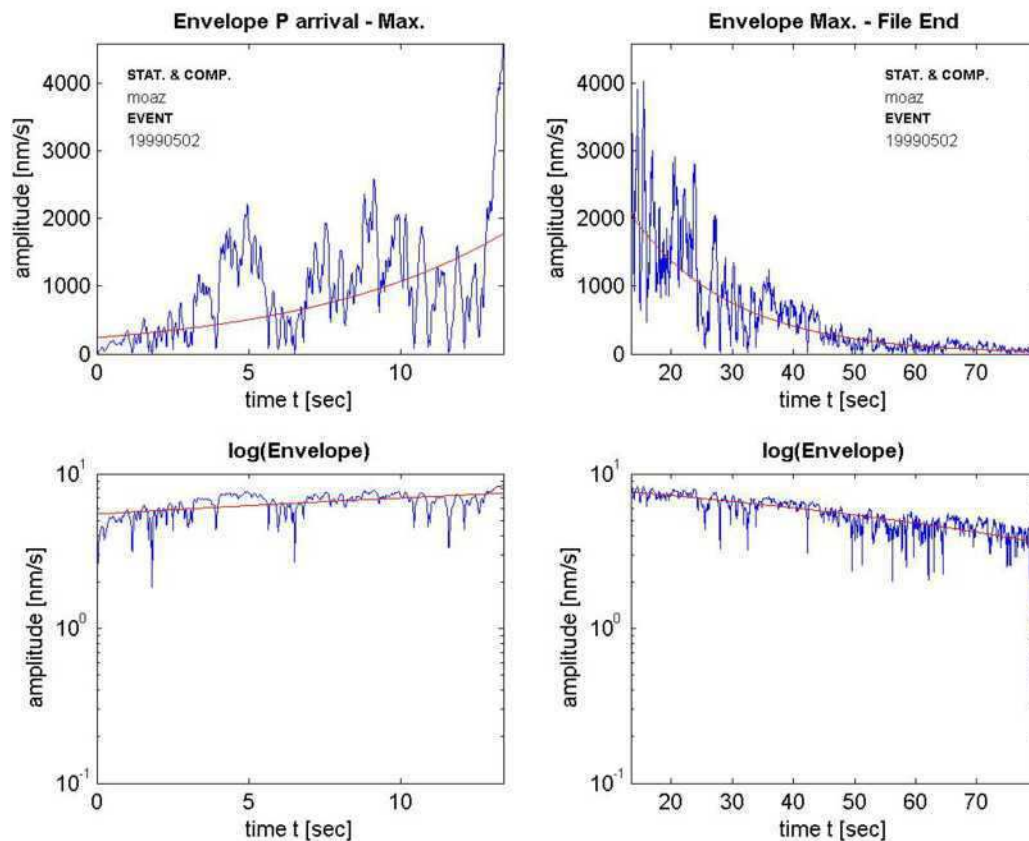


Figure 5-17 Envelope and exponential fit for the event of the 2nd of May 1999 on the left side from P arrival to the maximum value and on the right side for the remaining trace. Below the logarithm of the same traces is given with a linear fit. The traces refer to station MOA and the Z-component.

At first it should be noted that the maximum amplitude for the event in 2011 is approximately twice as big as the one in 1999 which cannot be explained with the help of the magnitudes as both events have one of 3.1. Still, for the later event a macroseismic intensity of 4 was assigned whereas no such value exists for the earlier one.

In general it can be said on the basis of Figure 5-17 that with the E-component having the most rapid increase in amplitude values for both events, the slope of the exponential fit for the increasing part characterizing the shape of the envelope decreases from the E-components to the Z-components. Comparing the traces for N-components one has to draw its attention to the time axis. While the maximum for the event in 2011 appears after about 15 seconds, for 1999 the maximum is already present much earlier after almost ten seconds. But considering the traces in detail, both events are rich in amplitudes at 10 and 15 seconds and can therefore be classified as events of the same source with equal signal shape. Traces of the Z-component bear an uncanny resemblance. Considering the maximum after about 5 seconds, the traces are similar.

5. Data Processing and Quantification

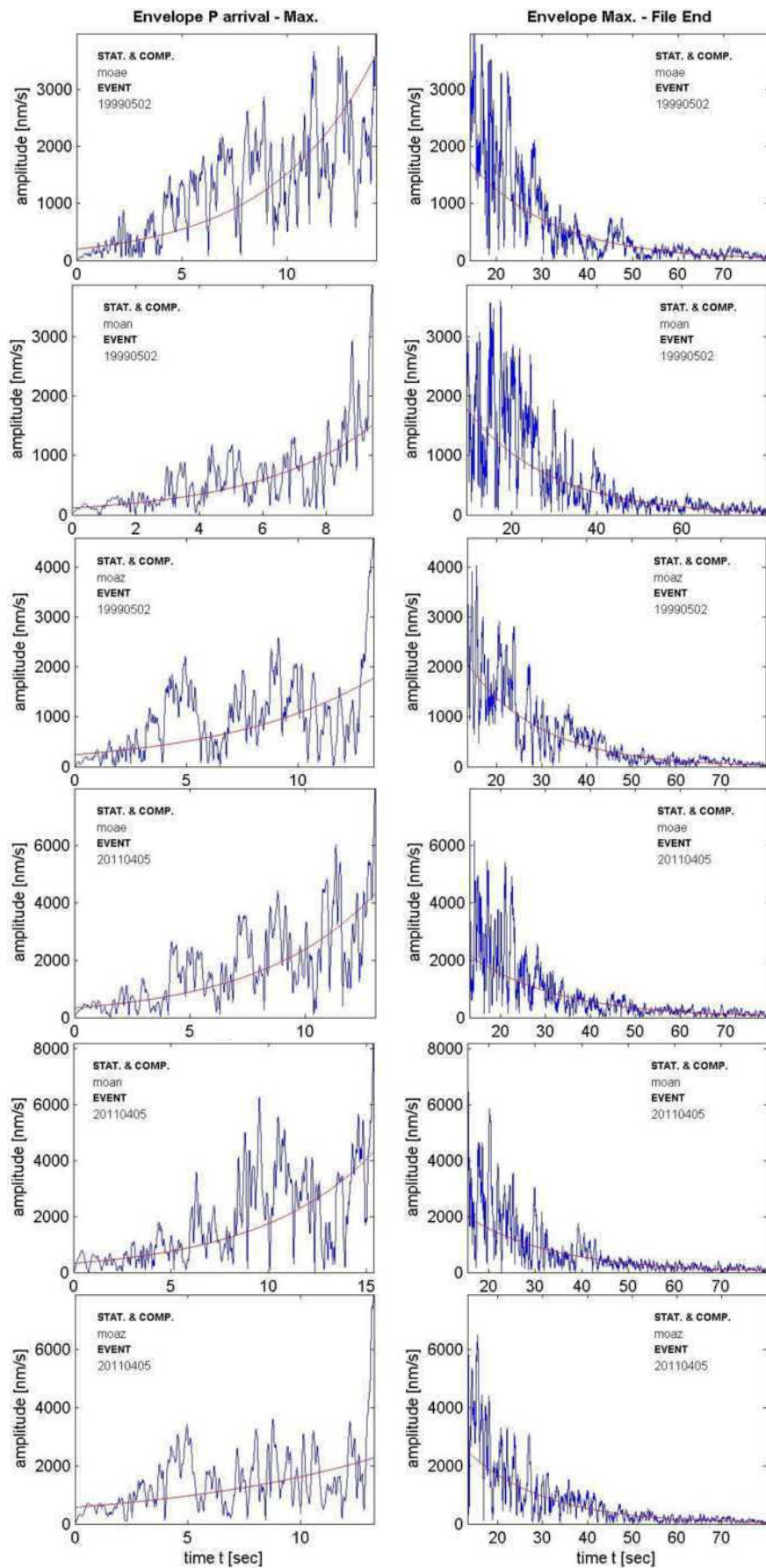


Figure 5-18 Envelope of all three components (E on top, N in the middle, Z at the bottom) for the events of the 2nd of May 1999 and 5th of April 2011 at station MOA. The traces are cut at their maximum value for applying an exponential fit.

5. Data Processing and Quantification

There is a continuous increase in amplitudes to about 5 seconds following a fast decrease with the minimum at approximately 6 seconds. Both events have their maximum at roughly 15 seconds after a very fast amplitude increase. Considering the down going part on all three components, no remarkable abnormalities can be detected.

To compare LPEs and earthquakes, the mean value of “a”, “ a_{exp} ” and “b” of the coda are calculated. The great variation in “a” and “ a_{exp} ” is most likely to be a result of calculating the mean value from all data. To obtain a more convincing result data of earthquakes with magnitudes greater than 3.1, which refers to the maximum amplitude of the long-period data, are neglected. The results are shown in Table 5-6 for the up going part starting at the P arrival ending at the maximum amplitude and for the down-going part with the remaining trace in Table 5-7.

Table 5-6 Mean values for the intersection with the ordinate (“a” and “ a_{exp} ”) and for the slope “b” for station MOA and KBA for LPEs and earthquakes for the up going part.

station	component	LPE			Earthquake		
		a	a_{exp}	b	a	a_{exp}	b
MOA	E	3.930	71.3	0.1458	4.796	223.5	0.1531
	N	3.829	62.5	0.1565	4.848	217.3	0.1576
	Z	3.945	83.6	0.1387	4.701	189.8	0.1339
KBA	E	3.647	56.4	0.1381	4.693	168.6	0.1891
	N	4.263	110.3	0.0682	5.044	287.2	0.1111
	Z	4.183	98.7	0.0758	4.847	160.7	0.1415

Table 5-7 Mean values for the intersection with the ordinate (“a” and “ a_{exp} ”) and for the slope “b” for station MOA and KBA for LPEs and earthquakes for the down going part.

station	component	LPE			Earthquake		
		a	a_{exp}	b	a	a_{exp}	b
MOA	E	5.658	686.8	-0.0393	6.362	1139.4	-0.0416
	N	5.711	706.1	-0.0395	6.517	1333.0	-0.0420
	Z	5.616	705.9	-0.0410	6.118	823.8	-0.0422
KBA	E	5.309	470.6	-0.0357	5.964	880.1	-0.0423
	N	5.208	406.4	-0.0351	5.657	648.1	-0.0366
	Z	5.375	522.0	-0.0346	5.592	470.8	-0.0353

Both tables explicitly reveal that for earthquakes the mean value of “a” is greater than the one for LPEs in the up going as well as the down going part for all three components and for both stations. The same statement can be made for the mean value of the slope as “b” for earthquakes is higher when compared with those of LPEs. It also has to be pointed out that for station KBA, the differences of the mean values of the two event types is clearer than for station MOA. Thus, calculating the envelope and its exponential fit can be of great help for separating source mechanisms.

6 Correlation

6.1 Correlation with Precipitation Data

In literature one finds several articles (e.g. , KRAFT, 2006 or KRAFT et al., 2006) referring to the interaction of precipitation and subsequent failure explained by hydromechanical coupling: an increase of the pore fluid pressure reduces the effective normal stress (HAINZL et al., 2006) For example HAINZL et al. (2006) states that earthquakes in a few kilometre depth can be triggered by precipitation as the crust reacts on tiny pressure variations and calculated an appropriate model as can be seen in Figure 6-1.

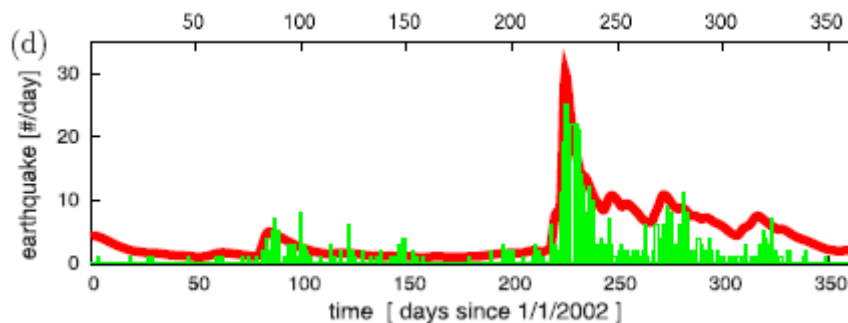


Figure 6-1 The daily number of detected earthquakes (green) in comparison with the theoretical rate for the 1-4 km depth interval (red). (HAINZL et al., 2006).

Depending on the geological and geomorphological setting of a region it can be more likely to trigger mass movements at the earth's surface. These mass movements can either occur more or less contemporaneously with the precipitation (COE et al., 2007) or be a consequence of preceding rainfall (CHLEBORAD et al., 2006). CHLEBORAD et al. (2006) define empirical rainfall thresholds as well as a formula for a cumulative rainfall threshold for Seattle, Washington. There, they consider the rainfall during the previous 3 and 15 days. Beside amount of rainfall and frequency and description of the resulting landslide, WIECZORE et al. (2009) additionally consider the duration and type of storm. They predict a threshold that represents minimum values necessary for triggering debris flows in the Blue Ridge of Central Virginia.

In this thesis the cause of the LPES is assumed to be some kind of a mass movement and therefore the correlation with the external factor of precipitation is taken into account.

6. Correlation

6.1.1 Meteorological stations

The epicentres of the events are spread around Bad Ischl with a maximum distance of 20 km and therefore the precipitation data of different meteorological stations is used for correlation (Table 6-1 and Figure 6-2). For each event the measurements of the closest station are taken.

Table 6-1 Meteorological stations of ZAMG with the TAWES (Teilautomatisches-Wetter-Erfassungs-System) name and number and its coordinates.

TAWES Name	TAWES Nr.	Longitude [°]	Latitude [°]
Bad Goisern	11354	13.6180	47.6425
Bad Aussee	11356	13.7827	47.6111
St. Wolfgang	11357	13.4527	47.7369
Bad Ischl	11361	13.6472	47.7061

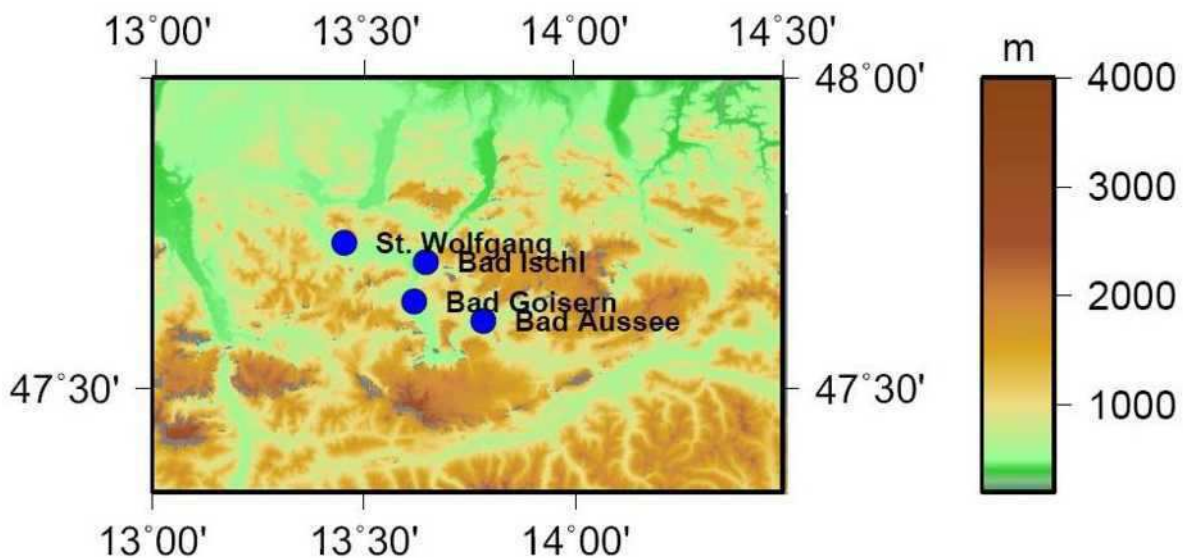


Figure 6-2 Meteorological stations for precipitation data in the surrounding of Bad Ischl.

6. Correlation

6.1.2 Precipitation data

The precipitation data were also contributed by ZAMG. Table 6-2 is an extract from a data sheet with measurements. More precisely, it belongs to the event on the 12th of October 2004 and aside the station number it displays the maximum time span of data used for a particular event. The considered time span starts 28 days before the day of the event and ends on that day. Measurements are taken every 10 minutes and are measured in $\frac{1}{10}$ mm. The corresponding time series is given in Figure 6-3 whereas these time series are later used for visually analyzing the data.

Table 6-2 Extract from a data sheet with precipitation values provided by ZAMG.

station number	date	time	precipitation
		hh mm	$\frac{1}{10}$ [mm]
11356	20040914	10	0
11356	20040914	20	0
...
11356	2004 10 10	320	0
11356	2004 10 10	330	0
11356	2004 10 10	340	6
11356	2004 10 10	350	1
11356	2004 10 10	400	1
11356	2004 10 10	410	0
11356	2004 10 10	420	8
11356	2004 10 10	430	11
11356	2004 10 10	440	5
11356	2004 10 10	450	7
11356	2004 10 10	500	3
11356	2004 10 10	510	0
...
11356	20041012	2350	0
11356	20041012	2400	0

6. Correlation

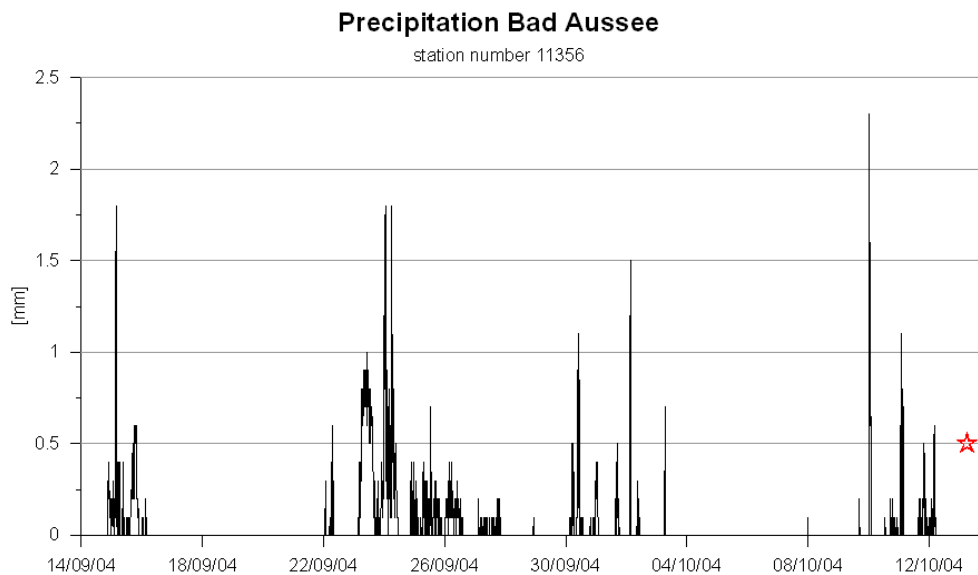


Figure 6-3 Example for a time series of precipitation. The event took place on the 12th of October 2004. The time series begins four weeks (28 days) before, namely the 14th of September 2004, whereas the next meteorological station is located in Bad Aussee. The red star indicates the focal time of the LPE.

6.1.3 Quantification

The data has to be quantified in some ways to compare the precipitation of the particular events. Its aim is to find regularities within four weeks (28 days) before the LPEs are possibly triggered. On that account the total amount of precipitation is calculated for each event. Primarily all values are summed up whereas thereafter only the sum of the last two weeks is considered.

The time series are also analyzed visually. The peaks of precipitation are roughly divided into separate precipitation periods whereas again the data is analyzed in total and separately for the last two weeks before the event. Beside the number of the periods a focus is also put on the time of its appearance, which leads to a classification based on broadly defined categories (Table 6-3).

Based on these five categories each time series is analyzed visually and the results are given in Table 6-4. Some explanations have to be made for a better understanding of the table. Primarily the data is sorted by stations and the date of the event. As additional information the magnitude is also listed. The following four columns give the amount of precipitation in mm for both four and two weeks together with the maximum precipitation within 10 minutes.

6. Correlation

Table 6-3 Description of broadly defined categories for precipitation quantification.

Category	Description
1	precipitation within the last 24 hours
2	precipitation within the last week
3	enhanced precipitation about 2 weeks before
4	enhanced precipitation about 3 weeks before
5	overall great amounts of precipitation

For detailed consideration these amounts are shown in Figure 6-4. The histogram on top represents the precipitation within the last four weeks before the LPE is triggered. As in each case only two events took place in the immediate vicinity of Bad Ischl and St. Wolfgang no clear statement can be made about a correlation of precipitation and mass movement. However, enough values are available for the other two stations. For Bad Aussee it can be said that within the last four weeks the full range from 30 to 220 mm of precipitation is evenly represented whereas for the last two weeks most events follow a period of precipitation between 20 and 80 mm. The precipitation data measured in Bad Goisern has a peak at 100 to 110 mm at four events. Also most events have less than 150 mm of precipitation within the last four weeks. An even more detailed statement can be made for the last two weeks, as more than half of the LPEs occur after precipitation periods of 20 to 60 mm. Furthermore it is worth mentioning that two events detected in the proximity of Bad Goisern even took place after a relatively small amount of less than 10 mm of precipitation. Combined with the fact that an event also took place with less than 30 mm within four weeks the mass movements are most likely a result of a complex mechanism with variable factors contributing.

Considering the data from the four stations altogether, the following conclusion can be made: If the correlation of precipitation and triggered mass movements is decisive in this thesis it can be said that analyzing the amount of precipitation within the last two weeks is quite useful as a peak is detected in the histogram. With precipitation of less than 80 mm a mass movement is likely to take place whereby the different regions are surely distinctive.

Also given in Table 6-4 are the results of the time series analysis based on the categories defined in Table 6-3. A dot (•) implies that the conditions are clearly complied, a plus (+) indicates that the category is fulfilled but only small amounts of precipitation were measured. The plus-minus sign (\pm) signifies that the category demands are only identifiable to some extent whereas a blank character () states that this category is not fulfilled.

In Bad Aussee most LPEs occurred during a rain period following greater amounts of precipitation within the preceding one to two weeks whereas for all events there was definitely precipitation in the last days before the mass failure. Considering the maximum value in the preceding two weeks only three values exceed 5 mm within 10 minutes. Also, generally speaking there is no need of great amounts of rain in the forgoing four weeks.

6. Correlation

Table 6-4 Results of the analysis of precipitation data.

Date	Magnitude	Precipitation [mm]				Precipitation Periods		Category				
		4 weeks		2 weeks		4 weeks	2 weeks	1	2	3	4	5
		total	max	total	max							
BAD AUSSEE												
1999 05 02	3.1	117.3	2.4	52.6	2.4			+	+	•	•	•
2002 06 30	2.0	180.9	5.6	63.2	5.6	5	4	+	•		•	+
2002 07 20	2.1	124.2	6.2	70.6	6.2	7	4		•		+	•
2004 05 08	1.5	61.0	1.7	37.8	1.7	7	4	+	+	•		±
2004 10 12	1.5	192.9	2.3	46.8	2.3	4	2		•	•	•	±
2006 02 22	3.0	88.8	0.8	60.9	0.8	3	2 - 3		+	•	•	
2006 05 27	2.3	140.2	2.1	116.5	2.1	5	3	+	•	•		+
2006 12 16	2.7	51.2	1.0	23.2	1.0	4	2		+	+		
2007 12 10	2.0	134.0	1.0	85.8	0.9	3	2	+	+	+	+	
2008 07 23	2.0	370.6	4.7	140.8	3.2			•	•	•	±	•
2010 01 19	2.7	47.1	0.9	22.3	0.9	6	2	•	•		±	
2010 01 23	2.3	32.0	0.9	22.6	0.9	5	2		+		+	
2011 04 05	3.1	91.3	1.2	42.4	1.1	5	3	•	+	+	+	
2011 08 10	2.0	111.5	5.4	68.8	5.4	3	1	•	•		+	+
2011 12 26	1.5	120.6	1.2	77.5	0.8				+	+	+	±
BAD GOISERN												
2000 04 18	2.3	97.3	1.3	38.1	1.1	9	5	+	±	+	•	±
2000 06 25	2.6	157.6	12.2	119.3	12.2	7	5	+	•	•	+	±
2000 08 29	2.1	81.1	2.5	6.5	0.5	3	2		±	•	•	+
2000 11 09	1.7	29.8	0.8	24.2	0.8	5	4		±	±	±	
2001 04 25	1.8	107.4	0.8	50.6	0.8			+	+	+	+	•
2002 11 18	2.0	169	1.2	97.9	1.2			+		•	•	•
2003 07 14	2.9	134.5	5.0	88.2	5.0	4	2		•	•	±	•
2003 09 18	2.1	193.9	3.1	133.5	3.1	2	2		•	+	•	±
2006 03 28	1.8	122.4	1.1	46.5	1.0			•	•	±	•	•
2006 04 27	1.5	97.7	1.7	39.6	1.2	7	4	•		+	•	+
2006 05 18	2.6	103.6	1.9	54.6	1.9	4	3	+	•		•	±
2006 08 22	2.3	50.3	4.0	39.7	4.0	4	3	•	•	+	±	±
2006 09 26	1.9	125.9	2.2	76.8	2.2	6	3	+		•	+	+
2006 12 15	2.9	42.4	1.0	23.7	1.0	5	3			+	+	
2007 03 18	1.4	106.3	1.1	31.4	0.7	4	3	+		•	•	±
2007 03 27	2.2	130.3	1.1	48.6	0.6	5	3		•		+	±
2007 06 04	1.0	149	2.1	43.9	2.1	7	5	+	+	±	•	•
2008 01 22	1.4	54.1	0.9	32.2	0.5	5	3	+	+	+	+	
2008 03 02	1.8	70.2	1.6	45.4	1.6	4	3	•	•		±	±

6. Correlation

Table 6-4 Continuation.

Date	Magnitude	Precipitation [mm]				Precipitation Periods		Category				
		4 weeks		2 weeks		4 weeks	2 weeks	1	2	3	4	5
		total	max	total	max							
BAD GOISERN												
2008 05 03	2.5	107.9	1.4	76.9	1.4			+	+	•	+	+
2009 01 06	1.3	124.3	1.3	7.2	0.4	2	1			•	•	+
2009 05 06	2.1	76.1	2.7	59.6	2.7	5	4	+	+	+	±	±
2010 01 24	2.3	33.9	0.6	22.6	0.6	3	2		•	+	±	
2010 04 23	1.4	86.7	0.9	39.6	0.9				±	±	±	±
BAD ISCHL												
2010 09 18	1.7	201.2	11.4	30.1	2.1			+	+	+	•	•
2010 10 23	2.4	50.5	1.1	23.9	1.1	5	2		•		+	±
ST. WOLFGANG												
2006 11 24	1.7	186.0	4.4	98.6	1.4	7	4		+	•	•	+
2010 05 03	2.2	49.2	1.1	12.4	0.8	6	4	+		+	+	±

When looking at the events in the vicinity of Bad Goisern, a consistency is detected in the precipitation data. At least one rain period predates every long-period seismic signal in the third week before. Except for three and six events respectively there is also a noticeable amount of precipitation in the second and the first week before. This leads to the fact that for that specific data set nine of 15 possible events do not require precipitation within the last 24 hours before the failure as trigger anymore. Another noticeable fact is that in most cases the maximum values measured in ten minutes are quite low. The data leads to the conclusion that in Bad Goisern there is no need for a lot of precipitation within a short time span but a great amount of precipitation over a longer time period is necessary to trigger mass movements which can also be seen in Figure 6-4 as the maximum in the upper graphic is about 100 mm precipitation in four weeks and about 40 mm in two weeks.

Data from Bad Ischl and Sankt Wolfgang cannot be interpreted due to the small number of events.

For further interpretation and correlation of the precipitation data the measurement values of each day are summed up and termed “S₁” for the sum of day one to “S₂₉” for the sum of day 29 respectively. To find consistency in rain periods S_i values of the different events are added up; this means that “S_i” of same days before each event are summed up and divided by the number of events. The results are visualized in Figure 6-5.

6. Correlation

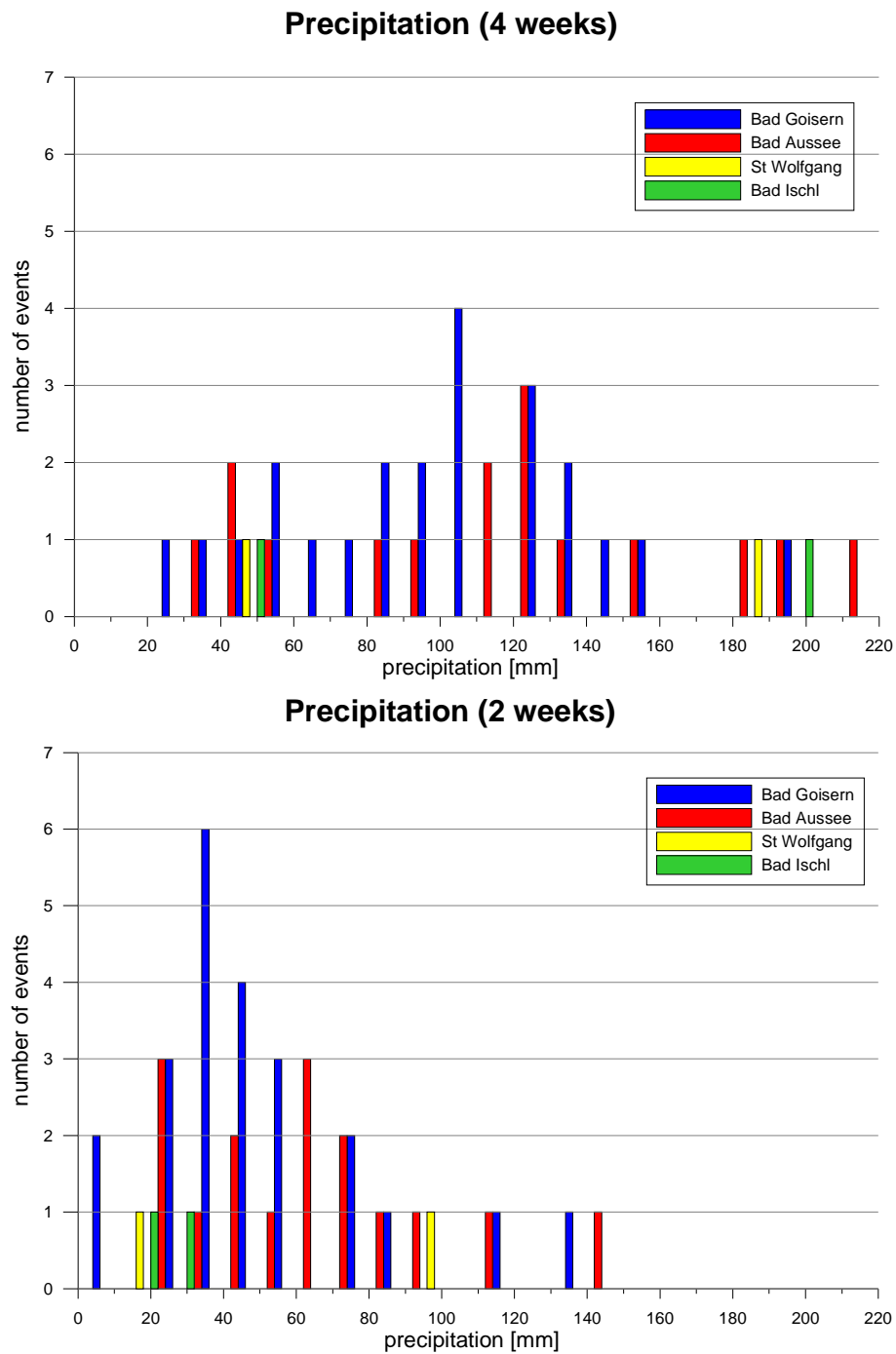


Figure 6-4 Histogram showing the number of events per amount of precipitation within the last 4 weeks (top) and 2 weeks (bottom) for the four weather stations.

6. Correlation

For the meteorological station in Bad Goisern the following can be said: Four peaks can be detected: one starting two days before the event, the second one from day six until day eleven, the third period lasts from day 16 until day 19 and passes over to the last period that has its peak at day 26 and 27. All in all the day of maximum precipitation is 18 days before the event whereas one minimum is located at day 14. Generally speaking a variation in amounts of precipitation can be found and might be responsible for mass movements triggering LPEs.

By contrast these four peaks cannot be found on the right side of Figure 6-5, which shows the precipitation data at station Bad Aussee. The graphic rather signalizes constantly precipitation with an increase within the last ten days. Most strikingly are the amounts of precipitation shortly before the event is triggered as well as on the day of the event. Of course, day 19 and day 23 do not fit to this observation but it is not obvious that these two days signalize the peak of a rain period.

With the help of Figure 6-5 it can be said that in case of a correlation with precipitation data the triggering mechanism of a mass movement depends on very specific local settings. The statements have to be made separately for each station. Also the small number of events does not allow for a distinct conclusion. Thus no general conclusion of a correlation of meteorological data and triggering mass movements can be made, but maybe a continuation of collecting LPEs from the surrounding of Bad Ischl can confirm the above detected characteristics.

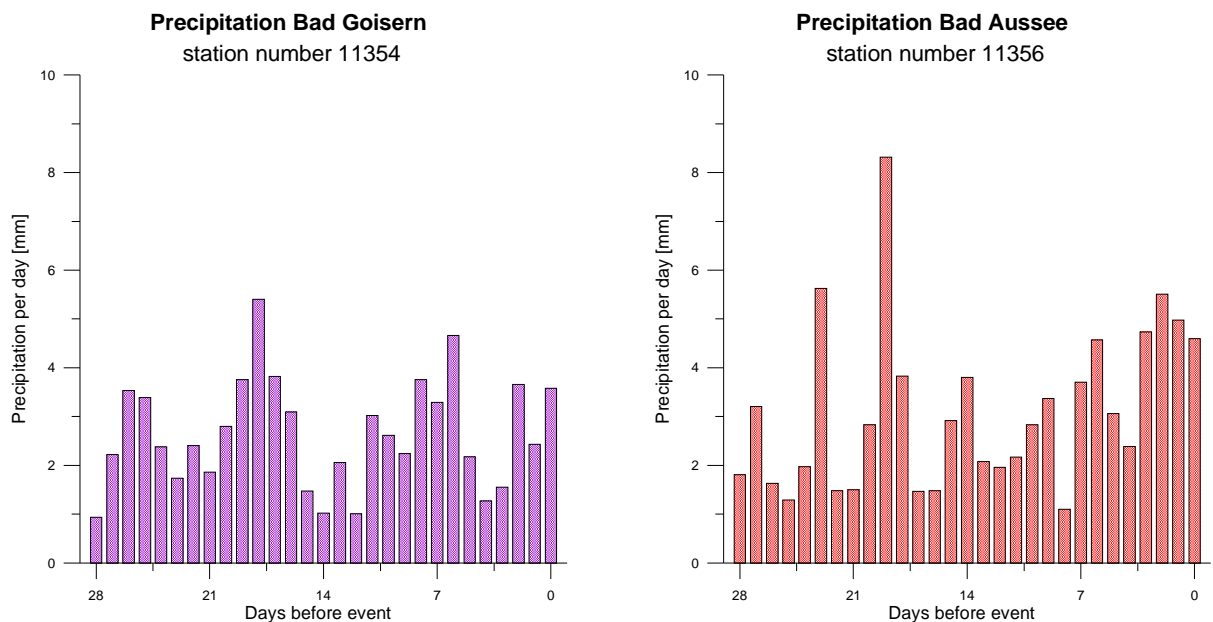


Figure 6-5 Precipitation data for Bad Goisern (left) and Bad Aussee (right). Data are summed up daily before every single event.

6. Correlation

Last but not least, the mean value of “ S_i ” for each event is calculated. Combined with the standard deviation further statements of the precipitation data shall be made. The results are presented in Figure 6-6.

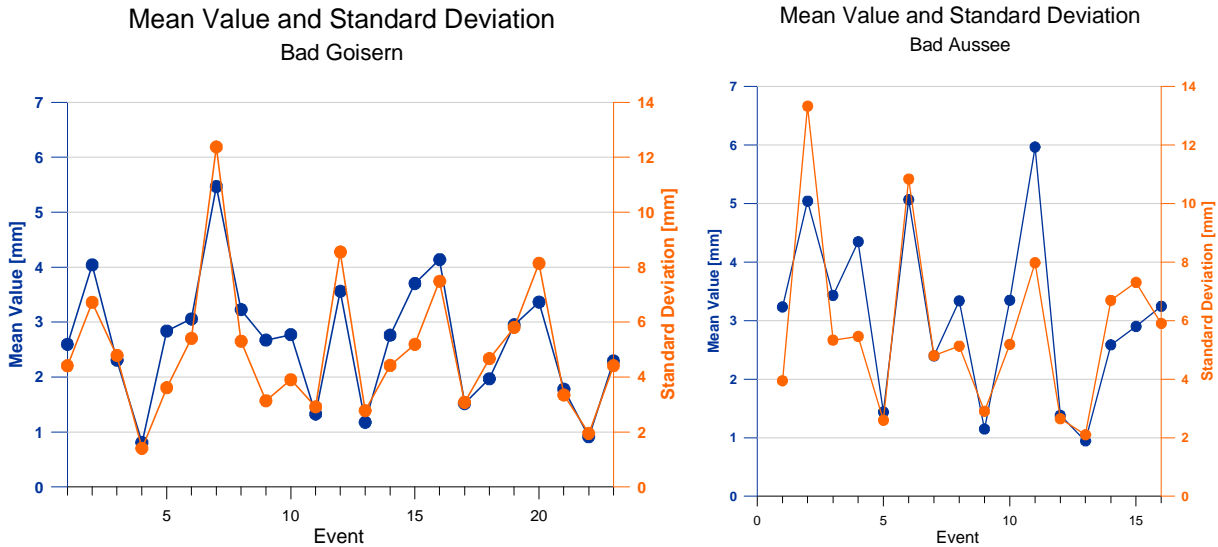


Figure 6-6 Mean values (blue) and standard deviation (orange) for the precipitation data measured at the station in Bad Goisern (left) and the station in Bad Aussee (right) for each event. Note, that the axis of the standard deviation is twice the one of the mean value.

Again the two stations are considered separately. On the left side of the figure the results from the meteorological station in Bad Goisern are displayed. It can be seen, that the curve of the mean value (blue) and the one of the standard deviation (orange) fit very well in most cases whereas the axis of the standard deviation is twice the axis of the mean value. Thus, for higher mean values also the standard deviation is greater, namely by a factor two. This means that for LPEs with a lot of rain in the four weeks before the event the precipitation did not occur always as the standard deviation is high. Therefore the assumption can be made that the precipitation came in separate rainfall periods lasting several days. This correlates with the previously found results that triggering the LPEs in the surrounding of Bad Goisern goes hand in hand with up to four precipitation periods within four weeks.

On the contrary, the curves for the mean value and the standard deviation do not fit as well when considering the data measured at the meteorological station in Bad Aussee. No general assumption can be made as in seven cases the mean values coincide with the standard deviation, in all remaining cases there is an obvious gap. As these fits and misfits also do not depend on the mean value itself, no general statement can be made for this analysis for the particular meteorological station.

6. Correlation

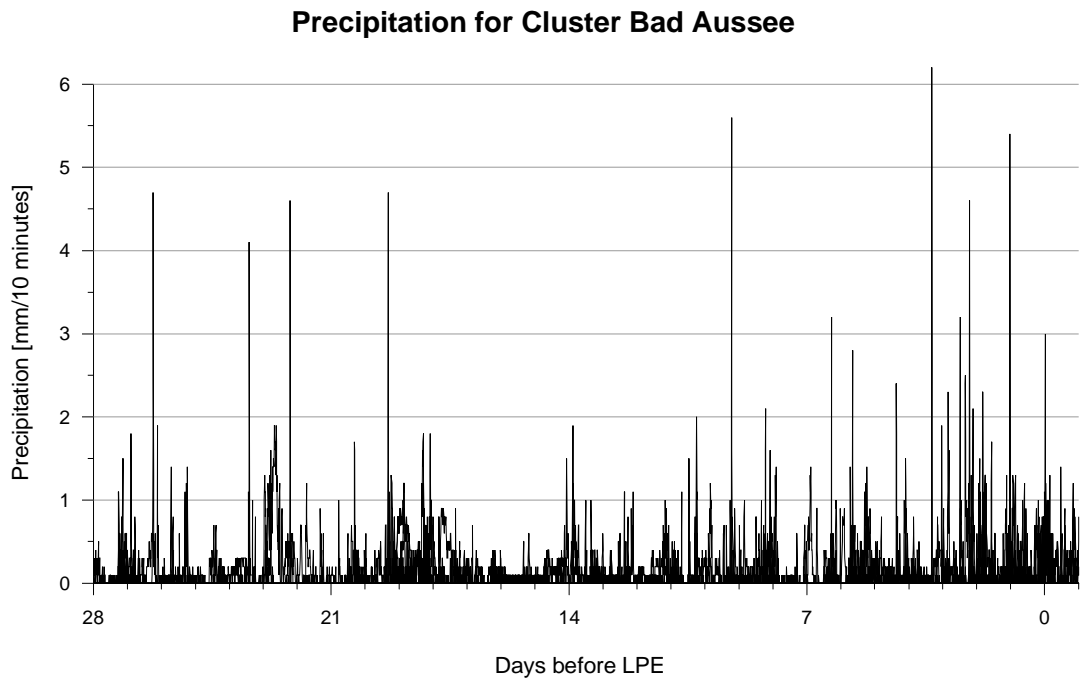


Figure 6-7 Precipitation data from all LPEs recorded closest to the meteorological station Bad Aussee.

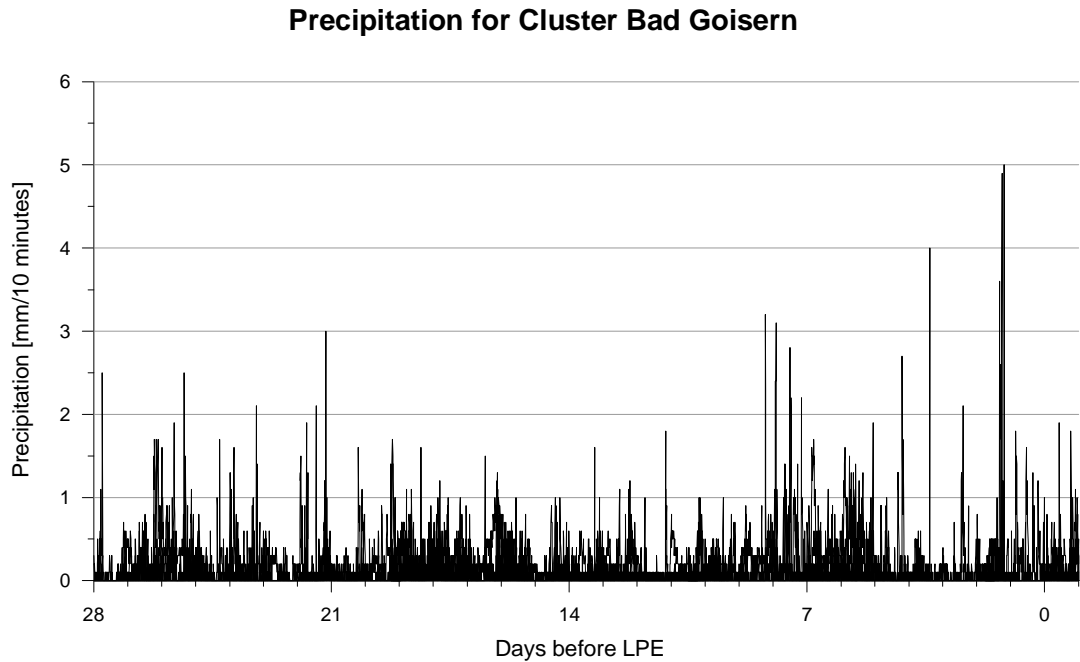


Figure 6-8 Precipitation data from all LPEs recorded closest to the meteorological station Bad Goisern.

6. Correlation

Finally, to discuss the precipitation data and the results from the methods applied previously, two more figures are added. Figure 6-7 and Figure 6-8 show the time series of all precipitation data used in this thesis for the respective station except for the event of the 25th of June 2000, because it exceeds the maximum value of the y-axis by a factor of two. From Figure 6-7 no statements can be made, but one noticeable detail can be extracted, namely the occurrence of single heavy precipitation events. Still, all in all no satisfying result can be achieved by the evaluation of the precipitation data in the close vicinity of Bad Aussee.

Figure 6-8 shows the time series recorded at station Bad Goisern. Again, up to four precipitation periods can be detected together with a low constant rate of precipitation. Combined with the other methods more useful information can be gained from evaluating the precipitation data at station Bad Goisern than at Bad Aussee.

Finally, from the above mentioned analyses of the precipitation data the following can be said: No general statements can be made for the individual methods as there are always apparent differences concerning various meteorological stations. Still, for Bad Goisern some regularity could be detected. Thus further investigations in analyzing precipitation data in respect to long-period seismic events are useful when having a larger data set.

6.2 Correlation with the geological and geotechnical Setting

In chapter 4 an overview of the geological and geotechnical setting was given. Considering the fact that from a geotechnical point of view most of the mass movements are related to the system “Hart auf Weich”, the calculation of the area of failure is of great interest.

First of all, the seismic moment has to be approximated with the help of the formula of HANKS and KANAMORI (1979)

$$M_W = \frac{2}{3} * \log(M_0) - 6.1 \quad (6.1)$$

where “ M_W ” is the frequency independent moment magnitude and “ M_0 ” is the seismic moment. It implies a constant stress drop of 10^{-4} of the shear modulus, which is reasonable for tectonic earthquakes. Still, a modification of the formula can be used in the case study of Bad Ischl as the stress drop of 10^{-4} of the shear modulus also approximates the cohesion along a tectonic fault plane. The local magnitude “ M_L ” is used instead of the moment magnitude (pers. comm. Lenhardt). Thus, the formula to calculate the seismic moment reads as follows

$$M_0 = 10^{(1,5 * M_L + 9,1)} \quad (6.2)$$

Furthermore the shear modulus “ μ ” and the displacement “ D ” are used to calculate the area of failure “ A ” based on the formula

$$M_0 = AD \quad (6.3)$$

e.g. LAY and WALLACE (1995). McGARR (1991) gives a calculation path for the displacement “ D ” with “ v_s ” as the S-wave propagation velocity, “ ρ ” as the rock density, “ R ” as the distance from the source, “ v_{max} ” as the far field peak ground with the assumption that the shear stress drop “ σ ” is $10^{-4} \mu$ (HANKS and KANAMORI, 1979):

$$\mu = v_s^2 \rho \quad (6.4)$$

$$R v_{max} = \frac{0.0686}{\rho v_s} \sqrt[3]{(10^{-4} \mu)^2 M_0} \quad (6.5)$$

$$D = \frac{8.1 R v_{max}}{v_s} \quad (6.6)$$

6. Correlation

With the values for “ M_0 ”, “ μ ” and “ D ” the size of the respective fault plane “ A ” is calculated with formula (6.3). In addition the square root of the plane “ A ” is calculated as an approximation to the side length “ S_L ” of the area of failure.

Values for the shear wave velocities “ v_s ” of limestone were taken from the internet (last access 06/06/2012). As there is a great amount of data available with differing information the area was calculated twice with a “ v_{min} ” of 1800 m/s and a “ v_{max} ” of 3300 m/s. This great variety arises from many different factors with one of them being the density. As limestone can be both porous and massive depending on its genesis, also a minimum and a maximum value are chosen for the density with “ ρ_{min} ” being 1.8 g/cm³ and “ ρ_{max} ” 2.8 g/cm³.

Thus, the fault plane was calculated three times with the respective values given in Table 6-5.

Table 6-5 Shear wave velocities and densities for limestone.

Shear wave Velocity v_s		Density ρ
[m/s]		[kg/m ³]
min	1800	1800
mean	2550	2300
max	3300	2800

The following Tables (Table 6-6 to Table 6-8) show the results for the three clusters separated in chapter 4.

Table 6-6 Displacement “ D ”, fault plane “ A ” and its side length “ S_L ” for minimum, mean and maximum shear wave velocity and density, respectively, for LPEs near Hallstatt.

HALLSTATT		MIN			MEAN			MAX		
date	mag	D	A	S_L	D	A	S_L	D	A	S_L
yyyy mm dd		[m]	[m ²]	[m]	[m]	[m ²]	[m]	[m]	[m ²]	[m]
2001 04 25	1.8	0.006	18966	138	0.004	10123	101	0.003	6296	79
2003 09 18	2.1	0.008	37842	195	0.006	20198	142	0.005	12562	112
2006 08 22	2.3	0.010	59976	245	0.007	32012	179	0.006	19910	141
2007 03 27	2.2	0.009	47641	218	0.007	25428	159	0.005	15815	126
2008 03 02	1.8	0.006	18966	138	0.004	10123	101	0.003	6296	79
2008 05 03	2.5	0.013	95056	308	0.009	50736	225	0.007	31555	178
2009 05 06	2.1	0.008	37842	195	0.006	20198	142	0.005	12562	112
2010 01 24	2.3	0.010	59976	245	0.007	32012	179	0.006	19910	141

6. Correlation

Table 6-7 Displacement “D”, fault plane “A” and its side length “S_L” for minimum, mean and maximum shear wave velocity and density, respectively, for LPEs near Bad Goisern.

BAD GOISERN		MIN			MEAN			MAX		
date	mag	D	A	S _L	D	A	S _L	D	A	S _L
yyyy mm dd		[m]	[m ²]	[m]	[m]	[m ²]	[m]	[m]	[m ²]	[m]
2000 04 18	2.3	0.010	59976	245	0.007	32012	179	0.006	19910	141
2000 08 29	2.1	0.008	37842	195	0.006	20198	142	0.005	12562	112
2003 07 14	2.9	0.020	238770	489	0.015	127444	357	0.012	79262	282
2006 04 27	1.5	0.004	9506	97	0.003	5074	71	0.002	3155	56
2006 05 18	2.6	0.014	119668	346	0.010	63873	253	0.008	39725	199
2006 12 15	2.9	0.020	238770	489	0.015	127444	357	0.012	79262	282
2009 01 06	1.3	0.003	5998	77	0.002	3201	57	0.002	1991	45
2010 04 23	1.4	0.004	7551	87	0.003	4030	63	0.002	2506	50
2010 10 23	2.4	0.011	75506	275	0.008	40301	201	0.007	25065	158

Table 6-8 Displacement “D”, fault plane “A” and its side length “S_L” for minimum, mean and maximum shear wave velocity and density, respectively, for LPEs near Bad Aussee.

BAD AUSSEE		MIN			MEAN			MAX		
date	mag	D	A	S _L	D	A	S _L	D	A	S _L
yyyy mm dd		[m]	[m ²]	[m]	[m]	[m ²]	[m]	[m]	[m ²]	[m]
1999 05 02	3.1	0.025	378424	615	0.019	201985	449	0.015	125622	354
2000 06 25	2.6	0.014	119668	346	0.010	63873	253	0.008	39725	199
2002 06 30	2.0	0.007	30059	173	0.005	16044	127	0.004	9979	100
2002 07 20	2.1	0.008	37842	195	0.006	20198	142	0.005	12562	112
2004 05 08	1.5	0.004	9506	97	0.003	5074	71	0.002	3155	56
2004 10 12	1.5	0.004	9506	97	0.003	5074	71	0.002	3155	56
2006 02 22	3.0	0.023	300593	548	0.017	160442	401	0.013	99785	316
2006 03 28	1.8	0.006	18966	138	0.004	10123	101	0.003	6296	79
2006 05 27	2.3	0.010	59976	245	0.007	32012	179	0.006	19910	141
2006 12 16	2.7	0.016	150653	388	0.012	80412	284	0.009	50011	224
2007 12 10	2.0	0.007	30059	173	0.005	16044	127	0.004	9979	100
2008 07 23	2.0	0.007	30059	173	0.005	16044	127	0.004	9979	100
2010 01 19	2.7	0.016	150653	388	0.012	80412	284	0.009	50011	224
2010 01 23	2.3	0.010	59976	245	0.007	32012	179	0.006	19910	141
2011 04 05	3.1	0.025	378424	615	0.019	201985	449	0.015	125622	354
2011 08 10	2.0	0.007	30059	173	0.005	16044	127	0.004	9979	100
2011 12 26	1.5	0.004	9506	97	0.003	5074	71	0.002	3155	56

To discuss the values, four parameters (sum, mean value, minimum and maximum) are calculated for the displacement, the fault plane and the side length. The results are given in Table 6-9. Only the values calculated with mean shear wave velocity and mean rock density will be discussed in greater detail.

6. Correlation

Table 6-9 Sum, minimum, maximum and mean value for displacement “D”, fault plane “A” and its side length “S_L” for minimum/mean/maximum shear wave velocity and density.

		MIN			MEAN			MAX		
		D	A	S _L	D	A	S _L	D	A	S _L
		[m]	[m ²]	[m]	[m]	[m ²]	[m]	[m]	[m ²]	[m]
Hallstatt	Sum	0.070	376266	613	0.051	200833	448	0.040	124906	353
	Minimum	0.006	18966	138	0.004	10123	101	0.003	6296	79
	Maximum	0.013	95056	308	0.009	50736	225	0.007	31555	178
	Mean Value	0.009	47033	217	0.006	25104	158	0.005	15613	125
Bad Goisern	Sum	0.095	793586	891	0.070	423578	651	0.055	263440	513
	Minimum	0.003	5998	77	0.002	3201	57	0.002	1991	45
	Maximum	0.020	238770	489	0.015	127444	357	0.012	79262	282
	Mean Value	0.011	88176	297	0.008	47064	217	0.006	29271	171
Bad Aussee	Sum	0.195	1803933	1343	0.142	962853	981	0.112	598836	774
	Minimum	0.004	9506	97	0.003	5074	71	0.002	3155	56
	Maximum	0.025	378424	615	0.019	201985	449	0.015	125622	354
	Mean Value	0.011	106114	326	0.008	56638	238	0.007	35226	188

Figure 6-9 shows the cumulative curve of the displacements of each cluster. It can be seen, that for the region next to Bad Aussee (red line) and the region near Bad Goisern (green line) there is a greater variation in the single displacements compared to the LPEs in the closer vicinity of Hallstatt. This could be related to the smaller magnitude range, with a minimum magnitude of 1.8 and a maximum one of 2.5. At first, the displacement is more or less constant, with a higher mass movement rate starting in 2006 with one to two events each year until 2010.

Also, for the region of Bad Aussee the displacement is at

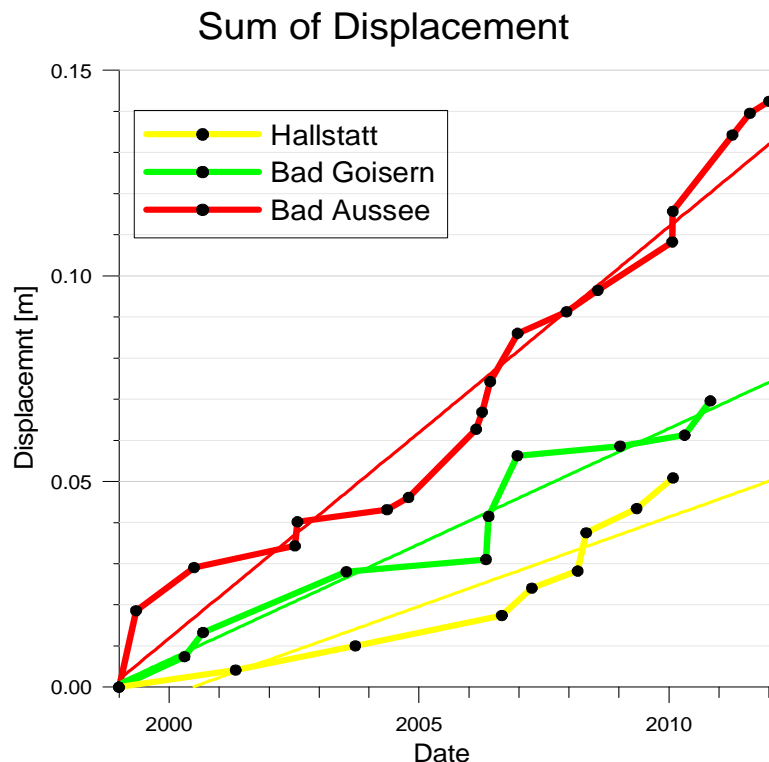


Figure 6-9 Cumulative curve of the displacement calculated for each cluster.

6. Correlation

a constant rate starting in 2006 with a minimum of mass movement from 2003 to 2005. Concerning the calculations at Bad Goisern a distinctive change in the displacement rate took place in 2006. Figure 6-9 reveals a step in 2006 and the other one starting in 2010.

All in all, the sum of the displacement in Bad Aussee comes up to nearly 0.15 metres in 13 years with 17 LPEs being detected. Also, a linear fit is applied to each curve. It shows that the displacement in the region of Bad Aussee (0.13 m) is far more than in the other two regions when extracting the values until 2012. Bad Goisern reaches a total displacement of about 0.07 m and Hallstatt of only 0.05 m.

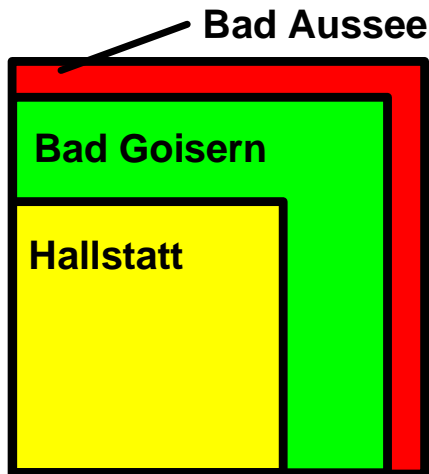


Figure 6-10 Size of fault plane when approximated by a square.

Another interesting aspect is to consider the fault plane and its different sizes in the three clusters. Therefore, the mean area of failure is approximated by a square (Figure 6-10). The LPEs near Bad Aussee appear to utilize the largest fault planes (238x238 m) while the ones near Hallstatt involve the smallest fault planes (158x158 m) respectively. Of course, this goes hand in hand with the cumulative curves of the displacement shown in Figure 6-9. Still the mean fault plane in the region of Bad Goisern is relatively big compared to the one in Bad Aussee as the total displacement in Bad Aussee is approximately twice the one of Bad Goisern.

To apply this information to the geological situation discussed in chapter 4 the smallest fault plane/displacement (Hallstatt) and the largest fault plane/displacement (Bad Aussee) are discussed.

As for Hallstatt, an up to 700 metres massive brittle cap-rock (e.g. Plassen) is located on an elastic basement (Alpine Haselgebirge). The above made calculations lead to the statement that a brittle rock with a base area of approximately 160x160 metres moves with approximately 9 mm on the softer basement. For all recorded LPEs the size of the fault plane as well as the displacement are more or less constant. To make statements about annual movements and compare them with the maximum annual movement of 16.6 mm mentioned by EHRET (2002) a more extensive seismic network in the closer vicinity is definitely necessary, so more LPEs can be detected with smaller magnitude (in case of occurrence).

To discuss the region northwest of Bad Aussee one has to remember that there were more possible locations where LPEs can be triggered and it was not a distinct unit like in Hallstatt. This can be one explanation for the greater variety in displacement. But in chapter 4 also an example of broken limy slabs on a softer basement was given (Sandling). The statement would then read as follows: A broken limy slab with a base area of approximately 238x238 metres moves with approximately 11 mm/a on a softer basement.

6. Correlation

Of course, the above mentioned statements are full of assumptions, but they still give a rough insight into the amounts of mass movements in the area of Bad Ischl and its surroundings. To get more detailed and significant information, a relocation of the LPEs is necessary. Then, with the help of geological expertise, the possible origins of the mass movement can be restricted and accurate rock density values as well as shear wave velocities can be determined. Thus, the calculation of displacement and fault plane would be more precise.

7 Discussion

Based on a data set of 43 long-period events (LPEs) near Bad Ischl, the aim of this diploma thesis discusses significant characteristics of LPE-seismograms. For that purpose various processing steps were applied to identify them reliably and distinguish them from tectonic earthquakes. Unfortunately, the next seismic station (MOA) from the seismological station network of Austria is approximately 50 km away from the region of interest, which is not suited to detect LPEs of magnitudes less than 1.0 and makes it difficult to detect significant characteristics in the low magnitude range (<1.0 to 1.5). In addition, the data of one more station was taken into account whereas the mean distance between source and receiver (KBA) amounts to almost 70 km.

Most of the processing was done with SAC (Seismic Analysis Code) as it meets all necessary demands. After considering the raw data attentively, it was concluded that a trace length of 80 seconds contains all necessary information, while the signal is still above the noise level. Table 7-1 lists the separate processing steps by alphabetical order and shows the abbreviations. All in all eleven different processing steps/calculations were applied to both the LPE data set and the tectonic earthquake data set to find out distinct differences.

Table 7-1 Processing steps and abbreviations.

Abbreviation	Processing Step
AC - s	AC - sum
AC - t	AC - time
AI	Arias Intensity
C	Coda
ES	Energy Signal
M	Magnitudes
RMS	Root Mean Square
SC	Spectral Content
SC - ma	SC - maximum amplitude
SC - mv	SC - mean value
SC - s	SC - sum

Thus, two tables are given below. They list all LPEs (Table 7-2) and tectonic earthquakes (Table 7-3) dependent on the processing steps (for abbreviations see Table 7-1). Applying each method, they show, whether the respective processed data fits very well (+) or not (-). Of course, not all results are clearly distinguishable and therefore another symbol is introduced for questionable results (~). Blank arrays indicate a lack of data. Additionally the magnitude is listed.

7. Discussion

Table 7-2 Very good fit (x), no fit (-) and questionable fit (~) of processed LPE data.

date yyyy mm dd	mag	Processing Steps										
		AC - s	AC - t	AI	C	ES	M	RMS	SC	SC - ma	SC - mv	SC - s
1999 05 02	3.1	x	x	x	x	x		x	x	x	x	x
2000 04 18	2.3	x	-	x	x	x		x	x	x	x	x
2000 06 25	2.6	x	x	x	x	~		~	x	x	x	x
2000 08 29	2.1	x	~	x	-	x		x	~	-	-	-
2000 11 09	1.7	-	~	x	-	~		~	-	x	x	x
2001 04 25	1.8	x	~	x	x	x		x	~	x	x	x
2002 06 30	2.0	x	x	x	x	x		x	x	-	x	x
2002 07 20	2.1	x	-	x	x	~		~	x	x	x	x
2002 11 18	2.0	x	x	x	x	x		x	~	x	x	x
2003 07 14	2.9	-	x	-	x	~		~	-	x	~	~
2003 09 18	2.1	x	x	x	x	x		x	-	x	x	x
2004 05 08	1.5	-	x	-	~	-		-	~	~	x	x
2004 10 12	1.5	~	x	-	x	-		-	~	x	x	~
2006 02 22	3.0	x	x	x	x	-		-	x	x	x	x
2006 03 28	1.8	-	x	x	x	~		~	~	-	x	x
2006 04 27	1.5	x	x	-	x	-	~	-	~	x	x	x
2006 05 18	2.6	x	~	x	x	x	~	x	x	x	x	x
2006 05 27	2.3	x	x	x	x	x	~	x	x	x	x	x
2006 08 22	2.3	x	x	x	x	x	~	x	x	x	x	x
2006 09 26	1.9	x	x	x	x	x	x	x	x	x	x	x
2006 11 24	1.7	x	x	x	x	x	-	x	~	x	x	x
2006 12 15	2.9	x	x	x	~	x	~	x	x	x	x	~
2006 12 16	2.7	x	x	x	x	x	~	x	x	x	x	x
2007 03 18	1.4	x	x	-	x	-	x	-	-	x	x	x
2007 03 27	2.2	x	x	x	x	x	~	x	~	x	x	x
2007 06 04	1.0	~	x	x	x	x	x	x	~	x	x	x
2007 12 10	2.0	x	x	x	x	x	x	x	-	x	x	x

7. Discussion

Continuation of Table 7-2.

date yyyy mm dd	mag	Processing Steps										
		AC - s	AC - t	AI	C	ES	M	RMS	SC	SC - ma	SC - mv	SC - s
2008 01 22	1.4	~	x	x	x	-		-	-	x	x	x
2008 03 02	1.8	x	~	x	x	x	x	x	~	x	x	x
2008 05 03	2.5	x	x	x	x	x	~	x	x	x	x	x
2008 07 23	2.0	x	x	x	x	~	x	~	x	x	x	x
2009 01 06	1.3	-	x	-	x	-		-	~	x	x	x
2009 05 06	2.1	x	x	x	x	~	x	~	x	x	x	x
2010 01 19	2.7	x	x	x	x	~	x	~	x	~	x	x
2010 01 23	2.3	x	-	x	x	x	x	x	~	x	x	x
2010 01 24	2.3	x	x	x	x	-	-	-	-	-	-	-
2010 04 23	1.4	x	x	-	-	-	~	-		~	x	x
2010 05 03	2.2	x	x	x	x	x	~	x	-	x	x	x
2010 09 18	1.7	-	-	-	-	-	x	-	x	-	-	-
2010 10 23	2.4	x	x	x	x	x	x	x	~	x	x	x
2011 04 05	3.1	x	x	x	~	x	x	x	x	-	~	~
2011 08 10	2.0	-	-	-	x	-	x	-	-	-	x	x
2011 12 26	1.5	x	x	-	x	-	x	-	~	~	-	~
Sum x		33	33	33	36	23	14	23	18	32	37	35
Sum ~		3	5	0	3	8	10	8	15	4	2	5

7. Discussion

Table 7-3 Very good fit (x), no fit (-) and questionable fit (~) of processed tectonic earthquake data

date yyyy mm dd	mag	Processing Steps										
		AC - s	AC - t	AI	C	ES	M	RMS	SC	SC - ma	SC - mv	SC - s
2001 04 15	2.6	x	-	x	-	~		~	x	x	x	x
2001 11 10	2.4	x	x	x	-	~		~	x	-	-	-
2004 02 22	2.4	x	~	x	~	x		x	x	x	x	x
2004 06 18	3.6	x	x	x	x	x		x	x	x	x	x
2005 06 23	1.9	x	x	x	x	x		x	x	x	x	~
2008 05 21	3.0	x	x	x	-	x	x	x	x	x	x	x
2008 05 21	3.6	x	x	x	x	x	x	x	x	x	x	x
2008 07 18	3.8	x	x	x	x	x	x	x	x	x	x	x
2010 08 04	3.3	x	x	x	x	x	x	x	x	x	x	x
2010 08 04	2.1	x	-	x	x	-	x	-	x	-	-	-
2010 08 04	1.4	~	~	x	x	-		-	x	x	x	x
2010 08 05	2.7	x	x	x	x	x	x	x	x	x	x	x
Sum x		11	8	12	8	8	6	8	12	10	10	9
Sum ~		1	2	0	1	2	0	2	0	0	0	1

7. Discussion

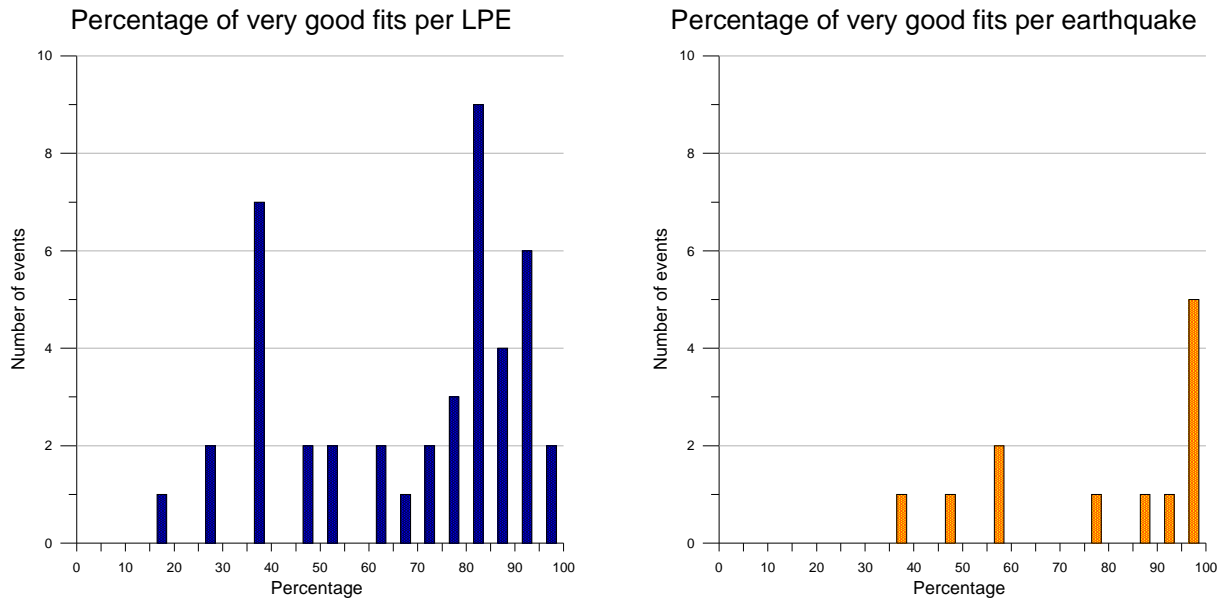


Figure 7-1 Percentage of very good fits per LPE (left) and earthquake (right).

To quantify the results of Table 7-2 and Table 7-3 two approaches are chosen. First, the percentage of very good fits per LPE and tectonic earthquake are given in Figure 7-1. The histogram shows that concerning the LPEs approximately two thirds of the events have more than 60 % of very good fits. Table 7-4 lists the LPEs, which have more than 60 % of misfit. Most of the events have low magnitudes (less than 2.0). There is one outlier with a magnitude of 2.9, which belongs to the event on the 14th of July 2003.

Table 7-4 Misfits greater than 60 %.

date yyyy mm dd	mag	fits per event	
		number	percentage
2000 08 29	2.1	4	40
2000 11 09	1.7	4	40
2003 07 14	2.9	3	30
2004 05 08	1.5	3	30
2004 10 12	1.5	4	40
2006 03 28	1.8	5	50
2006 04 27	1.5	6	55
2008 01 22	1.4	6	55
2009 01 06	1.3	5	45
2010 01 24	2.3	4	36
2010 04 23	1.4	4	36
2010 09 18	1.7	2	18
2011 08 10	2.0	4	36
2011 12 26	1.5	4	36

7. Discussion

Secondly, the percentage of very good fits for each processing step is shown in Figure 7-2. For seven different methods (AC – s, AC – t, AI, C, SC – ma, SC – mv, SC – a) about 80 % of the LPEs show very good results, whereas for the remaining four methods (ES, M, RMS, S) only approximately 50 percent of the processed data shows very good fits. For the sake of completeness the results for the same calculations are given for tectonic earthquakes.

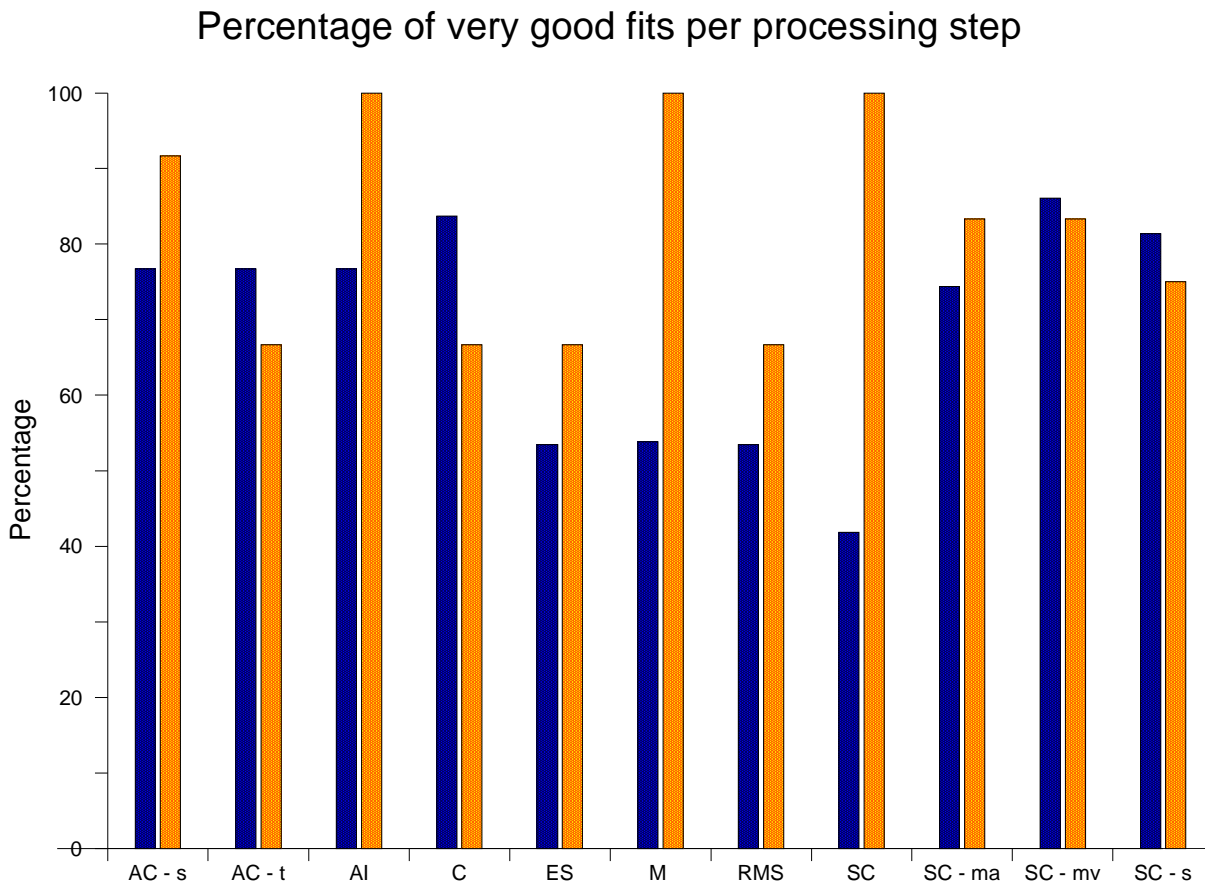


Figure 7-2 Percentage of very good fits per processing steps for LPEs (blue) and tectonic earthquakes (orange). Abbreviations see Table 7-1.

With all the data listed above, there is still a lack in information concerning the comparison of the content of a seismogram of an LPE and a tectonic earthquake. A very good fit does not conclusively lead to a separation of the two seismic sources as the results can be overlapping. It can either affect the whole magnitude range or only a limited division. For that reason, all processing steps have to be discussed separately to determine the most convincing methods.

Concerning the spectral content (SC, SC – ma, SC – mv, SC – s) it is best to have a look at the amplitude spectra itself, as the maximum amplitude range (0.5 to 3 Hz) and the low ratio at high frequencies can be visible. At least the second criterion is also visible for a low magnitude range,

7. Discussion

whereas a peak at the maximum amplitude range is only visible above magnitudes of 2.0. The bad fit in Figure 7-2 results from the strict classification, that a very good fit must reveal both criteria. To detect LPEs with low magnitudes with the help of the spectral content, it is useful to calculate the mean value (SC – mv) and the sum (SC – s) of the amplitudes in the characteristic spectral range from 0.5 to 3 Hz.

Another useful method is the comparison of body-wave magnitude and local magnitude. As the first one is always far less than the second one for earthquakes, this gap is not as big for LPEs. In some cases these magnitudes are even equal.

Calculating the Arias intensity (AI) of seismograms with a different source mechanism is also a useful tool. The results for LPEs are along the whole magnitude range less than the ones of earthquakes. By means of the exponential fit of the available data a greater separation for greater magnitudes is recognizable. The slope for LPEs accounts for 2.5 on average, while the one for tectonic earthquakes averages 3.7.

The same statements can be made for the energy signal (ES) and the root mean square (RMS) of the processed data. However, these are not very satisfying as there is hardly any difference between LPEs and tectonic earthquakes and the percentage of very good fits is less than 60 %.

This looks entirely different when calculating the auto correlation (AC) and “S₉₅”, which is the sum of the amplitudes at the point in time when 95 % of the signal has passed. Beside the minor width of the auto correlation function of earthquakes, their “S₉₅” is independent of the magnitude. It is at a more or less constant level of about 50 to 70 with an average slope of 2.11, while there is a steady increase for LPE data (slope averages 21.7). The values at low magnitude ranges can be separated but they should be verified with other methods. No such expressive information can be extracted from “T₉₅”, the point in time, when “S₉₅” is reached. Still it is a good example for a very good fit that does not conclusively lead to a separation of the two seismic sources, however.

Last, the coda (C) of the seismogram was analyzed. For that reason, the exponential fit was calculated for the increasing and the decreasing part of the seismogram with the maximum amplitude as separating peak value. In both cases the mean value of the slope for earthquakes is higher when compared with those of LPEs. Still, the separation of the seismograms with the help of the coda is restricted to magnitudes less than 1.5 and greater than 2.0.

To summarize the discussion of the processing steps Table 7-5 gives an overview of the different methods applied. It highlights, whether applying a method is very good, good, reasonable or nonviable. Calculating “S₉₅”, the exponential fit of the Arias intensity and analyzing the spectral content (SC, SC – mw, SC – s) of an unknown seismogram leads to a certain classification. The characteristics of LPEs are clearly distinguishable from the ones of tectonic earthquakes. Additionally, the result can be verified with the help of body-wave and local magnitude, as well as the Arias intensity and the maximum amplitude of the spectral content, whereas the last one is restricted to magnitudes greater than 2.0. There is no need in applying further processing steps, as calculating the energy signal or the root mean square did not perform well in the decision making process.

7. Discussion

Table 7-5 Final results for application and restriction of processing steps.

Processing Step	Abbreviation	Application	Restrictions
AC - sum	AC - s	very good	
AI - exponential fit	AI - ef	very good	
Spectral Content	SC	very good	$M > 2.0$
SC - mean value	SC - mv	very good	
SC - sum	SC - s	very good	
Arias Intensity	AI	good	
Magnitudes	M	good	
SC - maximum amplitude	SC - ma	good	$M > 2.0$
Auto Correlation	AC	reasonable	
Coda	C	reasonable	$1.5 < M < 2.0$
Energy Signal	ES	nonviable	
Root Mean Square	RMS	nonviable	

The second aim of the diploma thesis was to constrain the possible sources for LPEs from the closer vicinity of Bad Ischl. After consulting several papers on long-period seismic signals, the most obvious reason is thought to be some kind of mass movement on or very close to the earth's surface.

From the localization done by ZAMG, three clusters of events can be defined (west of Hallstatt, northwest of Bad Aussee and between Bad Ischl and Bad Goisern). Based on this partitioning a revealing conversation with M. LOTTER from the Geological Survey of Austria helped to figure out possible source mechanism: Beside landslides, basically the geological/geotechnical system "Hart auf Weich" implies a thick ductile basement overlain by a brittle cap rock. This limestone cap rock out of is forced by various factors to break up into several separate units.

To get an impression of size and movement, the fault plane of these limy broken slabs and the displacement were estimated. The area of failure in the clusters Bad Aussee and Bad Goisern are on average of similar size, but the mass movement within the last 13 years in Bad Aussee (0.14 m) exceeds the one in Bad Goisern (0.07 m) by a factor of two. Also twice as many events (17) occurred there and the final calculations show kind of a continuous mass movement. On the contrary, the data from Bad Goisern gives the impression of very low displacement rates with two strong LPEs in 2006. The results for the region west of Hallstatt reveal low constant displacements until 2006. After that more events with greater displacements occurred on small fault planes.

Also an attempt was taken to correlate mass movements with precipitation. Thus, data were retrieved from the nearest meteorological stations. The aim of the analysis was to correlate the precipitation in the previous four weeks before an LPE was recorded. Unfortunately, the meteorological stations do not correlate with the three defined clusters and thus the information to be extracted does not always refer to the closest vicinity of an event. Useful information could only be gained from the meteorological station of Bad Goisern, where four separate periods of increased precipitation were detected before most LPEs were triggered. The data from the meteorological

7. Discussion

station of Bad Aussee was also analyzed, but no conclusions could be drawn. Only in one case maybe a slight increase in precipitation within in the last few days prior to a LPE can be associated with.

7. Discussion

8 Conclusion

Testing various processing steps on the long-period seismic data set from the region of Bad Ischl allowed judging more of less selective methods. While some methods resulted in useful conclusions, others did not. Nevertheless, signal processing methods assist in separating LPEs from tectonic earthquakes.

A detailed analysis of the seismograms enables one to detect specific and distinct characteristics. Five out of eleven applied methods turned out to be very useful to make LPEs easily distinguishable from tectonic earthquakes:

- Sum of the auto correlation
- Exponential fit of the Arias intensity
- Spectral content
- Mean value of spectral content
- Sum of spectral content

In addition three other methods can be applied to confirm the results from the five above mentioned processing steps as they provide good results:

- Arias intensity
- Magnitudes
- Maximum amplitude of the spectral content

Analyzing the coda of seismograms is not expedient compared to the methods listed above and calculating the root mean square as well as the energy signal does not contribute to conclusive results.

The second part of the thesis placed special emphasis on the origin of the ground motion. From the localization done by ZAMG, three clusters were defined: Bad Goisern, Hallstatt, Bad Aussee. Combined with the geology and geotechnical situation, the three spatial separated regions were correlated with diverse forms of mass movements. Especially in the region of Hallstatt and Bad Aussee the system “Hart auf Weich” characterizes the instability of the masses on the earth surface while in the region of Bad Goisern several diverse mass movements (e.g. earth flows) are very likely to be responsible for triggering the long-period data. The respective calculated displacement rates within the last 13 years and the sizes of the fault planes are approximately 0.14 m/238x238 m (Bad Aussee), 0.07 m/217x217 m (Bad Goisern) and 0.05 m/158x158 m (Hallstatt).

A correlation with the external factor of precipitation did not lead to any significant conclusions, but four periods of precipitation were vaguely perceptible in the region of Bad Goisern and a slight increase in precipitation shortly before a LPE was triggered can be surmised for the region of Bad Aussee.

8. Conclusion

Altogether the analysis of long-period seismic data in the region of Bad Ischl led to satisfying results as processing steps were found to distinguish LPEs from tectonic earthquakes. In addition a reasonable correlation with the regional geology and geotechnical setting became obvious. However, there is still great potential in this field of work. The establishment of a more extensive seismic network in hazardous regions, a better localization of LPEs and a closer look at the geology in the field shortly after detecting an event might lead to an additional separation of source mechanisms in the range of mass movements based on the analysis of seismograms. This will minimize the risk to people habituated in hazardous regions and underlines the importance of seismically identifying and locating LPEs.

Acknowledgements

First of all, I would like to thank my supervisor Univ.-Doz. Dr. Wolfgang Lenhardt, who devoted his time and expert knowledge to this thesis.

I am grateful to Mag. Rita Meurers from ZAMG, who was an important contact person regarding the data, and Dr. Irene Bianchi from the University of Vienna, who was a great help concerning computer-related difficulties. Furthermore, I want to thank Dr. Michael Lotter from GBA, who supported this thesis with geological and geotechnical information.

Finally, I am grateful to my family and my boyfriend for their great support during my studies.

References

- ALLMANN, B. P., P. M. SHEARER and E. HAUSSON (2008). Spectral Discrimination between Quarry Blasts and Earthquakes in Southern California. *Bulletin of the Seismological Society of America*, 98, pp 2073-2079
- ARIAS, A. (1970). A measure of earthquake intensity, In R.J. Hansen (ed.): *Seismic Design for Nuclear Power Plants*, The M.I.T. Press, pp 438-483
- autoDRM, http://www.seismo.ethz.ch/prod/autodrm/index_EN, last access 01/03/2012
- BORMANN, P. (Ed.). *New Manual of Seismological Observatory Practice (NMSOP-1)*. IASPEI, GFZ German Research Centre for Geosciences, Potsdam, 2009
- BRODSKY, E. E., GORDEEV E. and H. KANAMORI (2003). Landslide basal friction as measured by seismic waves. *Geophysical Research Letters*, 30, No. 24, 2236
- CAPLAN-AUERBACH, J. and C. HUGGEL (2007). Precursory seismicity associated with frequent, large ice avalanches on Iliamna volcano, Alaska, USA. *Journal of Glaciology*, 33, No. 180
- CHLEBORAD, A. F., BAUM, R. L. and J. W. GODT (2006). Rainfall Thresholds for Forecasting Landslides in the Seattle, Washington, Area – Exceedance and Probability. U.S. Geological Survey Open-File Report 2006–1064
- CHOUET, B. A. (1996). Long-period volcano seismicity: its source and use in eruption forecasting. *NATURE*, 380, pp 309-316
- COE, J. A., GODT, J. W., WAIT, T. C. and J. W. KEAN (2007). Field Reconnaissance of Debris Flows Triggered by a July 21, 2007, Thunderstorm in Alpine, Colorado, and Vicinity. U.S. Geological Survey Open-File Report 2007-1237, 25 p.
- codeco3, http://www.seismo.ethz.ch/prod/software/codeco3/index_EN, last access 08/01/2011
- DAHLEN, F. A. (1993). Single-force representation of shallow landslides sources. *Bulletin of the Seismological Society of America*, 83, No. 1, pp 130-143
- DÖLLMANN, O. (2000). Untersuchung einer Großhangbewegung an der Sandling Südseite (Altaussee / Steiermark). Universität Karlsruhe (TH). Diploma Thesis unpublished
- EHRET, D. (2002). Geotechnische Untersuchung und GIS-gestützte Erfassung der Massenbewegungen zwischen Hallstatt und Plassen. Diploma thesis at Universität Karlsruhe (TH)
- FAUPL, P. (2003). *Historische Geologie*. WUV

- FRISCH, W. And H.-J. GAWLICK (2003). The nappe structure of the central Northern Calcareous Alps and its disintegration during Miocene tectonic extrusion-a contribution to understanding the orogenic evolution of the Eastern Alps. *International Journal of Earth Sciences*, 92, pp 712-727
- DIEGO, M., GOMEZ M. and ROBERTO A. TORRES C. (1996). Unusual low-frequency volcanic seismic events with slowly decaying coda wave observed at Galeras and other volcanoes. *Journal of volcanology and geothermal research*, 77, pp 173-193
- GEOLOGISCHE BUNDESANSTALT ÖSTERREICH (2007). Geologische Übersichtskarte Österreich. http://www.geologie.ac.at/RockyAustria/geologie_und_landschaft.htm, last access 05/05/2012
- GÖTZ, H. (1995). Einführung in die digitale Signalverarbeitung. Teubner Studienskripten
- HAAS, J., KOVACS, S., KRYSZTYN, L. and R. LEIN (1995). Significance of Late Permian - Triassic facies zones in terrane reconstruction in the Alpine - North Pannonian domain. *Elsevier Tectonophysics*, 242, pp 19-40
- HAINZL, S., KRAFT, T., WASSERMANN, J., IGEL, H. and E. SCHMEDES (2006). Evidence for rainfall-triggered earthquake activity. *Geophysical Research Letters*, 33, L19303
- HANKS, T.C. and H. KANAMORI (1979). A moment-magnitude scale. *Journal of Geophysical Research*, 84, pp 2348-2350
- HARP, E.L. and R.C. WILSON (1995). Shaking Intensity Thresholds for Rock Falls and Slides: Evidence from the Whittier Narrows and Superstition Hills Earthquake Strong Motion Records. *Bulletin of the Seismological Society of America*, 85, pp 1739-1757
- HAUSWIRTH, E. K. and A. E. SCHEIDEGGER (1988): Rock slide on the Red Wall above Hallstatt, Upper Austria. – *Proc. 5th Int. Symp. Landslides, Lausanne*, 2, pp 1333 – 1338
- HIGHLAND, L. M. and P. BOBROWSKY (2008). *The Landslide Handbook-A Guide to Understanding Landslides*. Reston, Virginia, U.S. Geological Survey Circular 1325, 129 p.
- HÖCHERL, A. (1991). Geologische und ingenieurgeologische Untersuchungen im Einzugsgebiet des Michelhallbaches zwischen Bad Goisern und Altaussee (Oberösterreich / Steiermark). Universität Erlangen- Nürnberg, diploma thesis [unpublished].
- HUNTER, G. and R. FELL (2001). "Rapid" Failure of Soil Slopes. Univeristy Report No. R-400, The Universtiy of New South Wales, Sydney.
- HUTCHINSON, J.N. and R. K. BHANDARI (1971). Undrained loading – a fundamental mechanism of mudflows and other mass movements. *Géotechnique*, 21, pp 353-358
- ISC, <http://www.isc.ac.uk/>, last access 12/03/2012

- KANAMORI, H. and W. GIVEN (1982). Analysis of long-period seismic waves excited by the May 18, 1980, eruption of Mt. St. Helens-a terrestrial monopole? *Journal of Geophysical Research*, 87, pp 5422-5432
- KRAFT, T. (2006). A new seismological network for Bavaria and its application to the study of meteorologically triggered earthquake swarms. LMU Munich, Faculty of Geosciences.
- KRAFT, T., WASSERMANN, J., E. SCHMEDES and H. IGEL (2006). Meteorological triggering of earthquake swarms at Mt. Hochstaufen, SE-Germany. Elsevier.
- LA ROCCA M., GALLUZO D., SACCOROTTI G., TINTI S., CIMINI G. B. and E. DEL PEZZO (2004). Seismic Signals Associated with Landslides and with a Tsunami at Stromboli Volcano, Italy. *Bulletin of the Seismological Society of America*, 94, No. 5, 1850-1867
- LAY, T. and T. C. WALLACE (1995). *Modern Global Seismology*. Academic Press
- LOTTER, M. (2001). Geotechnische und kinematische Untersuchungen an instabilen Felshängen im alpinen Raum. – Dissertation, Naturwiss. Fak. der Friedrich-Alexander-Univ. Erlangen-Nürnberg: IX + 325 S.; Erlangen. – [unpublished]
- LÜKE, H. D. (1992). *Signalübertragung: Grundlagen der digitalen und analogen Nachrichtenübertragungssysteme*. 5. Auflage, Springer-Verlag
- MANDL, G. W. (1984). Zur Trias des Hallstätter Faziesraumes – ein Modell am Beispiel Salzkammergut (Nördliche Kalkalpen, Österreich). – *Mitt. Ges. Geol. Bergbaustud. Österr.*, 30/31, pp 133 – 176
- MANDL, G. W. (2000). The Alpine sector of the Tethyan Shelf; examples of Triassic to Jurassic sedimentation and deformation from the Northern Calcareous Alps. *Mitteilungen der Österreichischen Geologischen Gesellschaft*, 92, No. 1999, pp 61-77
- McGARR, A. (1991). Observations constraining near-source ground motion estimated from locally recorded seismograms. *Journal of Geophysical Research*, 96, pp 16495- 16508
- MOSER, M., and K. CZURDA (1999). The evaluation of the risk of deep-seated mass movements to the cultural heritage sites of Hallstatt-Dachstein/Upper Austria. – IGCP Project, 425, Reports and Sub-Project Proposals, pp 61 – 70; Paris
- MOSER, M., LOTTER, M. and H. MEIER (2003). Großhangbewegungen des Hallstätter Raumes – Geotechnik – Kinematik – Bewegungsmechanismus. *Beiträge zur Geologie des Salzkammerguts, Gmundner Geo-Studien 2 Erkudok* ©Institut Museum Gmunden, pp 343-352
- NORRIS, R. D. (1994). Seismicity of rockfalls and avalanches at three Cascade Range volcanoes; implications for seismic detection of hazardous mass movements. *Bulletin of the Seismological Society of America*, 84, pp 1925-1939
- OKAL E. A. (1990). Single forces and double-couples: a theoretical review of their relative efficiency for the excitation of seismic and tsunami waves. *Journal of Physics of the Earth*, 38, 445-474

- POISEL, R. and W. EPPENSTEINER (1989). Gang und Gehwerk einer Massenbewegung Teil 2: Massenbewegungen am Rand des Systems „Hart auf Weich“. Felsbau 7, 1, 16-20, Essen
- ROHN, J., (1991). Geotechnische Untersuchungen an einer Großhangbewegung in Bad Goisern (Oberösterreich). Ph.D. thesis, Schriftenreihe Angewandte Geologie, 14, University of Karlsruhe
- ROHN, J., RESCH, M., SCHNEIDER, T., FERNANDEZ-STEEGER, T.M. and K. CZURDA (2004). Large-scale lateral spreading and related mass movements in the Northern Calcareous Alps. Bulletin of Engineering Geology and the Environment, 63, pp 71-75
- RÖNNAU, C. (2001). Zusammenstellung der geologischen und geotechnischen Karte der Hallstätter Zone von Bad Ischl – Altaussee mit ARC /Info (GIS). Universität Karlsruhe (TH), Diploma Thesis unpublished
- SAC, <http://www.iris.edu/software/sac/manual.html>, last access 01/04/2012
- SCHERBAUM, F. (2001). Of Poles and Zeros, Fundamentals of Digital Seismology. 2nd Edition, Kluwer Academic Publishers
- SCHNEIDER, H. (1998). Geologische und ingenieurgeologische Untersuchungen der Großhangbewegungen am Sandling bei Altaussee (Steiermark). Universität Karlsruhe (TH), Diploma Thesis unpublished
- SPÖTL, C. (1987). Eine klastisch-evaporitische Oberperm-Entwicklung im Hallstätter Salzberg (Salzkammergut, Österreich). Mitt. Österr. Geol. Ges., 80: 115 – 142, 9 Abb., 4 Tab., 2 Taf.; Wien
- Streckeisen STS-2, <http://www.passcal.nmt.edu/>, last access 01/03/2012
- STEIN, S. and M. WYSESSION (2003). An Introduction to Seismology, Earthquakes and Earth Structure. Blackwell Publishing
- SURINACH, E., VILAJOSANA, I., KHAZARADZE, G., BIESCAS, B., FURDADA, G., and J. M. VILAPLANA (2005). Seismic detection and characterization of landslides and other mass movements. Natural Hazards and Earth System Sciences, 5, pp 791-798
- TOLLMANN, A. (1964). Zur Frage der Faziesdecken in den Nördlichen Kalkalpen und zur Einwurzelung der Hallstätter Zone (Ostalpen). – Geol. Rdsch., 53 (1), pp 153 – 170
- TOLLMANN, A. (1976). Analyse des klassischen nordalpinen Mesozoikums: Stratigraphie, Fauna und Fazies der nördlichen Kalkalpen. Wien (Deuticke)
- TOLLMANN, A. (1976). Der Bau der Nördlichen Kalkalpen: Orogene Stellung und regionale Tektonik. Wien (Deuticke)
- TOLLMANN, A. (1982). Oberjurassische Gleittektonik als Hauptformungsprozeß der Hallstätter Region und neue Daten zur Gesamttektonik der Nördlichen Kalkalpen in den Ostalpen. Mitt. Österr. Geol. Ges., 74/75 (1981/1982), pp 167 – 195

- TOLLMANN, A. (1985). Geologie von Österreich: Band II Außerzentralalpiner Anteil. Wien (Deuticke).
- VAN DEN HAM, G. (2006). Numerical simulation and engineering-geological assessment of a creeping slope in the Alps. Dissertation, Universität Karlsruhe (TH)
- VILAJOSANA, I., SURINACH, E., ABELLÁN, A., KHAZARADZE, G., GARCIA, D., and J. LLOSA (2008). Rockfall induced seismic signals: case study in Montserrat, Catalonia, Natural Hazards and Earth System Sciences, 8, pp 805-812
- wikipedia.org, http://en.wikipedia.org/wiki/Prediction_of_volcanic_activity, last access 21/03/2012
- WEICHERT, D., HORNER, R. B. and S. G. EVANS (1994). Seismic Signatures of Landslides: the 1990 Brenda Mine collapse and the 1965 Hope Rockslides. Bulletin of the Seismological Society of America, 84, pp 1523-1532
- WIECZOREK, G.F., EATON, L.S., MORGAN, B.A., WOOTEN, R.M. and MORRISSEY, M., (2009). An examination of selected historical rainfall-induced debris-flow events within the central and southern Appalachian Mountains of the Eastern United States. U.S. Geological Survey Open-File Report 2009–1155, 25 p.
- ZAMG, <http://www.zamg.ac.at/lexikon/Erdbeben.php>, last access 02/05/2012

Curriculum Vitae

Persönliche Daten

Name: Mayrhofer Franziska
Geburtsdatum und -ort: 13.März 1987 in Wien 16
Nationalität: Österreich
Familienstand: ledig
Email Adresse: a0500656@unet.univie.ac.at

Schulische Ausbildung

[1993-1997] Privat Volksschule Zwettl
[1997-2005] Bundesgymnasium Zwettl
Abschluss: mit ausgezeichnetem Erfolg
[März 2003] 3. Platz beim Fremdsprachenwettbewerb in NÖ
Latein, Kurzform
[März 2004] 3. Platz beim Fremdsprachenwettbewerb in NÖ
Altgriechisch

Studium

[Oktober 2005 – Dezember 2006] Universität Wien: Diplomstudium Meteorologie und Geophysik, erster Abschnitt
[seit Dezember 2006] Universität Wien: Diplomstudium Meteorologie und Geophysik, Studienzweig Geophysik
[2008] Studentenvertretung in der Berufungskommission Geophysik
[seit Oktober 2009] Universität Wien: Bachelorstudium Erdwissenschaften
[September 2011] Archäogeophysikalisches Feldpraktikum in der Slowakei, veranstaltet von Christian-Albrechts-Universität zu Kiel
[seit Juni 2012] Mitglied der Studienkonferenz SPL28

Praktika/Berufserfahrung

[Juli/August 2008]	Geologische Bundesanstalt Wien, Praktikum in der Abteilung Geophysik
[Februar – April 2009]	Geologische Bundesanstalt Wien
[Juli 2010]	Geologische Bundesanstalt Wien, Messhelferin